CRANFIELD UNIVERSITY

JOSHUA HAKURI NWEN

NUMERICAL MODELING OF THE ELECTRO-KINETIC EFFECT ON PIPE-SOIL INTERACTION

SCHOOL OF WATER, ENERGY, AND ENVIRONMENT
ENERGY THEME

PhD Thesis

Academic Year: 2014 - 2017

Supervisor: Dr. Fuat Kara
Co-Supervisor: Professor John Oakey
OCTOBER 2017

CRANFIELD UNIVERSITY

SCHOOL OF WATER, ENERGY, AND ENVIRONMENT
Energy Theme

DOCTOR OF PHILOSOPHY (PhD)
Academic Year 2014 - 2017

JOSHUA HAKURI NWEN

Numerical modeling of the Electro-Kinetic Effect on Pipe-Soil Interaction

Supervisor: Dr. Fuat Kara
Co-Supervisor: Professor John Oakey

OCTOBER 2017

This thesis is submitted in partial fulfillment of the requirements for the degree of Doctor of Philosophy

ABSTRACT

The high pressure and high temperature (HP/HT) of operating fluid and soft soil content significantly account for the axial and lateral displacement of subsea pipelines. The ability of a pipeline to resist displacement depends on the soil strength. Due to low soil shear strength, the accumulation of displacement over a period of operating cycles leads to pipeline displacement. Increasing the pipe-soil interaction resistance will significantly reduce pipeline displacement. Soil contains solid, water and air particles. The levels of water, air and the solid particle size in the soil, govern its mechanical behaviour. Removal of pore water content from the soil voids may lead to consolidation with a resultant increase in effective stress.

One of the methods used to increase soil strength is the Electro-Kinetic (EK) process. This is applied to increase the strength of onshore and offshore soil foundations. An important advantage is a reduction in time taken for the soil to consolidate. A Numerical model is developed for the determination of the EK effect on soft soil using the ABAQUS software tool. Two stages involved in the EK analyses are electro-osmotic consolidation and dynamic pipe-soil interaction. Three different test series each for electro-osmotic consolidation and dynamic analyses were built. The electro-osmotic consolidation analyses determined the soil consolidation followed by a dynamic pipe-soil interaction process. The electro-osmosis considered the effect of voltage variations, time taking for the soil to consolidate and variations with numbers of electrodes. The dynamic analyses consider the effect of electro-osmosis due to the displacement of pipeline in the vertical, axial, and lateral direction.

From the electro-osmotic analyses, the soil settlement is due to its reduction in void volume as a result of the pore water pressure dissipation. A further interaction of pipeline on the (settled) consolidated soil indicates a significant improvement in the soil strength when compared with the non-treated soil.

PUBLICATIONS

1. Joshua, H. N., and Kara, F. (2018). “Numerical study of electro-osmotic consolidation effect on pipe-soil interaction.” *Applied Ocean Research*, 74, 11–27.
2. Joshua, H. N., and Kara, F. (2017). “Numerical investigation of Electro-kinetic effect on pipe-soil interaction.” *Proceedings of the International Conference on Offshore Mechanics and Arctic Engineering - OMAE*, American Society of Mechanical Engineers, Trondheim, Norway, 1–10.
3. Joshua, H.N. and Kara, F. (2018) ‘Numerical Investigation of Dynamic Pipe-Soil Interaction on Electro-Kinetic Treated Soil’. Manuscript under Review, Journal of Water-way, Port, Coastal and Ocean Engineering.
4. Joshua, H.N. and Kara, F. (2017) ‘Numerical Study of Electro-Osmotic Consolidation of Soft Clay for Pipeline Stability’, Paper accepted for presentation at the Proceedings of the ASME 2018 37th International Conference on Ocean, Offshore and Arctic Engineering, OMAE2018, June 17-22, 2018, Madrid, Spain.

Keywords:

Force, Displacement, Settlement, Soil-Consolidation, Finite Element, Electro-Osmosis, Electrodes, Pore Pressure, Void Ratio, Effective Stress

ACKNOWLEDGEMENTS

Wish to acknowledge the help and support of my supervisor, Dr. Fuat Kara, for his invaluable advice, prompt response to queries, and quality guidance during this great task. He has displayed great professionalism, intelligence, and commitment which inspired my success. I remain grateful and fortunate to have a supervisor who not only cares about my academics but also cares about my wellbeing.

My gratitude goes to Dr. David Parson the thesis review independent chairman and Dr. Nigel Simms my course adviser for their constructive comments during my review periods. I also wish to show my appreciation to the external examiner Prof Robert Sutton and internal examiner Dr. Patrick Verdin for their recommendations which did help to shape this work.

My acknowledgment also goes to the Petroleum Technology Development Fund (PTDF), Nigeria for granting the funding for this research.

My father, Rtd Rev Joshua Shirkat Nwen and my Late mother Mrs. Hanatu Nadit Joshua, have made an immeasurable sacrifice to ensure I received the best in life. Their love, guidance, and encouragement have inspired me to a greater height. They are a gift from God to me. I know my mom is smiling for this success as she looks down from heaven. I love you.

My appreciation also goes to my siblings: Maryamu, Filibus, Shadrach, Helen, Kyauta, Naomi, and Nenrit. My nice Hope and my nephew Michael. Thank you for standing with me and for your ceaseless prayers.

TABLE OF CONTENTS

LIST OF FIGURES

LIST OF TABLES

LIST OF ABBREVIATIONS

CTD	Coupled Temperature-Displacement
EK	Electro-Kinetic
FE	Finite Element
HP/HT	High-Pressure, High-Temperature
IT	Information Technology
NLGEOM	Non-Linear Geometry
PIP	Pushed In Pipe
PLET	Pipeline End Termination
SCF	Stress Concentration Factor
WIP	Wished In Pipe

NOMENCLATURES

A	surface areas	(m^2)
A_c	area of contact	(m^2)
A_e	external area	(m^2)
A_e	internal area	(m^2)
D	diameter	(m)
E	Young's modulus	(Pa)
F_e	effective axial force	(N)
F_w	the axial force on pipe wall	(N)
e	void ratio	
e_0	initial void ratio	
${F_{ap}}^u$	undrained axial peak force	(N)
${F_{ar}}^u$	undrained axial residual force	(N)
L	length	(m)
L_0	original length	(m)
n	soil porosity	
p_e	external pressure	(Pa)
p_i	internal pressure	(Pa)
S	soil saturation	
S_u	undrained shear strength	(Pa)
S_{up}	undrained peak stress	(Pa)
S_{ur}	undrained residual stress	(Pa)
T	temperature	(℃)
V	the total volume of soil	(m^3)
V_v	volume of soil void	(m^3)
V_s	volume of solid soil particle	(m^3)
V_a	volume of air particle	(m^3)
V_w	volume of water particle	(m^3)
W_s	weight of solid soil particle	(N)
W_w	weight of water particle	(N)
Z	depth of embedment	(m)
σ'	effective stress	(N/m^2)
σ_f	total normal stress	(Pa)
${\sigma_f}'$	effective normal stress	(Pa)
τ	shear stress	(Pa)
τ_f	total shear strength	(Pa)
${\tau_f}'$	effective shear stress	(Pa)

ω	moisture content	
ϕ'	effective friction angle (degree"°")	
C	cohesion intercept	
c'	effective cohesion intercept	
p	equivalent pressure stress	(Pa)
t	deviatoric stress	(Pa)
M	slope of critical state line	
a	yield surface size	(Pa)
a_o	initial yield surface size	(Pa)
α	adhesion factor	
u	pore water pressure	(Pa)
u_e	excess water pore pressure	(Pa)
υ	Poisson ratio	

CHAPTER 1: INTRODUCTION

1.1 Background

High operating temperature and pressure induce high compressive forces on pipelines leading to axial and lateral displacement. Due to the accumulation of displacement with each start-up and shut-down cycles, pipeline walking occurs [1,2], which may be undesirable for risers, expansion spools, and in-line structures. This occurs mostly in areas with low soil strength. The strength of the material is measured with regard to the greatest stress it can resist and geotechnical structures depend on the shear strength of the soil. Failure of the soil can lead to the collapse of structures resting on it.

Deepwater consists mostly of very soft clay with high water content, low shear strength and high compressibility [2,3]. Increasing the soil strength is a possible mitigating measure against pipeline displacement [3–7]. Increase in the soil shear strength can be achieved using the Electro-Kinetic (EK) process. This involves passing an electrical current through electrode (cathode and anode) and in this process pore water flows in the soil toward the cathode known as electro-osmosis and the negative charge moves toward the anodes and the movement of the ions towards the cathodes known as electrophoresis [8–10].

Shear box testing by White et al. [6] demonstrate how the reduction in the moisture content in the soil can be achieved by cyclic hardening leading to an increase in undrained shear strength due to the release of excess pore water pressure and expectedly, leading to a significant increase in the axial resistance Smith and White [5]. The EK concept relates to shear box test by White et al. [6] such that it also involves removal of pore water pressure from the soil by electro-osmosis. The EK process has an advantage in significantly reducing the time for soil consolidation. EK process has found its application in geotechnical problems aimed at increasing strength of soil in dams, slopes, onshore and offshore foundations, consolidation in bridge supports, and bearing capacity of pre-driven piles [11]. This method proved a great success for both onshore and offshore

structures, however, numerical studies on the effect of the EK process on the pipe-soil interaction has received no attention.

This study considers numerically the impact in which EK treated soil will have on pipe-soil interaction using a commercially available software package (ABAQUS). Two important stages in this EK analysis are the electro-osmosis followed by a dynamic analysis. The electro-osmotic stage considers the soil consolidation with variation in voltage, time and number of electrodes. The dynamic analyses determine the electro-osmotic consolidation effect on pipeline displacement in axial, lateral and vertical directions. Results from the EK analyses indicate a significant improvement in the soil shear strength and the force required to pull the pipeline in vertical axial and lateral directions.

1.2 Study Motivation

Research has been carried out to determine the challenges posed by the operational load on a pipeline leading to its displacement with less work being made to find answers posed by the uncertainties. Complex and costly mitigating measures are being employed for pipeline stability and the need for further investigation to explore more options is necessary. Increasing the soil strength has been identified as a possible mitigation against pipeline displacement. Electro-osmotic consolidation of soil is currently being employed to increase soil strength around offshore and onshore structures, but the effect on pipe-soil interaction has not been investigated. This aspect has received no attention in terms of numerical modeling or detailed experiment in this regard. This study considers numerical modeling of the EK effect on the interaction of pipelines in treated soft clay. With the less complexity of this model, this will serve as a new approach to mitigating against pipeline displacement and other subsea structures.

1.3 Aim and Objectives

The aim of this research is to develop a numerical model using a commercially available software to investigate the effect of pipe-soil interaction on Electro-Kinetic (EK) treated soil.

The objectives are as follows:

- To review the electro-osmotic consolidation process and current practices aimed at mitigating subsea pipelines and the pipe-soil interaction behaviour.
- To develop a model and to determine the behaviour of the electro-osmotic consolidation due to soil-electrodes interactions.
- To determine the dynamic pipe-soil interaction behaviour due to soil EK treatment.
- To determine and compare the effect of non-EK and EK treated soil.
- To validate the numerical model with the experimental results.
- To conduct sensitivity analyses.

1.4 Thesis Structure

CHAPTER 1 consists of introduction, motivation, aim, and objectives of this study.

CHAPTER 2 reviews the electro-osmotic concept for subsea soil consolidation, the various flow processes, and similarities to justify the method adopted for the soil modeling and works relating to the pipe-soil interaction behaviour in vertical axial and lateral directions. Also highlighted are the current mitigation approaches to pipeline displacement and their limitations.

CHAPTER 3 discusses the numerical models employed in this study. This includes the model development, the pipe-soil model and their properties, the electro-osmotic modeling and the dynamic modeling. Coupling of the electro-osmotic consolidation and the dynamic analyses to determine the EK effect on pipe-soil interaction is also considered.

CHAPTER 4 presents the results from the electro-osmotic consolidation obtained from the studies. Mesh sensitivity analyses, validation of the Finite Element Analysis (FEA) electro-osmosis procedure/element type adopted are presented. Variation with numbers of anodes, variation with voltages, transient and steady-state analyses are also considered. The discussion centres on the electro-

osmotic behaviour and the consolation due to the effect of voltage, time, and variations with the numbers of electrodes.

CHAPTER 5 presents results from the dynamic analyses for non-EK and EK treated soil in vertical, axial, and lateral directions and the behaviour for each of these process are reported. Results were also compared with experimental studies. Pipe-soil interaction due to pipeline displacement considering the peak and residual behaviour, comparison of the non-EK with EK treated soil. Project applicability in the offshore environment is also highlighted.

CHAPTER 6 gives the summary, conclusions, and recommendations for future work.

CHAPTER 2: THEORETICAL BACKGROUND

Pipeline ends are constrained by a riser and the seabed soil resistance [12]. For a pipeline to remain in position, the soil resistance must be greater than the expansion forces. The level of expansion is a very considerable factor in pipeline design in order to safeguard the seabed structure against failure. Resistance to pipeline displacement is relatively influenced by pipe embedment, the cyclic response due to loading/unloading and the friction factor involved in the pipe-soil interaction. Any attempt to raise the soil resistance, the pipeline displacement and walking rate will significantly be affected. Research has been carried out to determine the axial resistance of pipe-soil interaction due to volumetric hardening, pipe shearing and soil EK treatment, which indicate a positive outcome.

2.1 Clay Soil Formation/Physical Parameters

Clay soil can be described as flake-shaped very small particles consisting of mica, clay mineral and other minerals with particle size averaging less than 0.075mm [13]. Clay soils are cohesive in nature, capable of attracting water, forming plastic components by adhesion within the particles. Three main clay minerals are Kaolinite, illite, and montmorillonite. The soil contains solid, water and air particles as shown in Figure 2-1. Gaps created within the soil often called voids and may contain water or air. The level of water, air, and the solid particle size governs its mechanical behaviour. A soil that is fully saturated contains 100% water; the water levels may vary depending on the soil types [13].

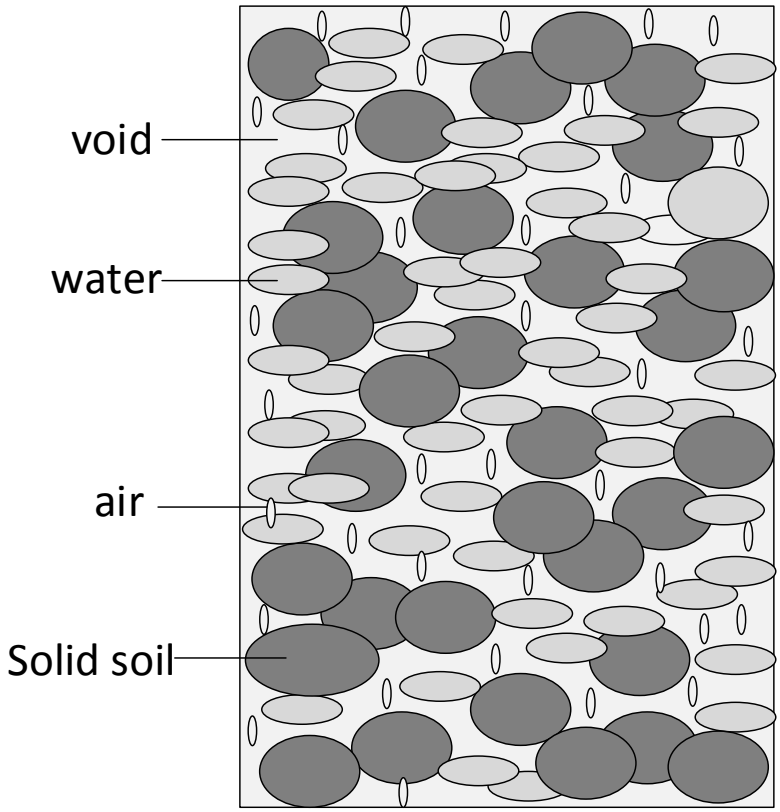

Figure 2-1 Soil Composition

From Figure 2-1, the volume of solid particles of the soil is V_s with no void and its weight is given as W_s, the volume of water component is given as V_w with the weight given as W_w, also the air contained in the soil contained a volume given as V_a with a negligible weight. The void volume in the soil V_v is a combination of $(V_a + V_w)$. Theoretically, the total volume V of the soil is given as [13]:

$$\boldsymbol{V = V_v + V_s = V_a + V_w + V_s} \tag{2-1}$$

The total weight W is given as,

$$\boldsymbol{W = W_w + W_s} \tag{2-2}$$

The void ratio e is the volume of voids V_v to the volume of the solid $V_{s,}$ is given as,

$$\boldsymbol{e = \frac{V_v}{V_s}} \tag{2-3}$$

The porosity of the soil n is defined as the volume of the void V_v to the total volume of the soil V given as,

$$\boldsymbol{n = \frac{V_v}{V} = \frac{e}{1+e}} \quad (2\text{-}4)$$

The level of the soil saturation S can be derived from the ratio of the water content V_w to the void volume V_v in the soil given as,

$$\boldsymbol{S = \frac{V_w}{V_v}} \quad (2\text{-}5)$$

Assuming a soil that is fully saturated, the voids volume V_v will be equal to the water content volume V_w, ($V_v = V_w$). In this case $S = 1$. While for a completely dry soil, $S = 0$ which implies that $V_w = 0$.

The moisture content ω in the soil is the ratio of water weight to the solid soil weight given by

$$\boldsymbol{\omega = \frac{W_w}{W_s}} \quad (2\text{-}6)$$

Soil composition and determination of soil parameters such as the void ratio, degree of saturation, specific gravity, soils and water unit weight are given in details elsewhere [13–15].

2.2 ABAQUS Constitutive Model

The ABAQUS tool has the capabilities to solve several geotechnical problems. Some of the approaches to solving the geotechnical problems are the Implicit Finite Element method, which has the capability to solve boundary value problems with little deformation with or without the pore water pressure taking into account. The Explicit Finite Element method is restricted to single-phase problems and capable of solving moderately to larger deformations. Also restricted to single-phase problems is the Coupled Eulerian-Lagrangian method, which has the capability of solving a larger deformation boundary. Soil constitutive models such as the Mohr-Coulomb plasticity, the modified Drucker Prager/Cap plasticity, and Modified Cam-Clay plasticity are introduced in the ABAQUS tool. The soil initial stress state, saturation and void ratio can be defined

using the initial state command implemented in ABAQUS. Other conditions such as the gravity load, concentrated and distributed load can also be defined [14].

The ABAQUS software can be used to determine the vertical penetration, lateral buckling, and axial walking of pipeline subjected to cycles of loading during shutdown and start-up. The finite element model considers the profile of seabed, nonlinear pipe-soil friction, pressure and temperature profile and the connected pipeline end termination (PLET) resistance, a pipeline can be modeled as a three-dimensional rigid or deformable surface. The quasi-static analysis is performed to simulate the axial displacement as the dynamic inertia loading is assumed to be negligible [7].

2.2.1 Mohr-Coulomb Plasticity Model

The stability of soil depends on the soil strength. The shear strength defines the soil internal resistance acting per unit area. Mohr-Coulomb failure criterion has found application in determining soil shear strength. The failure criterion combined the effect of shear stress τ and the normal stress σ, accounting for both the plastic flow and behaviour of the soil. This is defined by the equation [8]:

$$\boldsymbol{\tau_f = c + \sigma_f \tan \phi} \tag{2-7}$$

$$\boldsymbol{\tau_f{}' = c' + \sigma_f{}' \tan \phi'} \tag{2-8}$$

Where from Equation 2-7, τ_f is total shear stress on failure plane, σ_f is total normal stress on failure plane, ϕ is friction angle, c is cohesion intercept. Equation 2-8 defines the effective shear stress $\tau_f{}'$, the effective normal stress $\sigma_f{}'$, and the effective parameters for cohesive intercept c', and friction angle ϕ'. Equation 2-8 is more fundamental as the shear resistance of the soil depends on inter-particle interactions [8]. Other factors also account for the soil shear resistance; however, the focus is on the fundamental parameters based on equation 2-8.

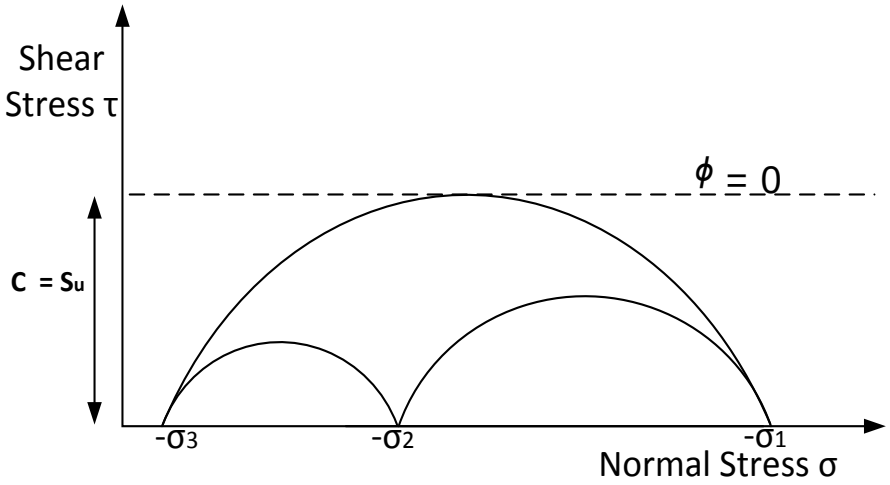

Figure 2-2 Mohr-Coulomb failure criterion of undrained saturated clay soil

A normally consolidated Kaolin clay has effective friction angle ϕ' ranging from 20° to 25° and decreases as the plasticity index increases. Assuming an incompressible saturated clay soil with the small size of the grain, the dilation and friction angle is neglected as there is very small or no dilation when subjected to shear. In this case, $\phi = 0$ and $c = s_u$ (soil undrained shear strength) [8] as shown in Figure 2-2.

2.2.2 Critical State (Clay) Plasticity Model

Critical state plasticity theory is an extension of the modified Cam-Clay model [16,17]. The model based on effective stress assumed a saturated soil with permeating fluid under pressure, flows with respect to Darcy's law. Modified Cam-Clay model considers the strain rate decomposition of the soil into elastic and inelastic parts, the theory of elasticity, yield surface; flow rule and hardening rule. Backward Euler integration of the flow and hardening rule were numerically implemented in plasticity models of ABAQUS [18].

The main features of the modified Cam-Clay model are the linear elasticity or porous elasticity which a material under compression indicates an increasing bulk elastic stiffness [18]. Models describing plasticity behaviour of clay are defined in ABAQUS. The Cam-Clay model shows how the inelastic behaviour of soil is

defined by non-variation of three stresses by a yield function. These are assumed to define the plastic strain rate and strain hardening in which the yield surface changes base on the volumetric strain [18]. The yield surface is described in equation 2-9 [18]

$$\frac{1}{\beta^2}\left(\frac{p}{a}-1\right)^2+\left(\frac{t}{Ma}\right)^2-1=0 \qquad (2\text{-}9)$$

Where p, the equivalent pressure stress; t, the deviatoric stress measure; and M, the constant defining slope of critical state line; β, the constant equal to 1 on dry the side of critical state line ($t > M, p$) and varies on the wet side of the critical state line. a, the yield surface size and as shown in Figure 2-3, k is the ratio of flow stress in triaxial tension to flow in triaxial compression.

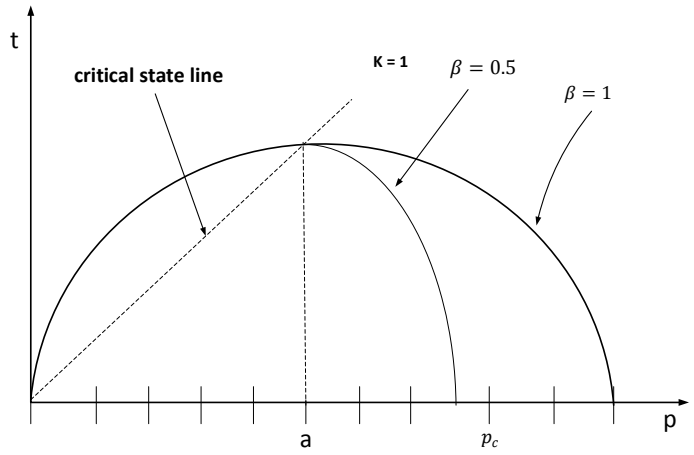

Figure 2-3 p—t plane showing clay yield surface (adapted from Dassault Systemes [18]).

2.2.2.1 Hardening Law

The hardening law is of two forms: exponential or piecewise.

THE EXPONENTIAL FORM has its application in the ABAQUS standard with respect to the porous elasticity media. The yield surface size a_0 can be determined from the initial hardening parameters value [18].

$$\boldsymbol{a = a_0 exp\left[(1 + e_0)\frac{1-J^{pl}}{\lambda-\kappa J^{pl}}\right]} \quad (2\text{-}10)$$

Where J^{pl}, the inelastic volume change (and J represent the ratio of the present volume to initial volume due to elastic deformation); $\kappa(\theta,\ f_i)$, gives the logarithmic bulk modulus for the porous Eleatic material; $\lambda(\theta,\ f_i)$, logarithmic constant for clay plasticity behaviour; e_o, initial void ratio defined by user. The yield surface size a_o is specified together with $\lambda, M, \beta, \kappa$ in ABAQUS [18].

PIECEWISE LINEAR FORM of Cam-Clay soil model is applicable for a normally consolidated and lightly overconsolidated clay soil. Capped Drucker Prager model is based on a linear surface corresponding to the Mohr-Coulomb failure criterion. This uses a partial ellipse taken the form of the Cam-Clay ellipse.

For a Cam-Clay model, the soil voids are assumed to be filled with water, soil plasticity occurs due to change in volume and water dissipation from the voids. Three parameters described in the critical state theory are mean effective stress p', deviator stress q, and void ratio e. The soil mean effective stress is calculated with respect to the principal effective stresses, σ_1', σ_2', and σ_3' given as,

$$\boldsymbol{P' = \frac{\sigma_1' + \sigma_2' + \sigma_3'}{3}} \quad (2\text{-}11)$$

The shear stress (deviator stress) q is derived from

$$\boldsymbol{q = \frac{1}{\sqrt{2}}\sqrt{(\sigma_1' - \sigma_2')^2 + (\sigma_2' - \sigma_3')^2 + (\sigma_1' - \sigma_3')^2}} \quad (2\text{-}12)$$

2.2.3 Drucker-Prager/Cap Plasticity Model

The modified Drucker-Prager/Cap plasticity model as constituted in ABAQUS tool is designed for material that the yielding parameter is pressure dependent. Two sections in the yield surface are the shear failure surface which mainly gives the shear flow and the cap for axis intersection due to pressure stress. A transformation usually occurs between these two sections giving a smooth surface. The cap section performs two functions: the yield surface bounded in

hydrostatic compression showing inelastic behaviour indicating compaction and control the volume dilation of a material, which yield due to shear. The cap sections use associated flow with the shear and transition sections using non-associated flow. The model responds well to larger stresses with reverse in the cap section while it is effective in the failure section mainly due to monotonic loading. It can be used with an elastic material model which indicate linear elastic behaviour or with the porous elastic material model when a creep is not represented [18].

Details regarding the constitutive soil model is not a major focus of this study. Refer to the above references for details.

2.3 Electro-Osmotic Concept

The concept in electro-osmosis involves the movement of liquid tangentially to a charged surface, discovered by F.F Reuss in 1808 with the theory first developed by H. Helmholtz and over the years, soil improvement using the electro-osmosis concept has generated interest in geotechnical engineering [19]. Laboratory equipment was build and tests conducted to determine the electro-osmotic effect on clay soil [20–28]. Casagrande [29,30] took the lead in the study to investigate the stability of slope using the electro-osmotic concept with successful field application being accounted [31–35]. Most studies in this regard as given by Yuan and Hicks [36] are based on laboratory studies.

An analytical solution for determining excess pore water in a one-dimensional uniform electrical field was first presented by Esrig [37]. A two-dimensional analytical approach for determination of excess pore water pressure due to an electrical field was developed by Su and Wang [38]. Further studies considering both numerical and analytical method for determining the soil consolidation by electro-osmosis were then carried out and presented [27,36,47–50,39–46]. Most field test as stated by Yuan and Hicks [36] is hardly being reported due to the simple geometry and material behaviours that are employed. Rittirong and Shang [10] however, carried out an analysis of the finite difference method based on a report represented by Bjerrum et al. [32].

A three-dimensional (3-D) model was analyzed by Micic et al. [51] considering the material behaviours and boundary conditions. Hu and Wu [52] also presented a two-dimensional (2-D) and 3-D numerical analyses of the field test conducted by Bjerrum et al. [32]. Yuan et al. [48] also conducted a numerical study base on the field test reported by Bjerrum et al. [32] in 2-D considering large strain and constitutive elastoplastic behaviour of the soil. Yuan and Hicks [36] presented numerical analyses of a multi-dimensional model base on field data given by Burnotte et al. [33]. The complex geometry with multiple electrodes and intermittent current were determined. Other conditions such as the material nonlinearity and the soil elastoplastic behaviour were considered.

2.3.1 Consideration for Electro-Osmotic Consolidation

To determine the electro-osmotic consolidation of the soil, the following procedures are generally followed as described by Jones and Glendinning [53]:

- Ascertain acceptability of the soil for electro-osmotic treatment.
- Ascertain the electro-osmotic permeability.
- Ascertain the soil resistivity.
- Choose the electrodes configuration.
- Ascertain layout of electrodes.
- Assess the current demand.

The electro-osmotic consolidation process to increase the strength of soil is conducted by applying an electrical voltage to electrodes. Due to voltage flow, the soil pore water pressure tends to move from the anode to the cathode as shown in Figure 2-4 [8,54]**.** The electric potential applied to soil will lead to the generation of negative pore pressure where the drainage condition is being determined by the anode and cathode of the electrode. The pore water pressure being generated will lead to an increase in the effective stress of the soil with the total stress experiencing no changes and subsequently, lead to consolidation due to soil compartment [53].

The induced water flow due to ion migration can also lead to movement of another contaminant in the soil, which depends on factors such as the soil and pore water

conductivity [55]. As given by Shang and Lo [26], factors influencing the EK process are categorized as internal and external. Internal factors include the soil grain size, salinity, pH, and hydraulic permeability while the eternal factors are: current density, types of electrode and configuration in which appropriate design should be considered.

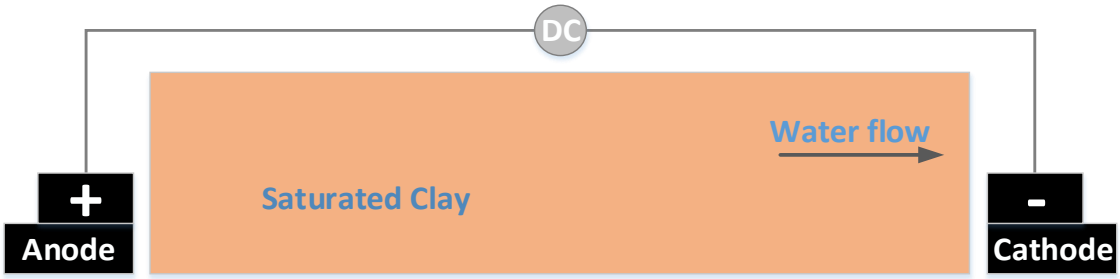

Figure 2-4 Electro-kinetic phenomena: electro-osmosis (adapted from Mitchell and Soga [8])

The EK process has found its application on both saturated and unsaturated soil. Electro-osmosis offers great benefits such that, the time taken for soil consolidation is highly reduced and surcharge loading avoided [56]. A normally consolidated soft clay have shown to be over-consolidated when treated and the over-consolidated ratio can be achieved in the range of about 1.2 and 1.7 while the soil shear strength can witness an increase of about 100% to 200% [57]. As stated by Lo et al. [57], the undrained soil shear strength increases further after the EK treatment, mainly due to the soil hardening as a result of ionic diffusion and is permanent. A considerable increase in the soil shear strength around the anodes [11] has been observed.

A more recent approach by Eton [58] of which the soil modification was applied to pipelines on soft clay soil indicates a considerable improvement in the soil strength.

2.3.2 Mathematical Model

Yuan and Hicks [36] give a model in which the soil skeleton is described using a Lagrangian coordinate and the porous liquid particle using the Eulerian coordinate with respect to the soil skeleton configuration. They consider a

reference configuration X, having a position x at time t. A mapping function φ which link the initial and current position vector. An updated configuration of the body with a typical time step as shown below [36]:

$$\boldsymbol{x} = \boldsymbol{\varphi}(\boldsymbol{X}, \boldsymbol{t}) \tag{2-13}$$

At a point x, the spatial velocity v is given by:

$$\boldsymbol{v} = \boldsymbol{v}(\boldsymbol{x}, \boldsymbol{t}) = \frac{\partial \boldsymbol{x}}{\partial \boldsymbol{t}} \tag{2-14}$$

Consider a moving particle phase π, with reference to arbitrary scalar function $f(x,t)$, this is defined by:

$$\frac{\boldsymbol{D^{\pi} f^{\pi}}}{\boldsymbol{Dt}} = \frac{\boldsymbol{\partial f^{\pi}}}{\boldsymbol{\partial t}} + \boldsymbol{\nabla f^{\pi}}.\boldsymbol{v^{\pi}} \tag{2-15}$$

The fluid velocity of πth phase relative to the solid (s) configuration velocity is given as:

$$\boldsymbol{v^{\pi s}} = \boldsymbol{v^{\pi}} - \boldsymbol{v^{s}} \tag{2-16}$$

From the above velocities, the derivative of material time f^{π} with reference to the solid phase is given by:

$$\frac{\boldsymbol{D^{s} f^{\pi}}}{\boldsymbol{Dt}} = \frac{\boldsymbol{D^{\pi} f^{\pi}}}{\boldsymbol{Dt}} + \boldsymbol{\nabla f^{\pi}}.\boldsymbol{v^{s\pi}} \tag{2-17}$$

Given an updated Lagrangian configuration, the equilibrium equation is given by

$$\boldsymbol{\nabla}.\boldsymbol{\sigma} + \boldsymbol{b} = \boldsymbol{0} \tag{2-18}$$

Where $\boldsymbol{\sigma}$ gives the total Cauchy stress vector and $\boldsymbol{b}$ force vector of the body. The total Cauchy stress relate with effective Cauchy effective stress $\boldsymbol{\sigma'}$ with respect to the pore water pressure p given as:

$$\boldsymbol{\sigma} = \boldsymbol{\sigma'} + \boldsymbol{pI} \tag{2-19}$$

Where $\boldsymbol{I}$ gives the identity vector. Rotation effect of a rigid body in the large-strain analysis is taking into account in a stress strain relationship. This can be obtained in the Joumann stress rate given below [36].

$$\boldsymbol{d\sigma'^{J} = d\sigma' - d\Omega.\, d\sigma' - \sigma'.\, d\Omega^{T} = D_{ep} d\varepsilon} \quad (2\text{-}20)$$

Where the spin tensor is given as Ω, the stress-strain matrix as D_{ep} and the strain vector given as ε.

2.3.3 Constitutive Equations

The mass conservation of water is given by the equation [36]:

$$\boldsymbol{\nabla.(v^{s} + \overline{v}) = 0} \quad (2\text{-}21)$$

Where the soil particle velocity is given as v^{s} and the water filtration velocity relative to the soil skeleton is $\overline{v}$. The fluid flow due to electrical and hydraulic gradient can be coupled to give a total flow [37,41,42]:

$$\boldsymbol{\overline{v} = -\frac{k_w}{\gamma_w}(\nabla p + \gamma_w z) - k_{eo}\nabla\phi} \quad (2\text{-}22)$$

Where the hydraulic conductivity, soil unit weight and the elevation are given by k_w, γ_w and z respectively, the electro-osmotic permeability is k_{eo} and electric potential is given as ϕ .

Assuming a charge conservation with steady state current, the electrical field governing equation is as shown below [36]:

$$\boldsymbol{-\nabla.j = C_p \frac{\partial\phi}{\partial t}} \quad (2\text{-}23)$$

Where the electrical current flux is given as j, the electrical capacitance per unit volume as C_p. Assuming C_p is negligible and based on Ohms law, the electrical flow can be represented as:

$$\boldsymbol{j = -k_{\sigma e}\nabla\phi} \quad (2\text{-}24)$$

Where the electrical conductivity is $k_{\sigma e}$.

For a constant hydraulic pressure, the excess pore water pressure p_e is obtained from equation [37,41,42]:

$$\boldsymbol{\nabla^2 p_e + \frac{k_{eo}}{k_w}\gamma_w\nabla^2\phi = -\frac{1}{C_v}\frac{\partial p_e}{\partial t}} \quad (2\text{-}25)$$

Where, $\boldsymbol{c_v = \frac{k_w}{m_v \gamma_w}}$ (2-26)

where c_v is the coefficient of consolidation.

2.3.4 Pore Water Pressure

Water contained in the soil void is referred to as the pore water while the pressure of the water in the void is referred to as the pore pressure. Effective stress σ' the principle is based on the difference between the total stress σ and the pore water pressure p for a saturated soil as given below [59],

$$\boldsymbol{\sigma' = \sigma - p} \quad (2\text{-}27)$$

The increase in the soil effective stress $\boldsymbol{\sigma'}$ due to the reduction in pore water pressure p is given by:

$$\boldsymbol{\Delta\, \sigma' = -\Delta u} \quad (2\text{-}28)$$

The soil compressibility and strength depend on the effective stress within the soil particles. The difference $\sigma - p$ controls the volume change ΔV that occur within the soil [59]. Total pressure consist of various component within the soil and is considered to be the same at every points under equilibrium conditions [59]. The flow of pore water can occur within the soil if a difference is created at certain points.

Total pore pressure consists of many components amongst which are the hydrostatic pressure and the osmotic pressure [59]. The hydrostatic pressure occurs due to incomplete saturation and externally applied load. The osmotic pressure usually occurs due to the difference in ionic concentration within the soil as previously described by Mitchell and Soga [8] in Figure 2-4, pore water flows from higher concentration to lower concentration. The osmotic effect has been one of the main cause of negative pore water pressure and could take place in both saturated and partially saturated soil [59].

2.3.5 Finite-Element (FE) formulations

Finite Element (FE) formulation of the governing equation represented in matrix form as given by Yuan and Hicks [36] with further details given by Yuan et al. [48]; Yuan and Hicks [50].

$$\begin{bmatrix} \boldsymbol{K_{nl}} & \boldsymbol{L} & \boldsymbol{0} \\ \boldsymbol{L^T} & \boldsymbol{0} & \boldsymbol{0} \\ \boldsymbol{0} & \boldsymbol{0} & \boldsymbol{K_{\sigma e}} \end{bmatrix} \begin{bmatrix} \dot{\boldsymbol{u}} \\ \dot{\boldsymbol{p}} \\ \dot{\boldsymbol{\phi}} \end{bmatrix} + \begin{bmatrix} \boldsymbol{0} & \boldsymbol{0} & \boldsymbol{0} \\ \boldsymbol{0} & \boldsymbol{K_c} & \boldsymbol{K_{\sigma o}} \\ \boldsymbol{0} & \boldsymbol{0} & \boldsymbol{0} \end{bmatrix} \begin{bmatrix} \boldsymbol{u} \\ \boldsymbol{p} \\ \boldsymbol{\phi} \end{bmatrix} = \begin{bmatrix} \dot{\boldsymbol{F}}^{\boldsymbol{ext}} \\ \boldsymbol{Q_p^{ext}} \\ \dot{\boldsymbol{Q}}_{\boldsymbol{V}}^{\boldsymbol{ext}} \end{bmatrix} \quad (2\text{-}29)$$

Where from the matrix, the displacement of the soil is given as u, the pore water pressure p, the Global coupling matrix function L, and the hydraulic flow matric K_c, the electro-osmosis flow metric $K_{\sigma o}$, the electrical conductivity matric $K_{\sigma e}$, the elastic stiffness matrix for small deformation K_e, the geometric stiffness matric determined from effective stress K_g, and $K_{nl} = K_e + K_g$, the external load vector from body load $\dot{F}^{ext}$, the external fluid supply vector Q_p^{ext}, and the external current supply vector $\dot{Q}_V^{ext}$.

2.3.6 Electro-Osmotic Consolidation

Electro-osmotic leads to water being removed and discharged at the cathodes, leading to the soil settlement. The soil consolidation and water flow rate are given as [10]:

$$\boldsymbol{q} = \int_v \boldsymbol{\nabla dV} = \int_v \boldsymbol{m_v} \frac{\boldsymbol{\partial_u}}{\boldsymbol{\partial_t}} \boldsymbol{dV} \quad (2\text{-}30)$$

Where V is the volume of soil and m_v the soil coefficient of volume change.

The value m_v reduces with increase in the effective stress σ' value and estimated from:

$$\boldsymbol{m_v} = \frac{\boldsymbol{1}}{\boldsymbol{1+e}} \frac{\boldsymbol{de}}{\boldsymbol{d\sigma'}} = \boldsymbol{0.434} \frac{\boldsymbol{C_c}}{\boldsymbol{(1+e)\sigma'}} \leq \boldsymbol{m_{v0}} \quad (2\text{-}31)$$

Where m_{v0}, is the initial soil coefficient of volume change and C_c, the compression index.

For a saturated soil, the total amount of water discharged at the cathode Q over time gives the volume decrease of the soil given as:

$$\boldsymbol{Q = \iint_{0\ v}^{t} m_v\,(x, y, \sigma'(t))\,\frac{\partial u}{\partial t}\,dV dt} \tag{2-32}$$

The soil settlement S_t on consolidation is derived from:

$$\boldsymbol{S_t = \frac{Q}{A}} \tag{2-33}$$

Where A is the area of treatment.

As stated by Eton [58] the excess pore water from the soil will drain into the water body for cathodes that are embedded in water.

2.3.7 Energy Consumption

The intensity of power being applied will also affect the corrosion rate of the electrodes. The cost of electrodes and power consumption will, therefore, play an important role in this case. Two major problems encountered with the EK process are the corrosion of the anode and high conductivity of marine clay which requires a high power supply, these challenges, however, can be addressed in part by applying an intermittent current [57]. Details on this electro-osmotic process are covered by Lo et al [57]; Yuan and Hicks [36].

Distribution of voltage between electrodes as observed by Lo et al. [60] is approximately linear with no significant drop, however, the conductivity of the soil experiences considerable decrease leading to drop in current flow at the soil-electrode-water interface [60]. Most studies assumed constant electrical and mechanical properties during the electro-osmotic consolidation process. Reports are also made by Micic et al. [9,61]; Wan and Mitchell [42] on the possibility of increasing the current density by using the polarity reversal method. However, this aspect was not considered in this study.

Equations defining the electrical properties in the EK treatment are giving by Lo et al [57] as outlined below.

The power consumption rate:

$$\boldsymbol{P = j \times \beta \times \Delta\emptyset/\Delta L} \quad (2\text{-}34)$$

Where the current density,

$$\boldsymbol{j = \frac{I}{A}\ (A/m^2)} \quad (2\text{-}35)$$

And

$$\boldsymbol{\beta = \frac{power\ ON\ time}{power\ ON+OFF\ time}} \quad (2\text{-}36)$$

(i.e. for the intermittent power supply) and $\frac{\Delta\emptyset}{\Delta L}\ (V/m)$ is the voltage gradient.

2.3.8 Electrochemical Consideration

Segall [62] described that the electro-osmosis and the electrolyte (clay-water) exhibit some electrochemical behaviour. The electrochemical process involves current flowing through the electrolytes within areas having a difference in electrical potential. The free electrons from the anodic reaction are being transported by the current to the cathodes and consequently the OH^- ions transported back to the anodes due to reactions with the electrons. In this process, OH^- ions combined with Fe^{2+} which lead to rust at the anodes to occur. Assuming iron electrodes is used, the process of oxidation takes place at the anode and reduction at the cathode described by the following equations [8,63,64]:

$$\text{Oxidation (anodic)reaction:} \quad Fe \rightarrow Fe^{2+} + 2e^- \quad (2\text{-}37)$$

And

$$\text{Reduction (cathodic)reaction:} \quad O_2 + +2H_2O + 4e^- \rightarrow 4OH^- \quad (2\text{-}38)$$

2.3.9 Flow Equations and Similarities

Provided the rate of flow is linearly related to the gradient and all properties and boundary conditions are well defined, the flow from one of the equations can be used to solve related problems [8]. Laws relating to heat, electrical, chemical and hydraulic flows are given in Table 2-1.

Table 2-1 Similarities of flows conduction in porous media (adapted from Mitchell and Soga [8])

	Fluid	**Heat**	**Electrical**	**Chemical**
Potential	Total heat h (m)	Temperature θ (℃)	Voltage ϕ (volts)	Concentration c or Chemical Potential μ (mol/m^3)
Storage	Fluid volume V (m^3/m^3)	Thermal energy u (J/m^3)	Charge Q (Coulomb)	Total mass per unit total volume, m (mol/m^3)
Conductivity	Hydraulic conductivity k_h (m/s)	Thermal conductivity k_t $W/m/$℃	Electrical conductivity σ (Siemens/m)	Diffusion coefficient D (m^2/s)
Flow	q_h (m^3/s)	q_t (J/s)	Current I (amp)	j_D (mol/s)
Gradient	$i_h = -\frac{\partial h}{\partial x}$ (m/m)	$i_t = -\frac{\partial \theta}{\partial x}$ $(℃/m^3)$	$i_e = \frac{\partial \phi}{\partial x}$ (V/m)	$i_h = \frac{\partial h}{\partial x}$ (mol/m^4)
Conduction	Darcy's law $q_h = -k_h \frac{\partial h}{\partial x} A$	Fourier's law $q_t = -k_t \frac{\partial \theta}{\partial x} A$	Ohm's law $I = -\sigma_e \frac{\partial \phi}{\partial x} A = V/R$	Fick's law $J_D = -D \frac{\partial c}{\partial x} A$
Continuity	$\frac{\partial V}{\partial t} + \nabla\left(\frac{q_h}{A}\right) = 0$	$\frac{\partial u}{\partial t} + \nabla\left(\frac{q_\theta}{A}\right) = 0$	$\frac{\partial Q}{\partial t} + \nabla\left(\frac{I}{A}\right) = 0$	$\frac{\partial (m)}{\partial t} + \nabla J_D = 0$
Steady state	$\nabla^2 q_h = 0$	$\nabla^2 q_t = 0$	$\nabla^2 I = 0$	$\nabla^2 J_D = 0$

2.4 Dynamic Process

2.4.1 Pipe-Soil Interaction

Deepwater exploration of oil and gas have made pipelines to become an important part of offshore subsea structures. The depth of pipeline embedment is an important part of design aimed at controlling it from the adverse effect of axial walking and lateral buckling. Due to increase in operating temperature, pipeline tends to release axial stress in the form of buckling. Control buckling has been one of the effective ways of controlling lateral buckling due to axial compression of the pipeline, this involves working with the pipeline [65]. Many studies and design were introduced to address this challenge. This ranges from understanding the behaviour of the pipeline response to force and displacement, loading cycles, and point of failure [65].

Designs have been introduced requiring the pipeline to displace laterally from its initial position to certain distance. Formation of the lateral buckle can be advantageous to mitigating pipeline walking as the axial force decreases and feed into the buckle. The build-up of compressive axial force in the pipeline depends on the soil strength and the operating conditions. The greater the compressive force, the greater the susceptibility of the pipeline to buckling. With regards to buckling and axial walking, it has been observed by Cormie et al. [65], the lower the axial friction of the soil, the susceptibility of pipeline walking increase, however, as the axial friction increase, its susceptibility to walking decrease while the lateral buckling increase. The design solution must incorporate a balance between these two conditions for a desirable response. As given by Cormie et al. [65], axial displacement of an operating pipeline occurs between 2m to 10m and between 100m to 300m for lateral displacement. Three conditions that control buckle initiation are [65]: an effective compressive force which depends on the axial resistance, the “out-of-straightness features, and lateral peak force. While these conditions may be conflicting with regard to identifying the resistance to be adopted, design for pipe-soil interaction resistance should be carefully considered in all the design stages [65].

2.4.2 Pipe Embedment

Pipe embedment is defined as the penetration depth of pipeline invert (bottom) relative to the seabed in an undisturbed condition. Embedment influences the contact area of pipelines with seabed [66]. Formulation of the pipe-soil interaction follows the same method as for the pipeline embedment and axial frictional force. Pipeline embedment that describes the initial state of the pipe after installation is significant at defining the axial resistance. Different parameters influence pipeline embedment which also include factors such as installation effect, conditions of soil and effective weight [66,67]. Observations made from as-laid pipes in offshore West Africa, the basic embedment in soft clay is of between one third and one diameter [67]. These boundaries are being utilized to fix the limit for calculations. Frictional resistance can be evaluated from embedment being predicted, one regular feature is the existence of peak and residual properties in the “load-deflection relationship”.

A finite element approach at determining the vertical penetration of a pipeline has been conducted by Merifield [68] with a pipeline placed at a predetermined depth known as wished in pipe (WIP) [69] and with a pipeline allowed to penetrate based on its own weight or operational load known as pushed in pipe (PIP) described in Figure 2-5. It was discovered that higher penetration force is required to displace the soil for the PIP than the WIP due to heave formation around the pipe surface as given by Merifield et al. [70]. A pipeline laid on an undrained clay soil will be sustained by the soil pore water pressure. A gradual dissipation of the pore pressure over time will account for the effective stress, and in this case, the soil skeleton will be involved. Further embedment (settlement) of the pipeline with pore water dissipation lead to local consolidation at the pipe invert surface. This takes place over a period and governs the drained or undrained behaviour of a pipeline. A better understanding of the pore pressure behaviour and the effective stress is vital in accounting for the pipeline initial embedment.

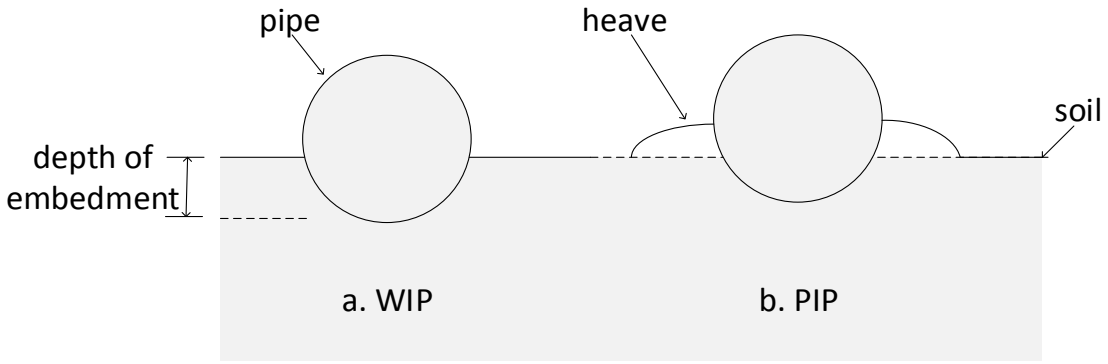

Figure 2-5 a. Wished in Pipe, (WIP) b. Push in Pipe, (PIP)

Total stress undrained analysis using the Mohr-Coulomb model with the pore water pressure dissipation and void ratio dependency are not represented. This limitation can be captured using the effective stress analysis with a Cam-Clay (critical state) model. The pore fluid analysis can be determined in terms of total or excess pore water pressure. The total pore pressure analysis considered the gravity loading to define the load on the soil while the excess pore pressure considered both the gravity and distributed body load. The soil weight forms an important part of the Cam-Clay model, unlike the Mohr-Coulomb. Total pore pressure approach was adopted as the consolidation was determined by electro-osmosis.

The relationship defining the undrained vertical displacement of the pipeline with the load as given by Muthukrishnan et al. [71] is represented by the parameters shown below.

$$\boldsymbol{V = f(E, S_u, D, z, v, \gamma', C_i)} \tag{2-39}$$

Where V is the vertical load per unit length; E, is the Young's modulus; $\boldsymbol{S_u}$, the soil undrained shear strength; D, pipe diameter; z, depth of embedment; v, soil Poisson ratio; and γ' soil effective unit weight; $\boldsymbol{C_i}$, adhesion of pipe-soil. The embedment of the pipe into the soil can be determine using the non-dimensional function.

$$\frac{\boldsymbol{V}}{\boldsymbol{DS_u}} = \boldsymbol{\phi}\left(\frac{\boldsymbol{E}}{\boldsymbol{S_u}}, \frac{\boldsymbol{z}}{\boldsymbol{D}}, \boldsymbol{v}, \frac{\boldsymbol{C_i}}{\boldsymbol{S_u}}, \frac{\boldsymbol{\gamma' D}}{\boldsymbol{S_u}}\right) \tag{2-40}$$

The vertical reaction law accounting for both the laying and dynamic installation effect for determining embedment of a pipeline is shown in the equation below [72–74]:

$$\frac{V}{DS_u} = \boldsymbol{a}\left(\frac{z}{D}\right)^{\boldsymbol{b}} + \boldsymbol{f_b}\frac{A_c}{D^2}\frac{\gamma' D}{S_u} \tag{2-41}$$

This can also be express with regard to a bearing capacity factor:

$$\frac{V}{DS_u} = \boldsymbol{N_c} + \boldsymbol{N_b}\frac{\gamma' z}{S_u} \tag{2-42}$$

$$\text{Where, } \boldsymbol{N_c} = \boldsymbol{a}\left(\frac{z}{D}\right)^{\boldsymbol{b}}, \quad \boldsymbol{N_b} = \boldsymbol{f_b}\frac{A_c}{Dz} \tag{2-43}$$

Where A_c the nominal submerged area of pipe cross section below mudline, N_c is the bearing capacity factor for the design, a and b are given as 6 and 0.25 respectively, based on power law coefficient, N_b is the buoyancy factor, N_c is a factor given as 1.5 due to heave formation and f_b is a factor that enhance the buoyancy effect. Due to uncertainty related to other effect such as installation, the accuracy can be estimated within the range ±10% [72]. Pipe embedment shows a non-linear elastic response, the coupling of axial resistance with pipe embedment will give a more realistic result and pipe embedment to a large extent depend on the area of contact [67,75].

According to Ballard et al. [3], the interaction of the pipe-soil in deepwater is usually in an undrained or partially undrained condition due to the existence of excess pore pressure. This depends on the consolidation coefficient, length of drainage path, level of stress subjected to the soil and the displacement rate in the axial direction. Deepwater soft clay soil is characterized by undrained shear strength of approximately zero at the mudline, with the strength gradient extending from 5-15kPa/m. The bearing pressure ranges between 1-10kPa Ballard et al. [3]. Determination of the drained and undrained conditions of soil are given in the equations below [76].

Fully drain condition, $\frac{vD}{C_v} < \mathbf{1}$ (2-44)

Fully undrain condition, $\frac{vD}{C_v} > \mathbf{20}$ (2-45)

Where v, pile velocity; D, diameter and C_v, soil coefficient of consolidation.

2.4.3 Pipe Axial Response

As the hot operating fluid passes through a subsea pipeline, it expands toward the pipeline free end "(least resistance direction)". The slippage of the expanding pipeline with the soil set up compressive force due to frictional resistance. The cold end will tend to build up compressive force to set up equilibrium. If the slippage zone does not reach the far end, there will be no displacement and if otherwise, it will undergo axial displacement. The slippage zone reaches it far end for a short pipeline when the thermal point is in the middle of the pipeline [1,2,77,78].

Length of the pipeline is an influencing factor when assessing walking. However, axial resistance has influence that is more considerable. Walking occurs more on a short pipeline that is fully mobilized, however, if the thermal gradient is adequately steep, then walking can persist through a section of full constraint [2]. The level of axially constrained force build-up during start-up and shutdown of the pipeline is a very important factor for consideration in assessing pipeline walking. This ranges from a state where the cyclic constrained is mobilized fully with no axial movement to fully mobilize with axial movement along the whole length of the pipeline [78].

The two stages considered in the design for axial pipe-soil response are the peak (breakout resistance) and residual resistance Figure 2-6. Initial axial movement of the pipeline or when pipeline moves after resting for some time is usually associated with peak resistance. The mobilization resistance occurs at the peak resistance [2,3]. As noted by Ballard et al. [3]; Carneiro and Castelo [79], the pipe-soil response is nonlinear and the high initial stiffness tangent being produced increasingly reduces till the peak resistance is attained. Residual resistance

accompanied with large displacement follows the breakout point of peak resistance. The residual resistance initially decreases rapidly and then slow down to a certain value.

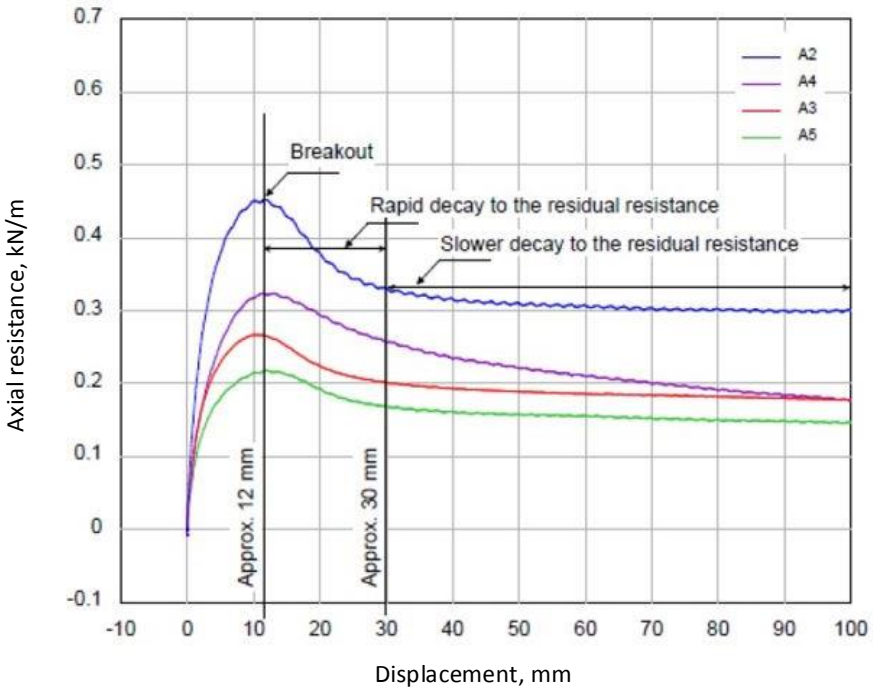

Figure 2-6 axial pipe-soil behaviours (adapted from Ballard et al. [3])

Peak friction is very significant at reducing the rate of walking leading to decrease in the anchor's load. The undrained axial resistance can be determined using the Alpha approach for both the peak and residual resistance [67,73,75]:

$$\boldsymbol{F = A_c S_u\, \alpha'} \tag{2-46}$$

$$\boldsymbol{{F_{ap}}^{u} = A_c S_{up}\, \alpha'} \tag{2-47}$$

$$\boldsymbol{{F_{ar}}^{u} = A_c S_{ur}\, \alpha} \tag{2-48}$$

S_u, the soil shear strength and α', the adhesion factor, ${F_{ap}}^{u}$ and S_{up} represent undrained peak axial resistance and shear strength, respectively. Similarly, ${F_{ar}}^{u}$ and S_{ur} represent undrained residual axial resistance and shear strength, respectively. A_c, is the the pieline area of contact with the soil given by the relationship:

$$A_c = D\cos^{-1}\left(1 - \frac{2z}{D}\right) \text{ for } 0 < z \leq \frac{2z}{D} \quad (2\text{-}49)$$

And

$$A_c = \frac{\pi D}{2} \text{ for } z > \frac{2z}{D} \quad (2\text{-}50)$$

Where z gives the initial embedded depth.

The axial resistance of a pipeline subjected to cyclic loading is centred on the decline in the peak resistance, typical thixotropic plot [67] show that peak axial resistance is effective for a period of few months. The operational loading cycles for the pipeline is normally designed to operate for few month and shut-down for few hour or days and soil thixotropic with regard to walking verified.

2.4.3.1 Mechanism Leading to Pipeline Walking

Factors leading to pipeline walking are [2,80,81]:

- Tension-induced by steel catenary risers on the pipeline.
- The slope of seabed along the length of the pipeline.
- Thermal transient along the pipeline due to variation in fluid temperature and thermal loading during start-up and shutdown cycles.
- In addition, Bruton and Carr [66] stated that multiphase flow behaviour during start-up and shut-down play a significant role in pipeline walking. Pipeline walking response rapidly to this mechanism. The difference in content density can increase the susceptibility of axial displacement down the slope.

2.4.3.2 Mitigations and limitations

Studies have shown that walking of a pipeline system can be reduced or eliminated by increasing the axial pipe-soil resistance. Jumpers/spool may only have the capacity to handle an expansion of around 1.2m, due to a limitation in the handling and installation capabilities [7]. Expansion of pipeline exceeding this limit will affect their integrity. As stated by Rong et al. [7] axial friction factor of 1.5

is needed to stop pipeline walking. This high axial resistance is difficult to achieve in the deepwater pipeline, which prompts the need for employing mitigating measures.

2.4.3.2.1 Concrete Weight Coating

Concrete weight coating can increase axial resistance, which may result in the reduction of axial displacement of pipelines. It can ensure controlled buckled occurs thereby reducing the axial feed-in to the buckle. However, the high axial resistance been set up can increase the possibilities of the uncontrolled lateral buckle. This can result in failure of field joint due to high-stress concentration factor (SCF). Moreover, the Installation of concrete coated pipe in deepwater is increasingly becoming less practicable due to a high level of top tension been set up [7].

2.4.3.2.2 Rock Dumping/Concrete Mattress

This method significantly reduces the end expansion and cycles of walking. It also helps toward a controlled buckle, which can lead to a decrease in the corresponding axial feed-in to buckle. However, a larger quantity of this material is needed and it proves to be very costly and taking too much of offshore time to complete, especially the concrete mattress. Special vessels are expected for this operation and its possibilities in ultra-deepwater should be well examined [7]. Figure 2-7 is an example of concretes mattress laid on the seabed.

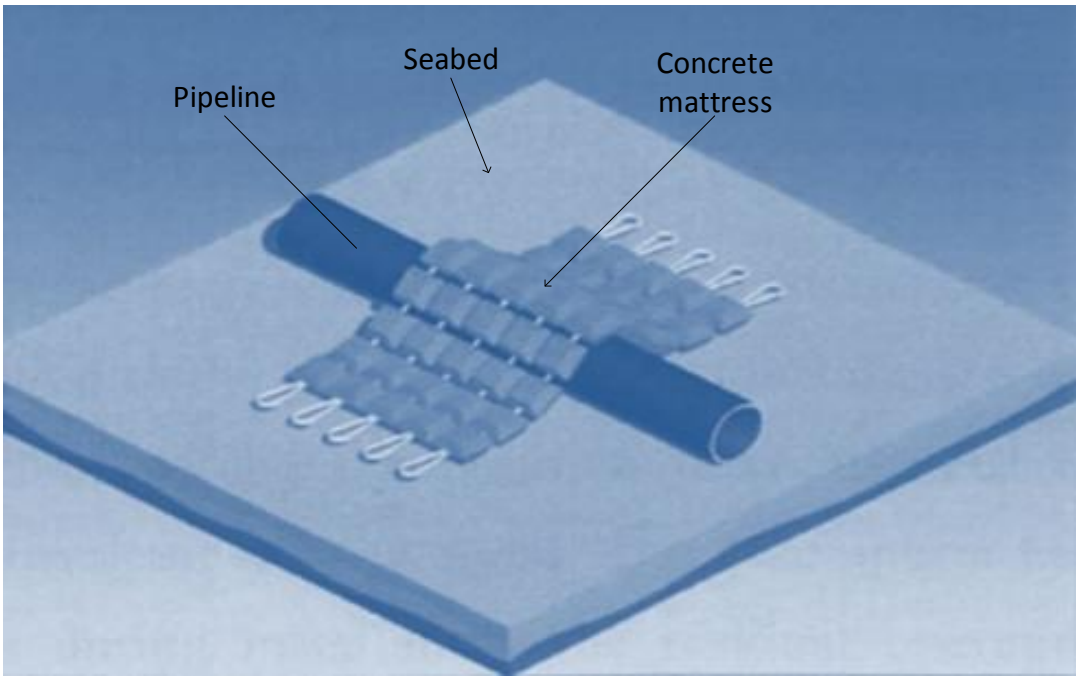

Figure 2-7 Concrete mattress

2.4.3.2.3 Controlled Buckles

The controlled buckle can be initiated to reduce the level of axial displacement of the pipeline. Snake–lay method has been employed for this purpose. However, in deepwater, this method is difficult to achieve due to uncertainties in determining the lateral soil resistance of the pipeline. The length of pipeline is also considered in this case; as the short pipeline is not sufficient to secure the initiation of the lateral buckle. Another method is to lay the pipeline over sleeper which also comes with its challenges as posed by the above methods [7].

2.4.3.2.4 Sleepers or Buckle Initiator

Various part of the pipeline can expand and feed into a particular area, which may lead to large localized lateral displacement and high curvature. Buckle initiator or sleeper as shown in Figure 2-8 is normally use at the point of lower lateral resistance and pipeline placed on it [82]. This method allows the pipeline to displace laterally in this direction thereby, relieving axial stress. The sleeper provides less resistance to a surface with the pipeline length raised above the seabed surface. Further measures are being adopted by including buoyancy at the intended area where buckle will occur. The buoyancy reduces the touchdown

point lateral resistance with buckle formation having a larger wavelength [82]. The additional coating is to ensure pipeline has positive submerged weight to avoid undesirable spans when emptying [82].

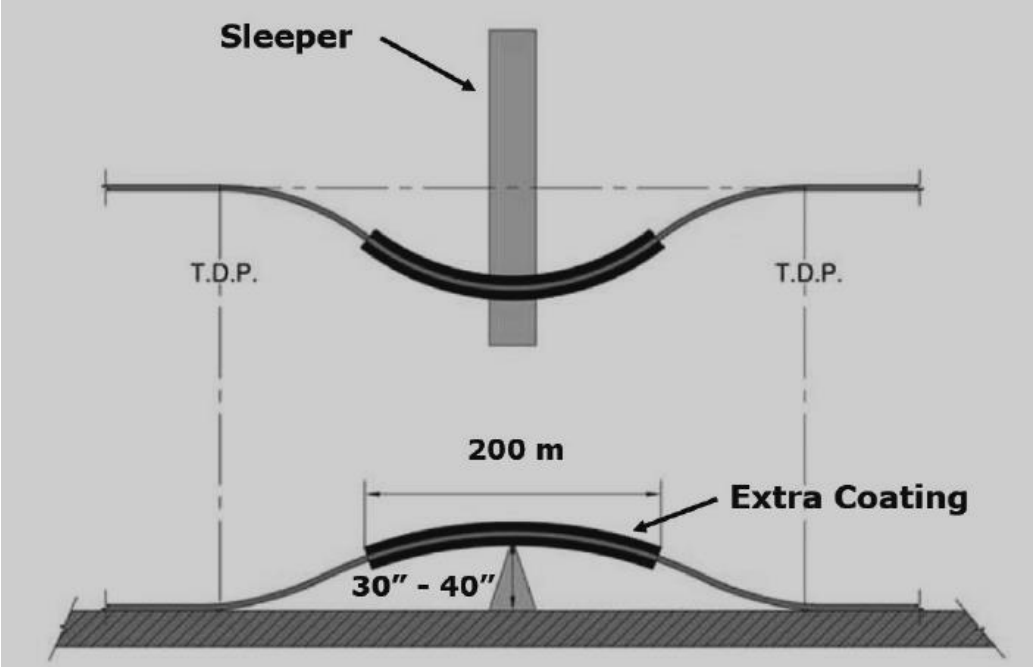

Figure 2-8 Sleepers (adapted from Perinet and Simon [82])

2.4.3.2.5 Anchoring

Anchors mainly suction pipes have been successfully installed in deepwater pipeline providing resistance to axial movement to mitigate end expansion. Anchors normally forces the virtual anchor point to share the same location on the pipe, it causes a mismatch of soil resistance to build up from the two ends. Anchors can be placed at any position of the pipeline, however, the best position to place the anchor is in the middle of the two virtual anchor point [7,77,83]. A typical example of pipe anchoring is described in Figure 2-9.

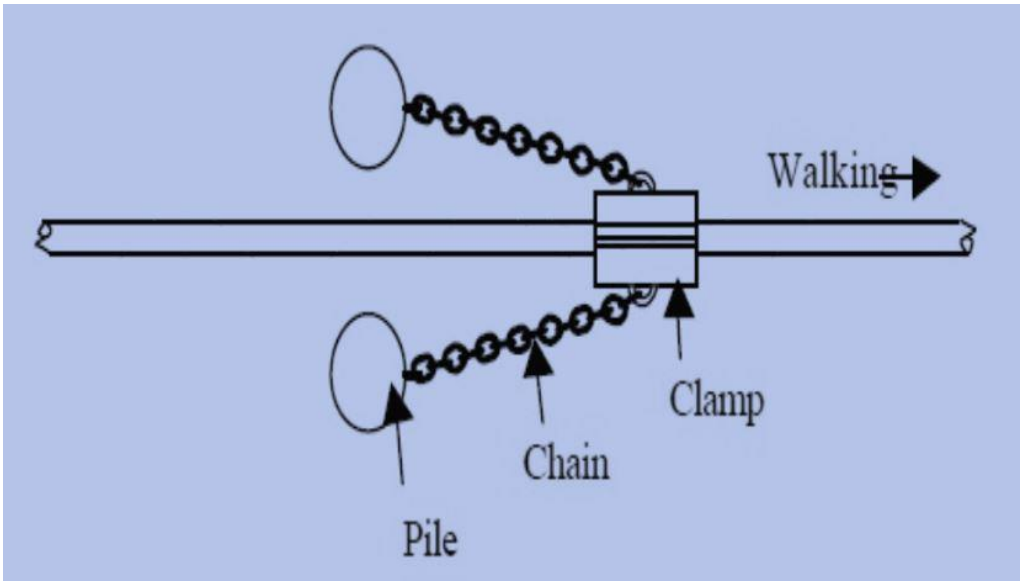

Figure 2-9 Pipe anchoring

However, installing anchors in soft soil posed greater challenges, which prompted the increase in the weight and size of the anchor being installed. This method is very expensive and requires the substantial vessel to install. Anchors can result in higher tension leading to route curve instability. This sets up a requirement for installing route curve with a greater radius of curvature more than necessary. This can compromise the field architecture [78,84].

2.4.3.2.6 SliPipe

SliPipe, as described in Figure 2-10, is developed by Norway's Det Norske Veritas (DNV), a new concept to mitigate the expansion of rigid pipeline ends due to high pressure/high temperature (HP/HT). This technology aims to reduce the effect of wall forces imposed at the tie-in by absorbing the end expansion through sliding within itself at the same time reducing the axial compressive force acting on the pipeline [85].

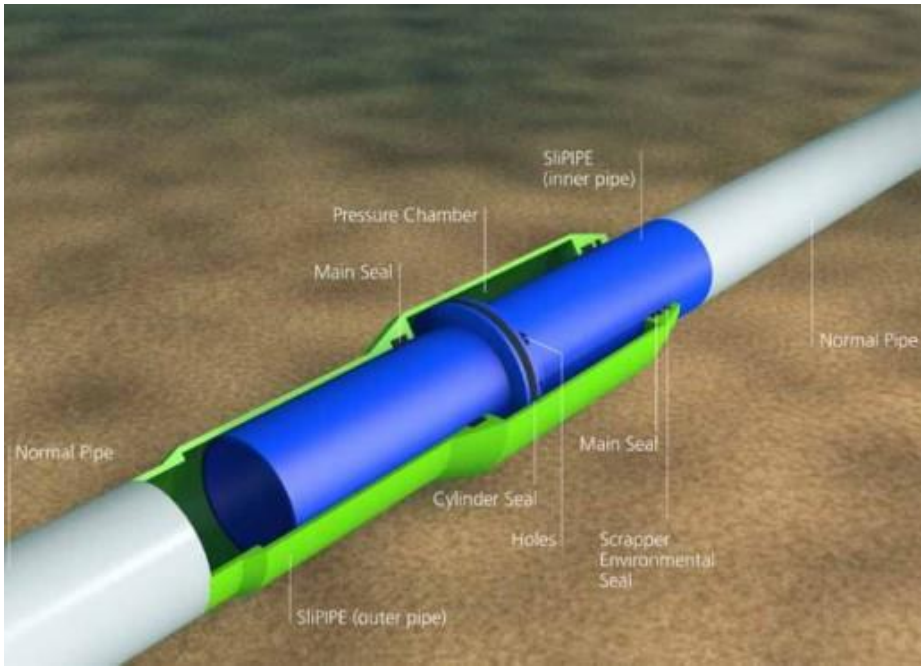

Figure 2-10 SliPIPE concept (adapted from Yew [85])

2.4.3.3 Effect of Axial Pipe-Soil Interaction Resistance

Effects of axial pipe-soil interaction are [65]:

- Pipeline maximum axial effective force.
- Pipeline effective force available for desirable buckle initiation.
- End expansion of pipe and lateral buckles feed-in.
- Pipeline walking.

2.4.3.4 Effective Axial Force

Understanding of the pipeline expansion mechanisms will require knowledge of the effective axial force, which is governed by the "(true) axial force on the wall of pipeline and the axial force due to fluids pressure. This is represented by the equation [3,78]:

$$\boldsymbol{F_e = F_w + p_e\ A_e - p_i\ .A_i} \tag{2-51}$$

Where, F_e is the effective axial force, F_w the axial force on pipe wall, p_e the external pressure, and p_i the internal pressure, A_e & A_i are the external and internal area of pipe respectively.

A state at which the axial strain is zero, the effective axial force F_e of a pipeline that is closed ended and fully constrained can be obtain by summing the axial increment in length, the internal and external pressure (considering the end effect) and the gradient of the temperature, $\Delta\theta$ [3].

$$\boldsymbol{F_e = \frac{\Delta L}{L_0} EA + (1 - 2v)(p_e A_e - p_i A_i) - EA\alpha\Delta\theta} \quad (2\text{-}52)$$

ΔL, is the length increment, L_0 is the original length, A the cross sectional area of steel pipe, p_e the external pressure, p_i the internal pressure, and E the Young's modulus of elasticity. A_e, and A_i are the external and internal surface area, respectively, υ is the Poisson ratio and α is the coefficient of thermal expansion respectively.

2.4.4 Pipe Lateral Response

2.4.4.1 Effect of lateral pipe-soil interaction resistance

Effect of lateral pipe-soil interaction as given by Cormie et al. [65] are:

- Lateral instability needed to initiate buckle.
- Instability of the route curve due to axial tension.
- Bending load of the lateral buckle at large displacements.
- Lateral buckle resulting from soil berm formation due to cyclic loading.

The main stages to consider in lateral buckling design are the break out force, the suction release the residual force, and the cyclic lateral frictional force [65]. A considerable peak force is observed when a pipe is about to move and depends on the embedment level during the process. The breakout force occurs with a suction effect inform of a crack between the wall of the pipe and soil, with little effect on its further behaviour. Under very slow loading and before a fully mobilized peak force is observed, the crack is formed. The initial breakout force usually takes place very fast, with tension to certain degree developed at the pipe rear, leading to soil failure experienced at both ends of the pipe.

During movement of the pipe, the peak force falls, leading to a residual lateral force, which raises and maintained at a steady state over a large displacement.

Residual force controls the displacement during first loading and determines the initial buckle shape and peak bending stress of the pipe [65]. Figure 2-11 shows an image of the lateral buckle of pipeline laying on the seabed.

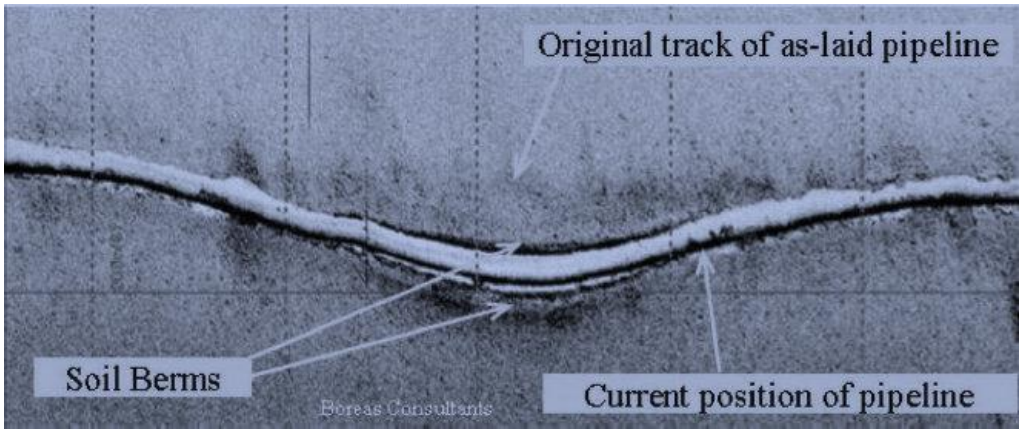

Figure 2-11 Side-scan sonar image of a lateral buckle (adapted from Bruton and Carr [66])

For cyclic lateral movement of the pipe, berms are formed on each side of the pipe. The berms contribute some resistance to pipe displacement and the buckle formation [65]. Many studies and design were introduced to address this challenge, this ranges from understanding the behaviour of the pipeline response to force and displacement, loading cycles, and point of failure [65]. Further details were discussed [2,86–89].

2.5 Experimental Pipe-Soil Interaction Test

Several models were tested to investigate the axial resistance of pipeline with regard to pipe-soil interactions, these include laboratory test, onshore model test, in-situ test, and numerical test [90]. The models investigated, indicates considerable improvement in the shear strength of soil due to loading/unloading with pore water dissipation, leading to an increase in the resistance to axial pipeline displacement. Axial resistance is a considerable factor in the design against pipeline displacement. Smith and White [5], had performed a large-scale test model of axial pipe on soft clay at the Norwegian Geotechnical Institute (NGI) Laboratory Oslo. The test was to determine axial resistance due to volumetric hardening based on hypothesis proposed by White and Cathie [91]. The report by Smith and White [5] indicates that the pipeline embedment increases from

initial 0.3D to 0.6D. Initial peak resistance is brittle and subsequently ductile. Residual resistance is about twice the initial value. The residual friction factor increases from 0.45 to 0.85 for the 13 sweep. Residual resistance increases to about 80%. Zone of hardening extended by approximately 40mm under the pipe at $D/3$. Soil strength increases by 35% and the water content indicate da ecrease of about 18%. This experiment established that volumetric hardening occurs due to cyclic loading because of pore water dissipation, leading to increase in axial resistance of the pipe-soil interaction.

The smart pipe in-situ model test by Ballard et al [3] have pipe length of 1200mm with outside diameter of 225mm. Pipeline coating is of polypropylene, the rate of displacement ranges from between 0.005mm/s – 1.15mm/s and according to Bruton et al [2], this represents the common ranges being encountered in the field. Soft clay soil undrained shear strength ranges from 0 to 5∽15kPa at depth of 1m. Bearing pressure ranges from 0 – 10kPa. The axial pipe-soil response is found to be mostly “undrained or partially undrained” with excess pore pressure generated. Pipe embedment depth ranges from 35% to 65% diameter (D) achieved with consolidation period of 4 hours to dissipate excess pore pressure. Peak resistance occurs at the axial displacement of 12mm (5%D). Residual resistance initially occurs rapidly at over 300mm (13%D) and subsequently followed by 100mm (45%D) when stabilizing. The test also indicates 55% to 80% residual resistance of the peak resistance. Unloading stiffness indicates a value 5 times greater than the “peak secant stiffness” in the loading test. Reloading cycle shows less pronunciation of peak resistance due to the time elapsed for the reloading to take place. The regaining of peak resistance could be attributed to the longer time taking for another cycle to initiate. Mobilization distance during reloading is similar to that of the initial peak. The SMARTPIPE test shows friction factor increasing from 0.25 to 0.55 for 14 loading/unloading cycles i.e. the friction factor increases by 0.02 per cycle. The result indicates walking rate decreases with increase friction factor. Axial peak and residual response of a pipe-soil are expected to reduce the pipeline-walking rate, which may be a very significant consideration in design.

Physical modeling at the University of Western Australia was conducted by Boylan and White [92] to determine the axial sliding resistance of pipe-soil interaction of a model pipe using a geotechnical beam centrifuge modeling. The model pipe has a length of 140mm with a diameter of 20mm made of aluminum. To achieve rough surface, the pipe was attached with a uniform fine-grained sand particle with the size, $d_o = 160\mu$m. The soil used was carbonated soil (Silt with mud) sample obtained from the North West Shelf of offshore Australia. Four axial test were conducted with displacement rates of 0.002mm/s, 0.02mm/s, 0.2mm/s and 2mm/s. Time elapsed between each cycles is 1000s. Initial embedment at 1.7kPa (at prototype scale pipe weight of 3.4kN/m) for the first to the fourth test are 0.22, 0.22, 0.24, and 0.22 with a corresponding final embedment z/D of 0.41, 0.39, 0.35 and 0.34 respectively. The amplitude for the cycles ranges from ±10mm to ±5mm. The test indicate a peak value of resistance for the first test of 8kPa (at prototype scale axial resistance of 4kN/m). The residual friction factor ranges form 0.7 – 3 and the longer steady value of 1 - 1.5 in contrast to the SMARTPIPE value of 0.3 - 0.6 as reported by Ballard et al [3].

Eton [58], conducted a large-scale model test on Kaolin clay to investigate the effect of EK treated soil on the displacement of subsea pipeline. Results of the experiment indicated that the water content before treatment of about 70% decreases by 10% to 3% just below the bottom of the pipe. The axial breakout force shows that the Peak force raises from 63N to 182N due to EK effect, representing a 190% increase.

2.6 Concluding Remarks

Literature being reviewed have underscores the importance of safeguarding a pipeline against adverse effect resulting from its displacement in vertical, axial and lateral directions. Various mitigation measures are currently being employed for the stability of pipeline with their limitations. Factors influencing pipeline stability ranges from its depth of embedment to the soil strength. Increasing soil strength has been shown to be a possible mitigating measure against pipeline displacement. The EK concept has been successfully deployed in strengthening structural foundations of both onshore and offshore environment with little or no

consideration given to pipeline structures. ABAQUS tool has the capability for solving complex geotechnical problems with wide range of constitutive soil models such as the Mohr-Coulomb, Cam-Clay, and the Drudger Prager model. The Critical state plasticity model which is an extension of the Cam-Clay Model have accepted wide usage with regards to its capabilities at capturing the soil effective stress. Other ABAQUS capabilities were the Coupled Temperature-Pore Pressure element to mimic Coupled Electrical-Pore Pressure element. A major consideration of the pipeline displacement behaviours is the peak and residual forces. The level of this forces depends on the conditions at which the pipeline is subjected to and is driven mainly by the internal temperature and pressure of the operation fluid. Estimation of the effective force on the pipeline has been a very considerable factor with regard to the soil strength required to resist it displacement. A good assessment of the EK process considering the power consumption, the numbers and types of electrodes, soil types and its suitability for electro-osmotic consolidation plays a major role. The Electro-osmotic consolidation of the soil and the resultant increase in the soil effective soil will have a significant influence on the dynamic behaviour of pipelines.

CHAPTER 3: NUMERICAL METHODOLOGY

3.1 Model Development

The ABAQUS finite element tool contains a large library capable of solving different problems. ABAQUS/CAE is the Complete ABAQUS environment that serves as an interface for model creation and the analyses results. This study uses the ABAQUS 2016 to demonstrate its capabilities in solving EK problems. The process of creating a model using ABAQUS generally follows the steps outlined below:

- Creating the model geometry and part in 2-D or 3-D.
- Material properties are applied to the models.
- Assembling parts of the models.
- The configuration of steps for analysis.
- Load and boundary conditions are applied.
- The created model is meshed.
- Submission of the created jobs for analysis.

Three phases are developed for this study: the first phase is the verification of the different flow process in ABAQUS. This help to confirm the capability of any of the flow process to mimic electrical flow due to their similarities as shown in Table 2-1. The second phase is the verification of the coupled temperature–pore pressure element for the electro-osmotic consolidation of the clay soil. The third phase consists of three series in which both electro-osmosis and dynamic analyses were conducted to confirm the effect of EK treated soil on pipe-soil interaction. The resistance developed due to pipe-soil interaction from EK and non-EK treated soil are then measured and compared.

3.1.1 ABAQUS Unit

The ABAQUS tool does not have a specific unit, the user decides on the unit to use in the analyses. However, consistency must be adhered to on the unit being adopted. For example, a unit of length is the metre, force is the Kilo-Newton, and time is the seconds. Other units can be derived from these.

3.1.2 Models Assumptions

Assumptions made for the analyses are:

1. The electrodes: anode and cathodes are of the same materials.
2. Electrical potential at the cathodes is zero.
3. There is constant electrical conductivity at the electrodes, soil, and water during the analyses
4. There is zero electrical potential at the soil/water surfaces.
5. A voltage gradient is directly proportional to the fluid velocity
6. Effect of electrochemical reaction is not considered.
7. Uniform pore pressure is assumed in the soil

3.1.3 Model Analyses/Procedure Verification

3.1.3.1 PHASE 1: ABAQUS Heat Transfer, Electrical, and Chemical Flow Verification

The first step in verification of procedure being adopted is the determination of BAQUS heat transfer capability to mimic electrical flow due to similarities are shown in Figure 3-1 and detailed earlier in Table 2-1.

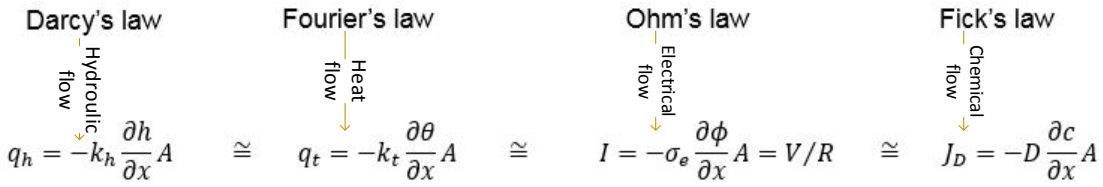

Figure 3-1 Description of flow equations similarities: can be used to mimic each other

A numerical analysis was conducted based on parameters obtained from Hansen and Saouma [63] on steel corrosion and concrete cracking as shown in Table 3-1. The geometry consists of concrete dimension 10.16cm x 6.03cm and electrodes dimension of 6.03cm x 0.16cm as shown in Figure 3-2. Current density, q at the model surface were set at zero. The boundary at the anode was set with a voltage of 0.440V and at the cathode with -0.417V. The concrete serve as the electrolyte while the potential at the anode and cathode represent the mass concentration (for an electrochemical reaction). A two dimensional (2-D) analysis in which, heat transfer, mass diffusion and electrical flow procedure in ABAQUS

were considered for comparison. The heat transfer and mass diffusion flow process was modelled with DC2D4 (a 4-node linear heat transfer quadrilateral) element. The electrical flow process is modelled with DC2D4E (a 4-node linear coupled thermal-electrical quadrilateral) element. Coupled temperature-displacement procedure is modelled with CPE4RT (a 4-node plane strain thermally coupled quadrilateral, bilinear displacement and temperature, reduced integration, hourglass control.

Table 3-1 Flow process verification parameter [63]

Properties	**Values**
Resistivity of concrete	5000 Ohm-cm
Potential at anode	0.440V
Potential at cathode	-0.417V
Analysis time	Steady state

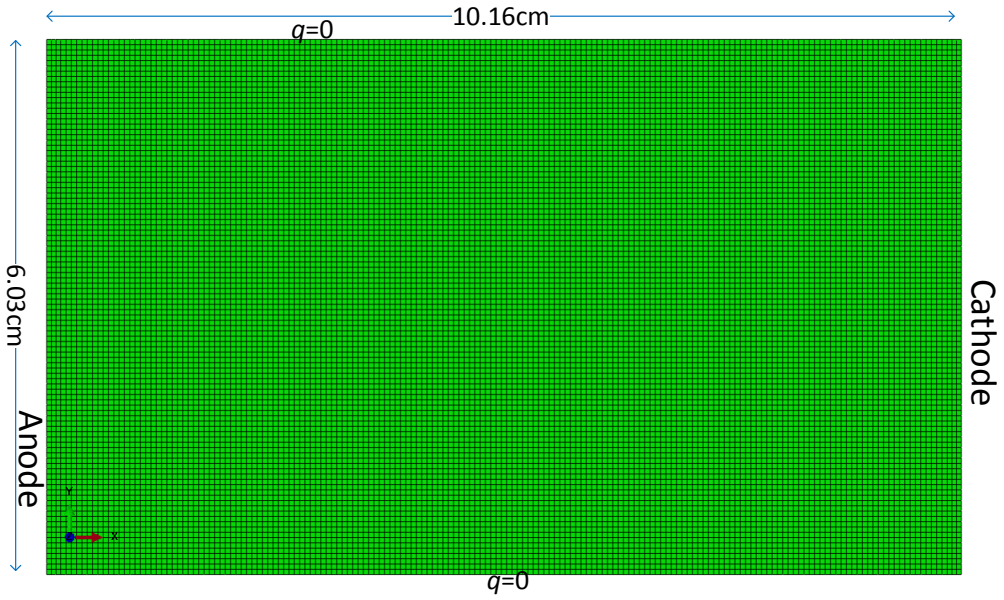

Figure 3-2 ABAQUS heat transfer, electrical and chemical flow verification model

3.1.3.2 PHASE-2: ABAQUS Coupled Temperature-Pore Pressure Elements Verification

To verify the capability of coupled temperature-pore pressure elements for the EK analyses, a numerical study was conducted and compared with a numerical analysis conducted by Yuan and Hicks [36]. The model as shown in Figure 3-3.a and b consists of 12 anodes and 12 cathodes of steel electrodes each 5m long and 0.17m in diameter. The anode and cathodes were arranged in four rows spaced at 3m, each of the rows consist of six anodes or six cathodes separated 2m apart. All electrodes were set at the same levels extending to depth of 14m from the top surface of the soil. The clay soil dimension consists of 49m x 20m x 20m. The water table is set at 3.1m and the pore water pressure above the water table set to zero. The vertical and bottom surface boundaries were assumed to be impermeable with free drainage allowed at the top vertical surface of the cathodes. The cathode each has a voltage of zero and voltage gradient of 0.33V/m between pairs of electrodes (anode and cathode). The boundary condition is applied to prevent any displacement in horizontal directions with the boundary assumed to be impermeable. The bottom surface boundary is fixed and also assumed to be impermeable with free drainage allowed at the cathodes.

Treatment time for the electro-osmosis is 50 days. The tie constraint between the electrode and the soil is set with the electrodes being the master surface and the soil being the slave surface. The FE models for electrodes and soil are modeled with the 10-nodes modified quadrilateral tetrahedron, pore pressure, and temperature, hourglass control, C3D10MPT. A modified Cam-Clay soil model is based on parameters obtained from Burnotte et al. [33]; Yuan and Hicks [36] shown in Figure 3-2. Critical state line, M is 0.567, poison ratio, ν of 0.3, and pre-consolidation pressure is 120kPa, hydraulic conductivity, k_w of $1.5\ x\ 10^{-12} m/s$ and electro-osmotic permeability, k_{eo} of $3.5\ x\ 10^{-9}\ m^2/V.s$. The model assembly is described in Figure 3-4, further details on the arrangement are given by Burnotte et al. [33]; Yuan and Hicks [36].

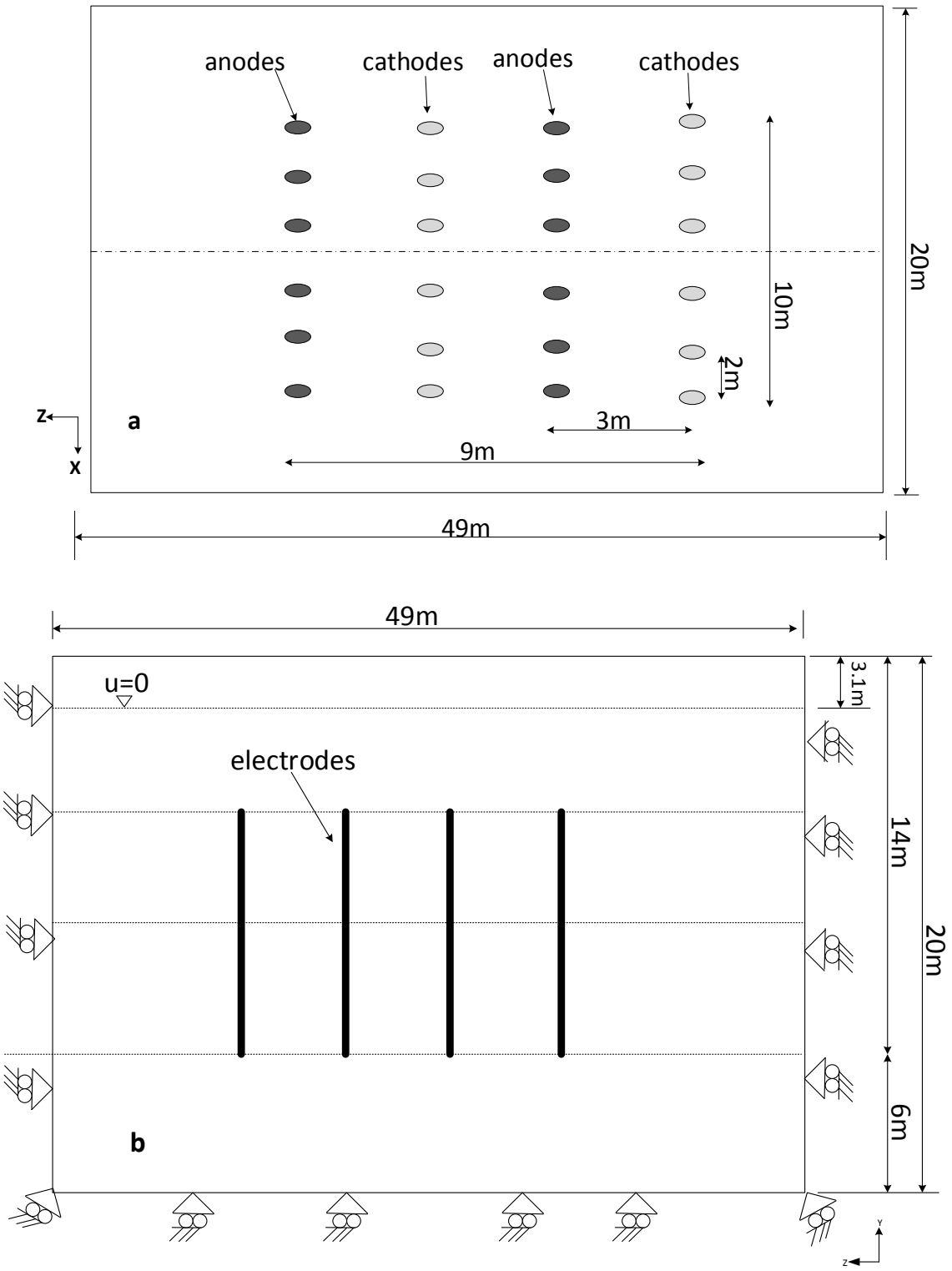

Figure 3-3 Series-2 Electro-osmotic consolidation model geometry description: (a) plan view (b) vertical side view

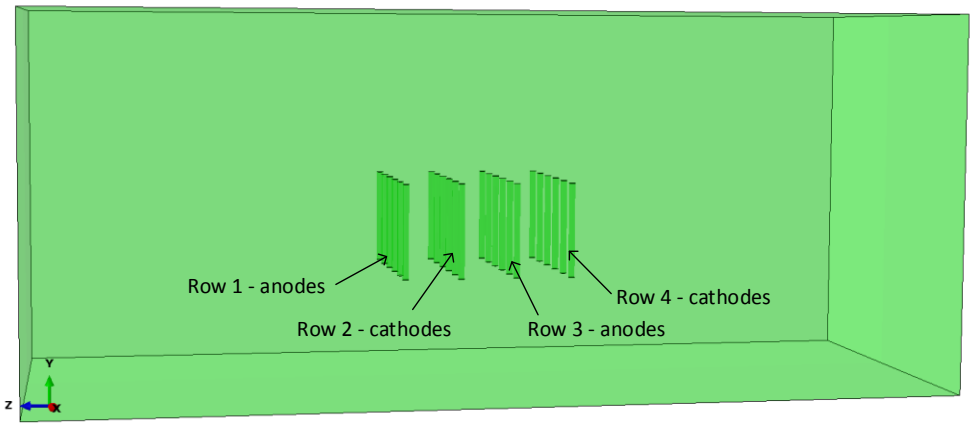

Figure 3-4 Series-2a Model Assembly

Table 3-2 Soft clay soil parameters (adapted from Burnotte et al. [33]; Yuan and Hicks [36])

Properties	**Values**
Hydraulic conductivity, k_h	$1.5\ x\ 10^{-12} m/s$
Electro-osmotic permeability, k_{eo}	$3.5\ x\ 10^{-9}\ m^2/V.s$
Electric conductivity, $k_{\sigma e}$	$1.0\ S/m$
Virgin consolidation line, λ	0.316
Recompression/swelling line κ	0.045
The slope of the critical state line	0.567
Poisson's ratio ν	0.3
The coefficient of earth pressure at rest, K_0	1.0*
Unit weight of soil, γ	$16.4\ kN/m^3$

3.1.3.3 PHASE 3: EK Pipe-Soil Interaction Model

This section explains the procedures followed in the analyses for pipe-soil behaviour with and without EK treatment. Three stages are involved in the simulation: geostatic, electro-osmosis (consolidation), and dynamic analysis. The measurement and comparison of the resistance developed between the EK and non-EK treated soils are determined. To ensure stress equilibrium of the soil, the first step in the analysis is the geostatic step. In this step, ABAQUS assumed a displacement of zero and where a non-zero is obtained, this value is neglected. The second step is the soil consolidation (EK) step in which the procedure "SOIL" in ABAQUS is adopted. The third step is adopted using the dynamic implicit procedure to determine resistance generated due to pipeline displacement before and after the EK treatment of the soil.

Three series were developed each for electro-osmotic consolidation and the dynamic analyses. Each series in this phase generally follows the procedures outlined in Figure 3-5.

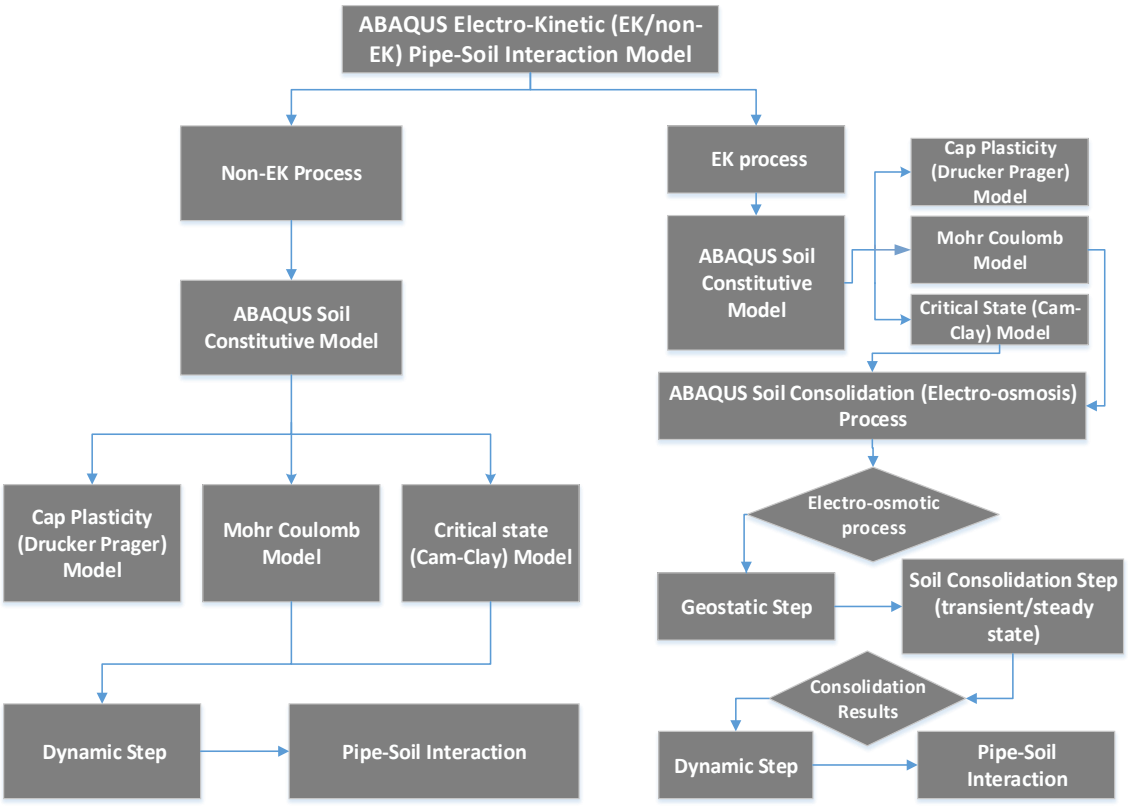

Figure 3-5 Flowchart: ABAQUS EK/non-EK test process

The electro-osmosis series-1a, 2a, and 3a give the analysis of the soil consolidation. To carry out the dynamic analysis, the results from the electro-osmotic consolidation of soil, series-1a, 2a, and 3a were inputted into the dynamic series-1b, 2b, and 3b respectively. The dynamic series gives the resultant effect of the soil consolidation due to pipe embedment, axial, and lateral displacement.

3.1.3.3.1 Electro-Osmotic Consolidation Modelling

ABAQUS software tool has no direct capabilities to support electro-osmotic process, however, based on the relationship with different flow processes as given in phase one and two, the mass diffusion or heat transfer analysis procedures can be used to mimic the electrical flow [63]. The governing law relating the flow process: fluid, electrical, chemical and heat transfer are shown in Table 2-1. Thermal conductivity in the heat transfer procedure in ABAQUS tool is based on the Fourier law shown in Table 2-1. The conductivity k_t can be isotropic, anisotropic orthotropic [18].

Based on relationships with the different flow process, couple temperature-pore pressure and couple temperature-displacement element in ABAQUS software package were adopted as described in the model of series-1, 2, and 3**.** A tie interaction constraints between the soil/water and the electrode is applied to ensure electrical contact. Initial time increment for the electro-osmotic model is determined from Equation 3-1 [93,94].

$$\Delta \boldsymbol{t_{initial}} = \frac{\boldsymbol{h^2 \gamma_w}}{\boldsymbol{6E'k}} \tag{3-1}$$

Where h, the average dimension of element k, soil permeability; and E, soil effective Young's modulus. To account for non-linearity in the geometry the Non-Linear Geometry (NLGEOM) parameter is set on, through all the analyses.

3.1.3.3.1.1 Pipeline Properties

Material properties of the pipelines are shown in Table 3-3. Further details are given for each of the model series in subsequent sections.

Table 3-3 Material properties of pipeline

Properties	Values	
Pipe material	Carbon steel	
Standard/Material Grade	ISO 3183, L450	
Density kg/m^3	7850	
Seawater density	1025 (kg/m^3)	
Pipe Elastic properties	Young's Modulus MPa	210x 10^3
	Poisson ratio	0.3
Pipe Plastic Properties	Yield Strength (MPa)	450
	Tensile Strength (MPa)	535

3.1.3.3.1.2 Soil Properties

The materials to be selected will be based on suitability, known physical and chemical properties and the ability to be compared with a known test that had been conducted. Polwhite E grade kaolin is a common constituent of many actual clay soils with suitable geotechnical and chemical properties is considered based on the experiment by Eton [58] Its main constituents are hydrous aluminium silicate clay mineral kaolinite. Further details on the soil compositions are given for each of the model series in the subsequent sections.

3.1.3.3.1.3 Electrode Materials Consideration

Electrode material selection is based on its availability, suitability for EK treatment and cost. Materials often used includes copper, mild steel and aluminium with consideration to their durability, conductivity, and chemical properties. EK soil treatment is related to the intensity of the electrical field, which depends on the layout of the electrode in consideration. Hence, the appropriate selection of the electrode materials will determine the optimum performance in service. In field applications, the cathode normally acts as the drain, however, due to its application in seawater, the seabed surface will act as the drain. Seawater has higher conductivity than clay and as given by Eton [58] its resistivity can be neglected. The seawater, in this case, is treated as the cathode, which gives a

reason for adopting fewer numbers of cathodes (and in this case two) when compared with numbers of anodes.

This study does not consider different types of electrodes materials as only the iron electrodes are employed. Eton [58] indicates that iron material is more effective for a partially embedded material in the soil. The iron material also has its limitations with regards to its faster rate of corrosion in the aggressive saline environment. Studies by Bergado et al. [95]; Mohamedelhassan and Shang [96]; Xie and Shang [97] shows that the electrode type is significant in the EK process, this depends on the material conductivity and its resilience during the treatment time. Further details on the material properties are given in subsequent sections for each of the model series.

3.1.3.3.1.4 Model Schematic Overview

The WIP method as described in Figure 2-5 is adopted in this study mainly to allow for electrical contact between the soil and anodes. The disadvantage of this method is the absence of initial pore water pressure generated during the pipe penetration as reported by Gourvenec and White [98]; Krost et al. [99] which is encountered in PIP. The pore water pressure generated is due to further embedment from the predefine WIP depth. This relatively will account for a lower penetration force to be observed than when PIP method is adopted. However, this study compares the non-EK and EK process under same conditions with regard to the WIP method to account for the soil settlement and the related strength developed on pipe-soil interactions. Unloading and reloading analysis of the pipe was not considered.

The layout of the electrodes for the electro-osmotic analysis is shown in Figure 3-6. The electrodes equal in length to the pipe are installed together and separated by supporting rings shown in Figure 3-11**.** The anodes are embedded in the soil inclined at an angle of $10°$ in series-1a and 2a, and $20°$ in series 3a. The same applies to the cathodes except they are embedded in the water. The pore water is assumed to flows in the vertical direction and the distance x between the anodes and cathodes create the potential gradient $i_e = \frac{\partial \phi}{\partial x}$ given in

Table 2-1. Zero potential assumed at the soil surface allows the electrical flow to be noted in all direction. However, as derived from Rittirong and Shang [10] the thickness W and width of the soil (soil/water) L is far greater than the distance between the anodes and cathodes x $(i.e\ W, L \gg x)$, the flow can be consider in two dimensions, x-y plane.

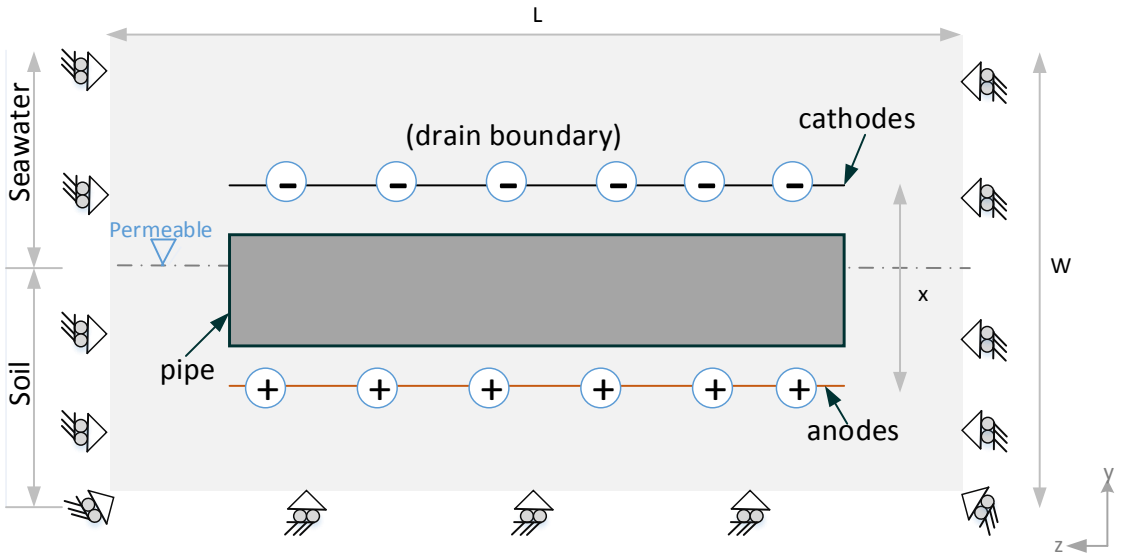

Figure 3-6 Schematic model configuration of the electro-osmotic process

Below is a schematic of the model arrangements for the pipe-soil interaction, conducted regards to the pipe vertical pulling/penetration in Figure 3-7, the pipe axial displacement in Figure 3-8, and the pipe lateral displacement in Figure 3-9. These represent all the tests conducted for both the electro-osmosis and dynamic analyses in Phase-3 of this study, which includes series-1a, 1b; 2a, 2b; and 3a, 3b. These are detailed in the next sections below.

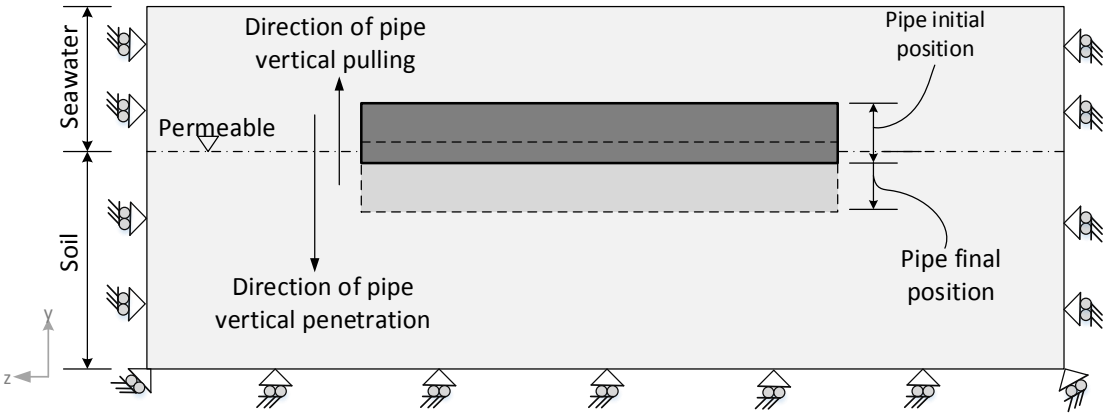

Figure 3-7 Schematic Side view of model position for pipe vertical pulling/penetration test

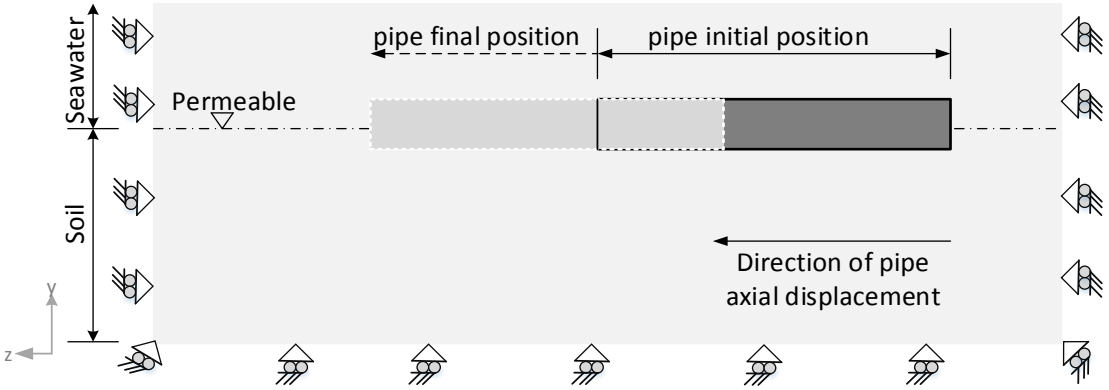

Figure 3-8 Schematic of model position for pipe axial displacement test

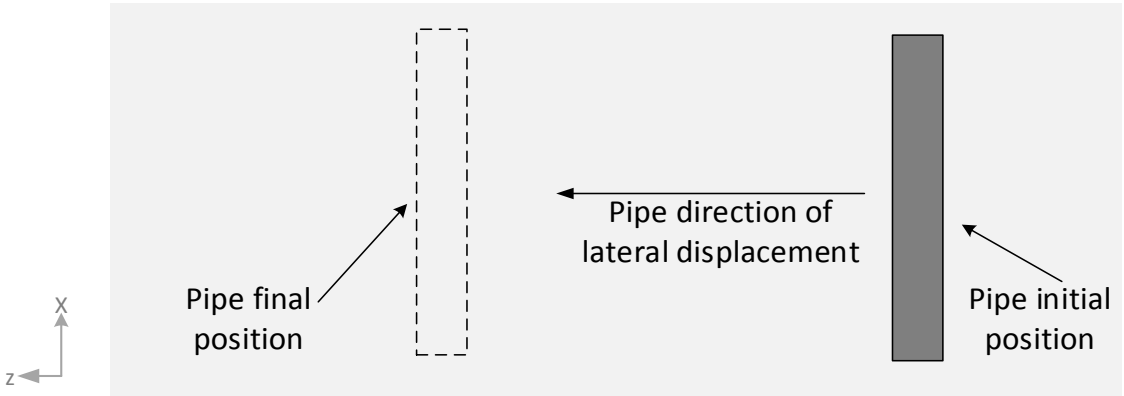

Figure 3-9 Schematic Plan view of model position for pipe lateral displacement test

3.1.3.3.1.5 Boundary Conditions

The electrodes boundary conditions are assigned with temperature $\theta = \theta(x,t)$ to mimic the voltage $\phi = \phi(x,t)$. The pipeline model is assumed to be straight with the end boundary conditions assumed unconstrained. The vertical boundaries beside soil surfaces are set to allow for displacement and permeable in the vertical direction with no displacement in the horizontal surfaces. The bottom surface of the soil is fixed and impermeable. The water level is set at the top surface of the soil and permeable with zero pore water pressure assumed. Other conditions are defined in each of the test series in subsequent sections.

3.1.3.3.1.6 Test Series - 1a

Series - 1a was derived from the small-scale experiment conducted by Eton [58]. The pipe-soil model is described in Table 3-4 and the electro-osmotic properties in Table 3-5. The soil dimension of 0.39m x 0.21m x 0.21m represents soil/water with a water depth of 0.06m and soil depth of 0.15m. Properties of materials for the Cam-Clay soil model used for the electro-osmotic analyses are given by Ansari et al. [93]; Dingle et al. [100]. The Finite Element (FE) models for electrodes, support rings, and soil/water are modeled with 10-nodes modified quadrilateral tetrahedron, pore pressure and temperature, hourglass control, C3D10MPT and the pipe is modeled with 6-node triangular thin shell element STRI65 [18]. These elements with reduced integration and hourglass control have lower computational cost while maintaining accuracy [93]. Two supporting rings, two cathodes, and the six anodes were adopted.

Table 3-4 Pipe/Soil Model: series – 1a, 1b

Parameters		**Values**
Soil	length	0.39m
	wide	0.21m
	depth	0.21m
Pipe	length	0.15m
	diameter	0.0508m
Electrodes	length	0.15m
	diameter	0.003m
Supporting rings	outside diameter	0.07m
	inside diameter	0.0508m
	thickness	0.004m
	holes diameter	0.003m
	angle between holes	10°

Table 3-5 Electro-osmotic/Cam-Clay model parameters: series - 1a, 1b

PARAMETERS		MATERIALS	VALUES	UNITS
Electrical Conductivity $k_{\sigma e}$	[8,64,101]	Soil	1.0	S/m
		Seawater	4.8	S/m
		Iron electrode	1.0×10^{7}	S/m
Hydraulic conductivity k_h		Soil	$1x10^{-9}$	m/s
Electro-osmotic conductivity k_{eo}		Soil	$5.5x10^{-9}$	$m^2/V.s$
Saturation S		Soil	90	%
Void ratio e_o		Soil	1.5	
Virgin consolidation line, λ	[93]	Soil	0.4	
Recompression/swelling line k		Soil	0.115	
Slope of Critical state line M		Soil	1	
The coefficient of earth pressure at rest, k_o		Soil	1	
Wet yield surface size		Soil	1	
Poisson ratio ν		Soil	0.333	
Young Modulus E		Soil	$1.8x10^{6}$	MPa
Dry density γ		Soil	1121	kg/m^3
Electrical potential (ϕ)	Anodes		10	V
	Cathodes		0	
Time (t)	6 – 12hrs			s

The model arrangement of series-1a, 1b, for the vertical penetration analysis as shown in Figure 3-10 and Figure 3-11 is the same as with the axial arrangement. The seabed soil considered uniformly homogenous, considering pipeline impact on the soil is relatively small. Kaolin clay, which gives a relatively good representation of deepwater soft soil, is adopted. The soil assumed to be in a normally consolidated state for a saturated soil with 90% water content and void ratio of 1.5. The mudline strength of 2.3kPa and the unit weigh γ_w given as $6.5kN/m^3$ [71,93,100]. Anodes and cathodes are of the same iron material adopted due to its suitability for a partially buried pipeline [58]. PVC pipe with rough machined surface assumed for the model. The mechanical behaviour of the pipeline is assumed linear elastic. Further details on these properties are given by Eton [58]. The pipe was WIP, embedded at a depth of 0.5D

The electro-osmotic effect on pipe-soil interaction due to pipe axial and vertical pull-out/penetration is conducted, subjecting the soil to treatment time of 6 and 12 hours at 10V. The aim is to compare the results with Eton [58], thus setting the pace for further studies.

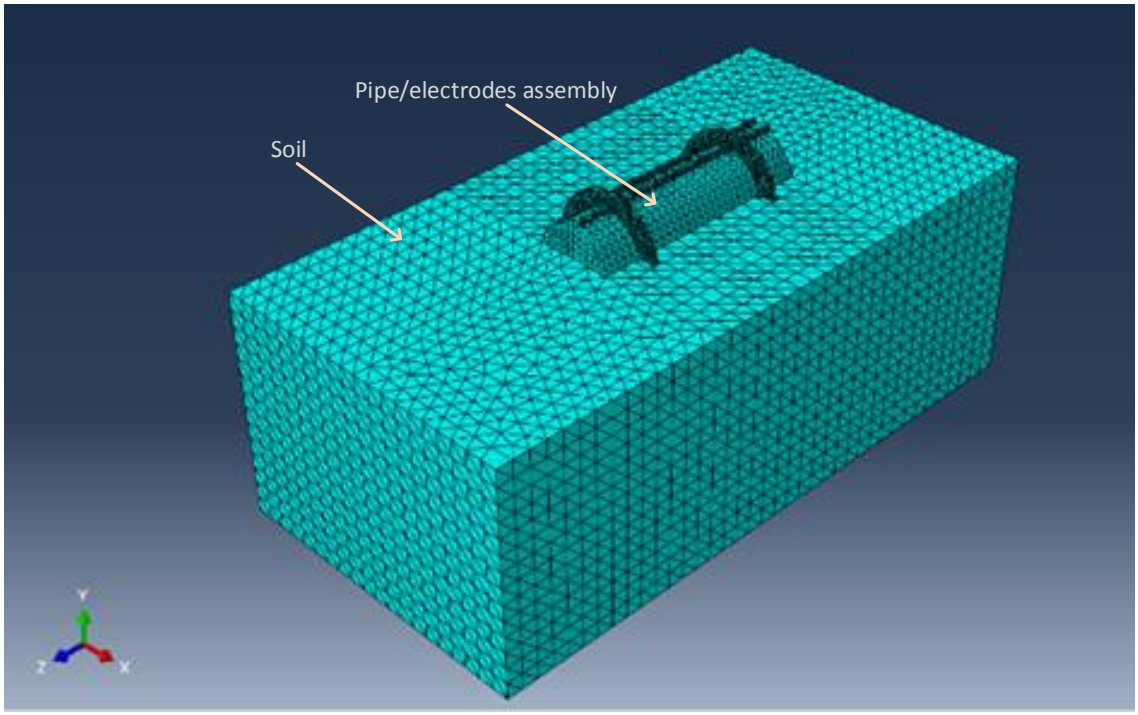

Figure 3-10 Model series 1: Section view – 3D FE vertical penetration pipe-soil interaction model

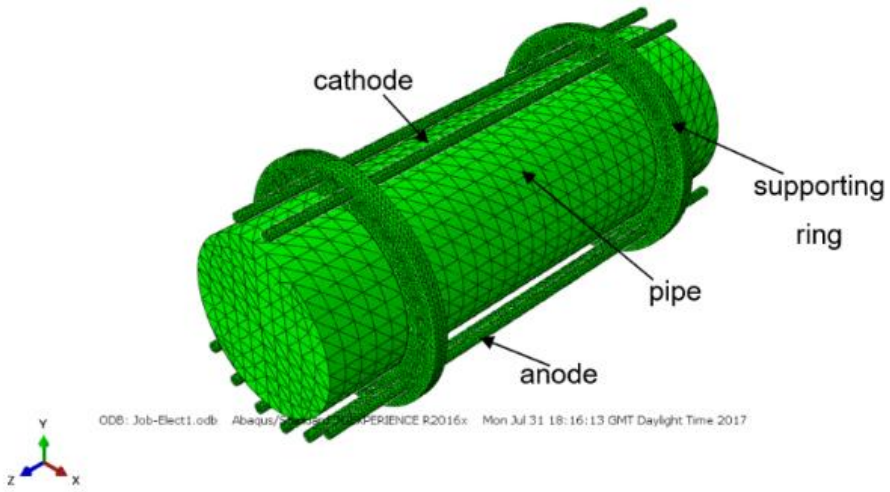

Figure 3-11 Model Series 1: Pipe-electrodes assembly

3.1.3.3.1.7 Test Series - 2a

Series-2a is based on a large-scale experiment conducted by Eton [58]. The pipe-soil model is described in Table 3-6 and the electro-osmotic properties in Table 3-7. The soil dimension of 2m x 0.9m x 0.7m represents soil/water with a water depth of 0.3m and soil depth of 0.4m. The seabed soil is considered uniformly homogenous. Kaolin clay as in series - 1a above is used, the soil assumed to be in a normally consolidated state for a saturated soil with 70% water content and void ratio of 1.5. The Cam-Clay model is given by Ansari et al. [93]; Dingle et al. [100] are used. Anodes and cathodes are of the same iron material. Steel pipe with the mechanical behaviour assumed to be linear elastic. The pipe is WIP at a depth of 0.5D for the vertical, axial and lateral pipe-soil interaction.

Table 3-6 Pipe/Soil Model: series – 2a, 2b

Parameters		**Values**
Soil	length	2m
	wide	0.9m
	depth	0.7m
Pipe	length	0.8m
	diameter	0.13m
Electrodes	length	0.8m
	diameter	0.0076m
Supporting rings	outside diameter	0.17m
	inside diameter	0.13m
	thickness	0.03m
	holes diameter	0.0076m
	angle between holes	10°

Table 3-7 Electro-osmotic/Cam-Clay model parameters: series - 2a, 2b

PARAMETERS		MATERIALS	VALUES	UNITS
Electrical Conductivity $k_{\sigma e}$	[8,64,101]	Soil	1.0	S/m
		Seawater	4.8	S/m
		Iron electrode	1.0×10^{7}	S/m
Hydraulic conductivity k_h		Soil	$1x10^{-9}$	m/s
Electro-osmotic conductivity k_{eo}		Soil	$5.5x10^{-9}$	$m^2/V.s$
Saturation S		Soil	70	%
Void ratio e_o		Soil	1.5	
Virgin consolidation line, λ	[93]	Soil	0.4	
Recompression/swelling line k		Soil	0.115	
Slope of Critical state line M		Soil	1	
The coefficient of earth pressure at rest, k_o		Soil	1	
Wet yield surface size		Soil	1	
Poisson ratio ν		Soil	0.333	
Young Modulus E		Soil	$1.8x10^{6}$	MPa
Dry density γ		Soil	1121	kg/m^3
Electrical potential (ϕ)	Anodes		2.5.25	V
	Cathodes		0	
Time (t)	Steady State and Transient			s

The element types for electrodes, support rings, pipe and soil/water are same with series-1a in section 3.1.3.3.1.6. Two supporting rings, two cathodes, and the six anodes were adopted using the critical state model. Figure 3-12 described the pipe-electrode assembly. The axial pipe-soil model arrangement is shown in Figure 3-13 while the section view is shown in Figure 3-14. The section view of the vertical and lateral pipe-soil interaction model is shown in Figure 3-15 and Figure 3-16 respectively.

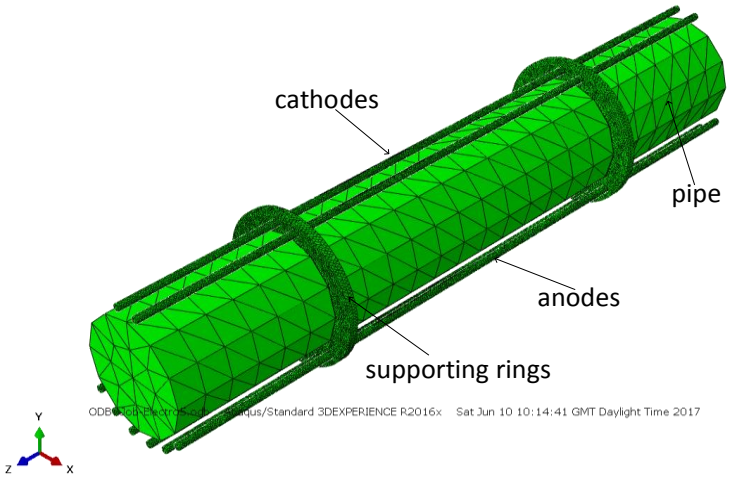

Figure 3-12 Model Series 2: Pipe-electrodes assembly

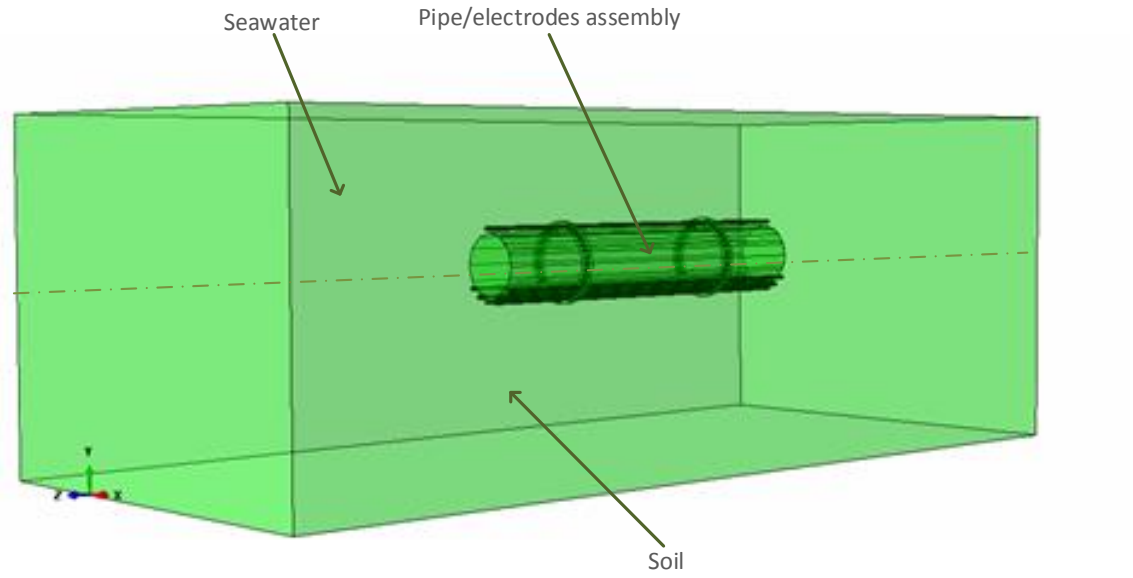

Figure 3-13 Model series 2: 3D FE axial pipe-soil interaction model – pipe/electrodes assembly embedded in soil/seawater

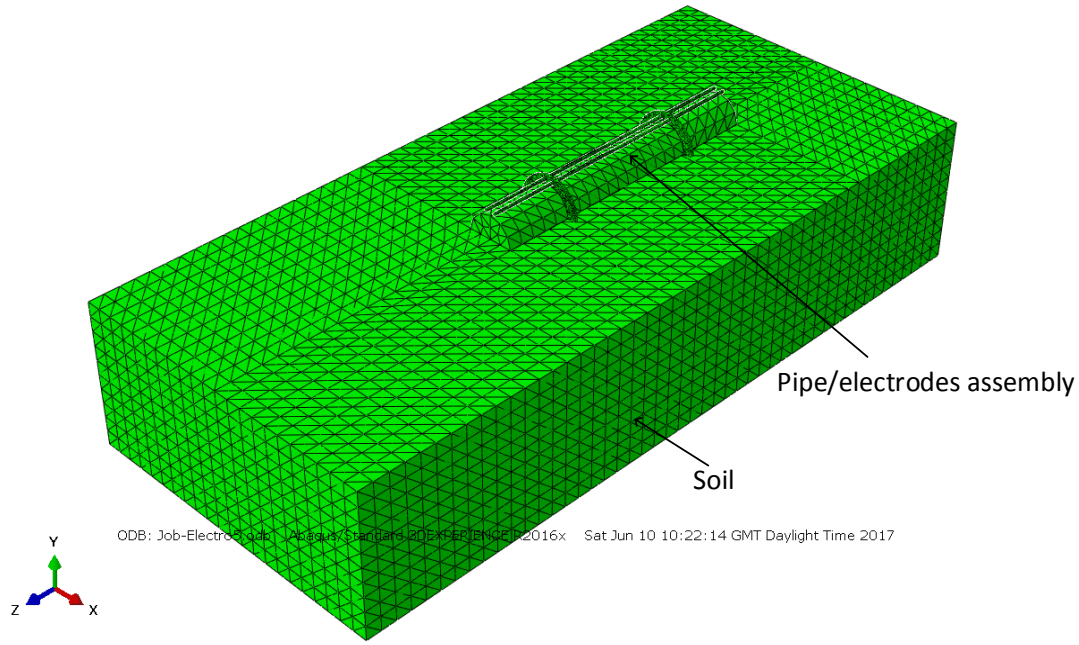

Figure 3-14 Model series 2: Section view – 3D FE axial pipe-soil interaction model

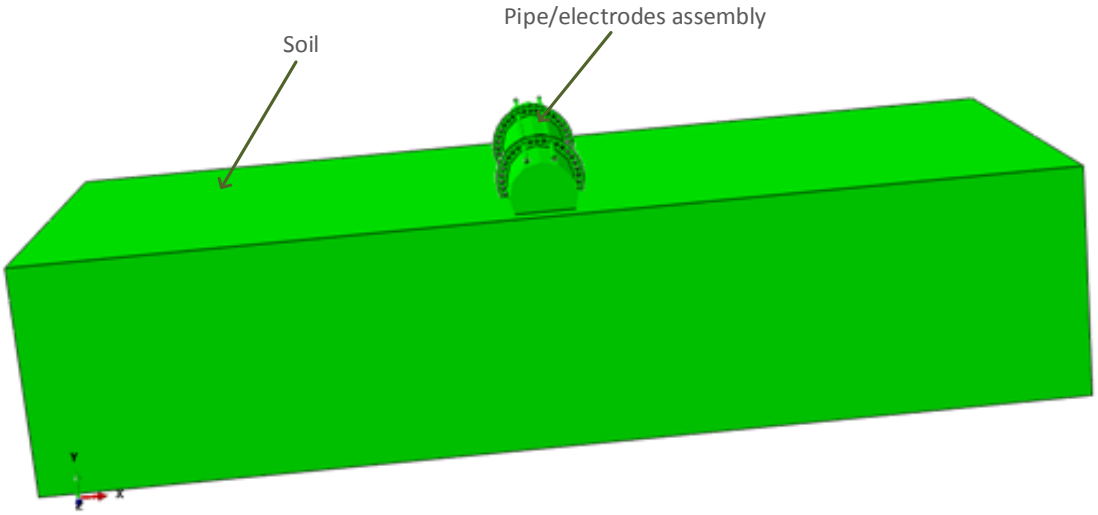

Figure 3-15 Model series 2: Section view - 3D FE vertical penetration pipe-soil interaction model

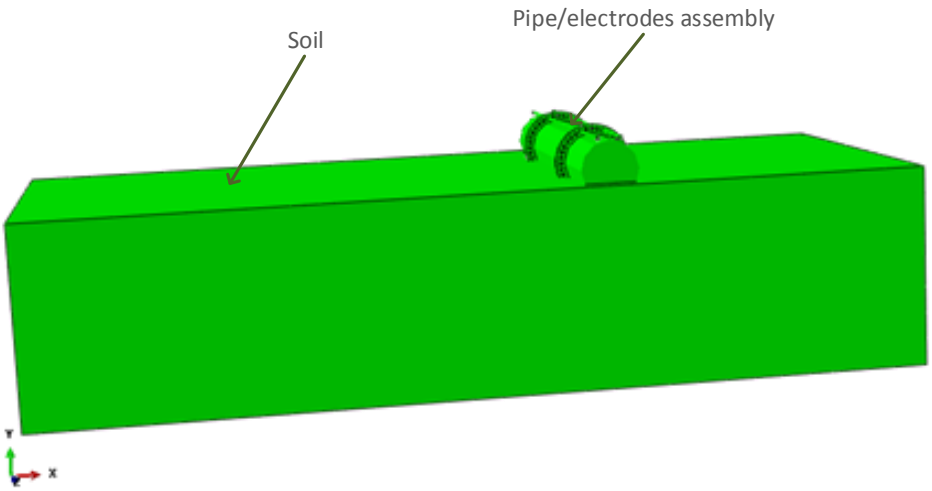

Figure 3-16 Model series 2: Section view – 3D FE lateral pipe-soil interaction model

The EK pipe-soil interaction analyses in vertical, axial, and lateral directions were conducted for both steady state and transient analyses. The time duration of 6, 12, and 24 hours were considered for the electro-osmotic process, subjecting the soil to electrical voltages between 2.5–25V.

The Mohr-Coulomb plasticity model which is based on total stress analyses was also explored for the present studies, using the coupled temperature displacement element with electrodes varying from two to six. The electrodes, support rings, and soil/water are modeled with solid volume element C3D8RT and the pipe is modeled with shell element S4RT [18].

3.1.3.3.1.8 Test Series - 3a

The pipe-soil model is described in Table 3-8 and the electro-osmotic properties in Table 3-9. The soil has dimension of 0.258m x 0.084m x 0.16m. The pipe dimension has a diameter of 0.02m and length of 0.08m. The water has the depth of 0.055m and the soil depth of 0.105m. The data were obtained based on small-scale modeling by Dutta et al. [102] and is scaled by a multiplier factor of 40 to represent the large-scale experiment conducted by Dingle et al. [100]. This series is based on a steady-state analysis of the soil.

Table 3-8 Pipe/Soil Model: series - 3a, 3b

Parameters		**Values**
Soil	length	0.258m
	wide	0.084m
	depth	0.16m
Pipe	length	0.08m
	diameter	0.02m
Electrodes	length	0.08m
	diameter	0.001m
Supporting rings	outside diameter	0.026m
	inside diameter	0.02m
	thickness	0.0015m
	holes diameter	0.0012m
	angle between holes	20°

Table 3-9 Electro-osmotic/Cam-Clay model parameters: series - 3a, 3b

PARAMETERS		MATERIALS	VALUES	UNITS
Electrical Conductivity $k_{\sigma e}$	[8,64,101]	Soil	1.0	S/m
		Seawater	4.8	S/m
		Iron electrode	1.0×10^{7}	S/m
Hydraulic conductivity k_h		Soil	$1x10^{-9}$	m/s
Electro-osmotic conductivity k_{eo}		Soil	$5.5x10^{-9}$	$m^2/V.s$
Saturation, S		Soil	120	%
Void ratio e_o		Soil	3	
Virgin consolidation line, λ	[93]	Soil	0.4	
Recompression/swelling line k		Soil	0.115	
The slope of Critical state line M		Soil	1	
The coefficient of earth pressure at rest, k_o		Soil	1	
Wet yield surface size		Soil	1	
Poisson ratio ν		Soil	0.333	
Young Modulus E		Soil	$1.8x10^{6}$	MPa
Dry density γ		Soil	1121	kg/m^3
Electrical potential (ϕ)	Anodes		10	V
	Cathodes		0	
Time (t)	Steady state			s

The soil is assumed to be in a normally consolidated state for a saturated soil with 120% water content and void ratio of 3. The Cam-Clay soil model is used in the test with Kaolin clay having Young's modulus E of 1.8MPa, the mudline strength is 2.3kPa, the unit weight of soil γ_s and water γ_w given as $6.5kN/m^3$ and $9.81kN/m^3$ respectively. Bot anodes and cathodes are of the same iron material. An Aluminium pipe is used with the mechanical behaviour of the pipelines assumed linear elastic. For each of the constituent parts: electrodes, support rings, pipe and soil/water, the FE model has the same element types as series-1a given in section 3.1.3.3.1.6. Figure 3-17, Figure 3-18 and Figure 3-19 shows the model arrangement and sectional view of the pipe-soil analyses. Further details on these properties are given by Dingle et al. [100].

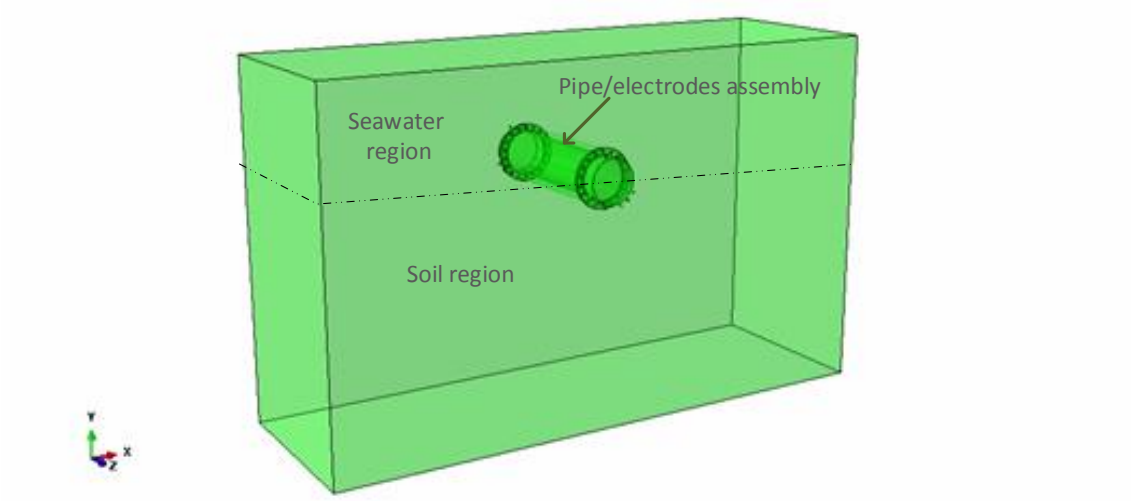

Figure 3-17 Model series 3: 3D FE vertical pipe-soil interaction model – pipe/ electrodes assembly embedded in soil/seawater

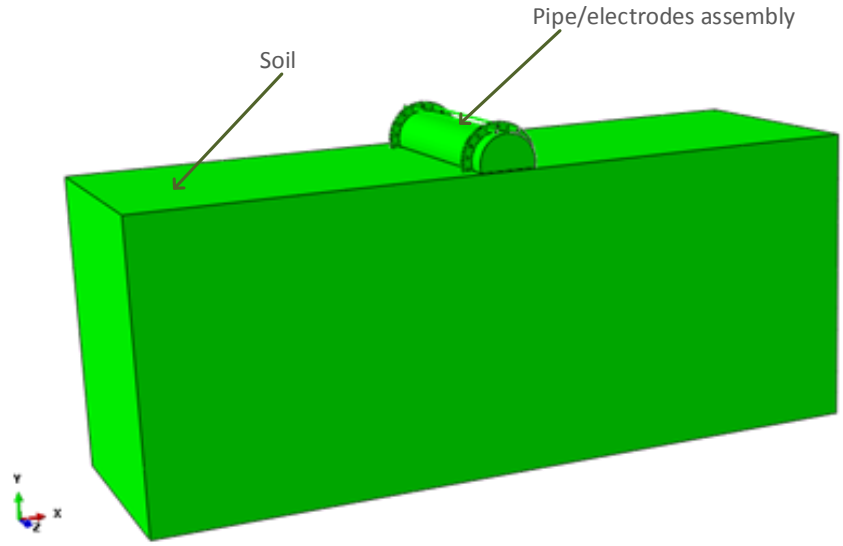

Figure 3-18 Model series 3: Section view - 3D FE vertical pipe-soil interaction model

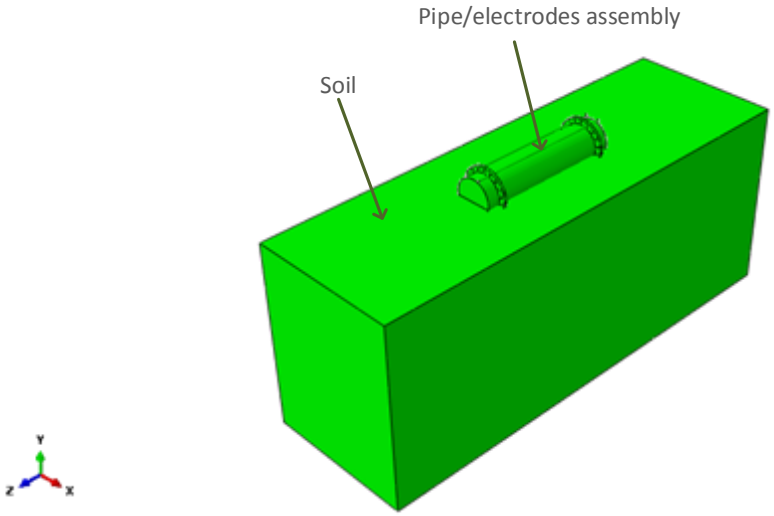

Figure 3-19 Model series 3: Section view - 3D FE axial pipe-soil interaction model

3.1.3.3.2 Dynamic Modelling

The dynamic section of this study consists of three series-1b, 2b, and 3b. Both dynamic EK and non-EK analyses were conducted and results obtained between the two are compared. The dynamic non-EK analyses are conducted without the effect of electrical flow while the EK is conducted to determine the effect of electrical flow (electro-osmosis) on the pipe-soil interaction. The dynamic EK pipe-soil interaction is achieved by importing results from series 1a, 2a, and 3a into series-1b, 2b and 3b respectively.

3.1.3.3.2.1 Test Series-1b

Properties for this model, series-1b is the same with series-1a as given in Table 3-4 and Table 3-5. The 3D dynamic implicit procedure is used for the dynamic analysis of the pipe-soil interaction. Properties for the electrodes, support rings, and soil/water are the same as for the electro-osmotic series-1a. The contact properties have tangential behaviour with a coefficient of friction set to rough ($\mu = \infty$), and normal behaviour set to hard contact. Surface to surface interaction set to the finite sliding formulation is adopted with the soil and pipeline being the master and slave surface respectively. The vertical boundaries of the soil surface are set to allow for displacement in the vertical direction only, while the bottom surface is fixed. A vertical pulling/penetration velocity of 0.0003m/s is set to displace the pipeline, and as given by Randolph and House [76] in Equation 2.45, these velocities are sufficient to cause the undrained condition in the soil to occur. This conditions were analysed in details [72–74].

3.1.3.3.2.2 Test Series-2b

The properties of this model, series-2b, is outlined in Table 3-6 and Table 3-7 which is the same as for series-2a. The analyses follow the same trend as described in series 1b. However, in the contact formulation, the pipeline is the master surface and soil the slave surface. The velocity of 0.0003m/s is applied for the vertical penetration while the axial and lateral displacement with a velocity of 0.0005m/s. As explained in section 3.1.3.3.2.1, these velocities satisfy the conditions for undrained occurrence in the soil. Mohr-Coulomb soil model was

also tested to determine the dynamic behaviour of the soil in vertical and axial directions and the variation with numbers of the anode is considered. The friction and dilation angle is zero with Poisson ratio of 0.49.

3.1.3.3.2.3 Test Series-3b

The model properties for this series-3b are given in Table 3-8 and Table 3-9 which is the same as in series-3a. Detail analysis with regards to vertical penetration of pipeline has been discussed by Dingle et al. [100]; Dutta et al. [102]. However, the dynamic analysis investigates further the EK effect on the pipe under the same and also different conditions for a non-EK treated soil and EK treated soil. During the vertical analysis, the pipeline is penetrated further from the initial depth of 0.375D to a depth 0.825D. The axial and lateral analyses also undergo the same treatment as for the vertical analysis with regard to the initial embedment. The contact formulation and other properties for this model are discussed in series-2b above. The vertical velocity of 0.015D and axial/lateral velocity of 0.0002m/s applied to pull the pipeline. These velocities satisfy the undrained conditions in the soil as earlier explained in section 3.1.3.3.2.1

3.2 Concluding Remarks

Chapter 3 described the numerical methods used in this study. The method for the validation of heat flow to mimic electrical flow have been determined which led to the adoption of the coupled temperature-pore pressure element and procedure. The pipe-soil model development, materials/model properties have been given. Numerical models were developed for the determination of EK effect on soft soil using ABAQUS software tool. Two stages involved in the EK analyses are electro-osmotic consolidation and dynamic pipe-soil interaction. Three different test series each for electro-osmotic consolidation and dynamic analyses were built. The electro-osmotic consolidation analyses determined the soil consolidation followed by dynamic pipe-soil interaction process. The electro-osmotic consolidation process determines the effect of voltage variations, time and numbers of electrodes. Soil models such as the Cam-Clay and Mohr-Coulomb were tested. The dynamic analysis considers the electro-osmotic effect

due to the displacement of pipeline in vertical, axial, and lateral direction. Details analyses on mesh sensitivity are considered. This allows for the adoption of the correct elements sizes for accuracy. Validation of the procedures adopted and the element types for this study were effectively covered.

CHAPTER 4: ELECTRO-OSMOTIC CONSOLIDATION ASSESSMENT

Results from the electro-osmotic analyses of pipe-soil interaction are presented in this section. The analyses ranged from verification of the flow processes and the pore-pressure elements procedure being adopted for consolidation analyses of the soil using the ABAQUS tool. Both transient and steady-state analyses with varying voltages are presented.

4.1 Mesh Sensitivity Analyses

In Finite Element (FE) analysis, the element type, shape, and size are very important for the accuracy of results. The quality of a model analysis depends on the mesh density, in most cases by increasing the mesh density the analysis accuracy increases. Selecting the approximate global size of elements is not straightforward, however, the optimal number of elements was determined by considering all cases ranging from coarse to fine mesh in the mesh refinement analyses. A convergence test is one of the effective means being considered for determining the element size adopted. In a convergence test, the error resulting from the calculated values tend to converge to zero as the number of elements increases.

In all cases for this study, the slave surface is finer than the master surface to avoid substantial penetration into the master surface for more accurate results. The test was conducted with the soil mesh density being the varying factor. The convergence test for test series-1 is shown in Figure 4-1 with an element size of soil 0.013m being adopted. The same applies to test series-2 and 3 with element sizes of 0.033m, and 0.0075m in Figure 4-2 and Figure 4-4 respectively. The mesh convergence test of series-2 for the Mohr-Coulomb plasticity model using coupled temperature-displacement elements is presented in Figure 4-3. Soil element size of 0.031m is adopted in this regard.

The types of an element chosen for each of the test series have been discussed in section 3.1.3.3. Further details on soil, pipe, electrodes and rings sizes, the

total number of elements for model series-1, 2, and 3 are given in Appendix A.1, A.2, and A.3 respectively.

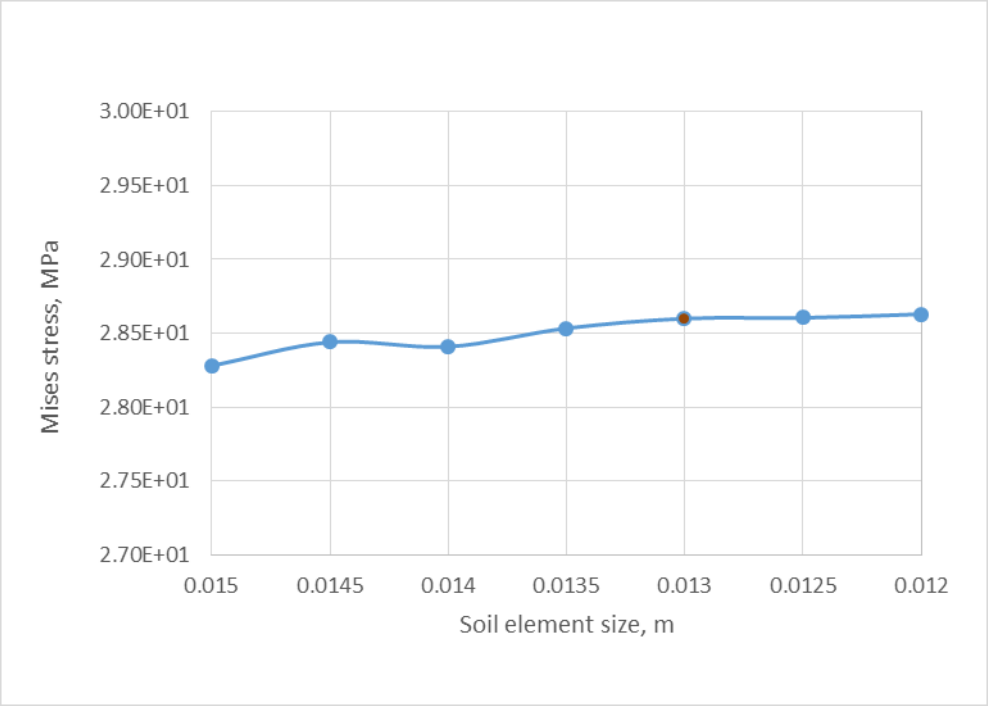

Figure 4-1 Test series-1: Mesh convergence test

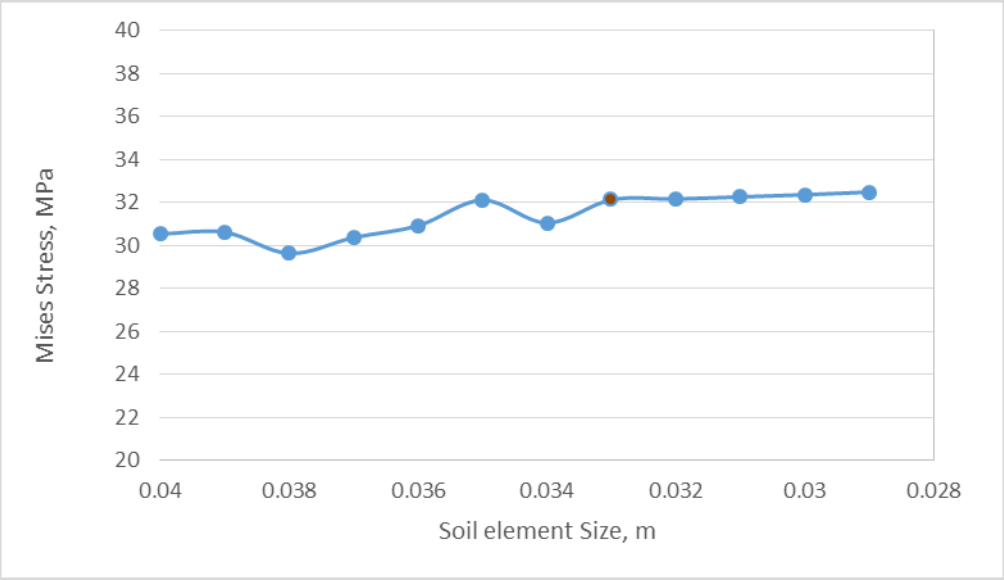

Figure 4-2 Test series-2: Mesh convergence test

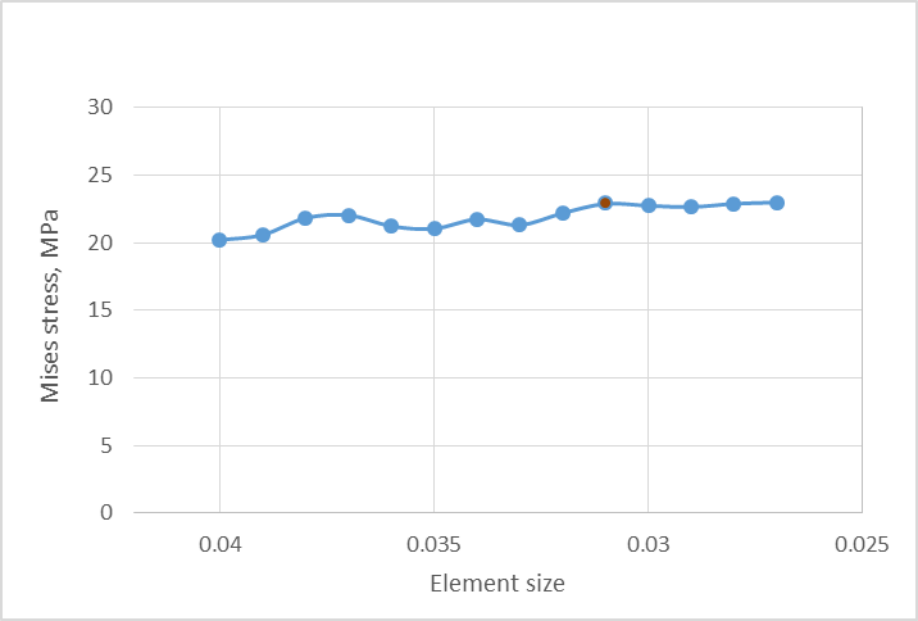

Figure 4-3 Test series-2: Mesh convergence test for Mohr-Coulomb model with CTD element

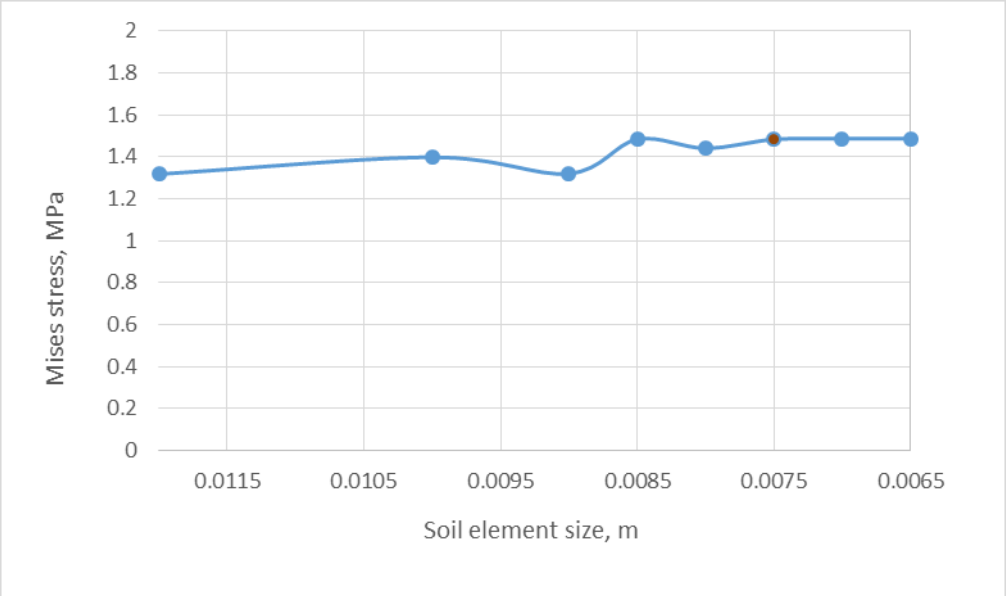

Figure 4-4 Test series-3: Mesh convergence test

4.2 FEA Procedure Verification

4.2.1 PHASE-1: ABAQUS Heat Transfer, Electrical, and Chemical Flow Verification

To determine the capability of ABAQUS using the various flow process outlined in Table 2-1, analyses were conducted for each of the processes. As given in Figure 4-5, any of the flow processes in ABAQUS has the capability to mimic each other and in this case, the electrical flow. Nodal temperature (NT11) from the result shown in Appendix B mimic the voltage (V). From Figure 4-5, the flow process originates from the anode to cathodes. By conduction, voltage is passed from anode to concrete and from the concrete to the cathodes. Areas embedded with anodes have the same potential of 0.440V and consequently decrease as it moves away from the anodes. Results of the different flow process indicate the same trends as shown in Figure 4-5. This verifies the choice of the ABAQUS heat flow to mimic the electrical flow.

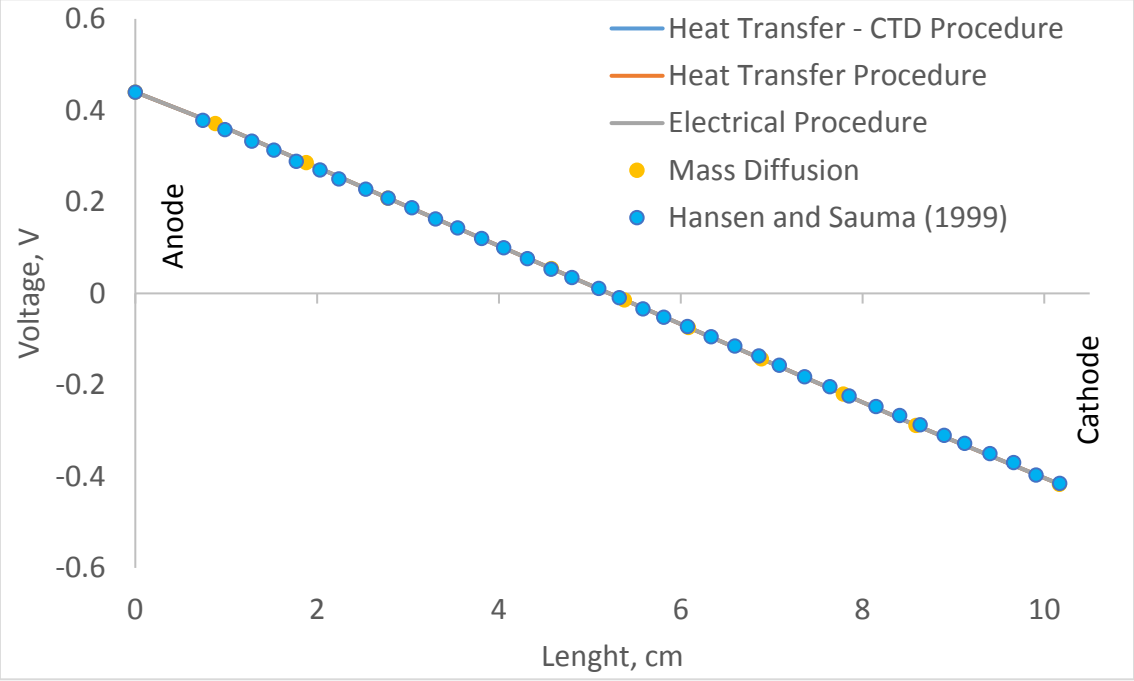

Figure 4-5 ABAQUS flow process verification using chloride diffusion cracking of concrete

4.2.2 PHASE-2: ABAQUS Temperature-Pore Pressure Elements Verification

To further confirm the capacities of the coupled temperature-pore pressure procedure in the ABAQUS tool, an analysis was conducted and the results are shown in Figure 4-6 and Figure 4-7. From the Figure 4-7, soil behaviour indicates higher settlement for the first 40 days of the treatment when compared with Burnotte et al. [33]; Yuan and Hicks [36]. However, from day 40, a contrast to the analysis by Yuan and Hicks [36] is observed, the soil settlement shows a rebound. This could be attributed to less influence of the soil treatment within these periods. From the experiment, rebound of soil settlement is due to absent of voltage, however, this analysis does not consider intermittent voltage flow. While the analysis by Yuan and Hicks [36] were in 2D, a detail 3D analysis merit further studies to determine this behaviour. Results show that the coupled temperature-pore pressure element can be used for the electro-osmotic consolidation of the soil,

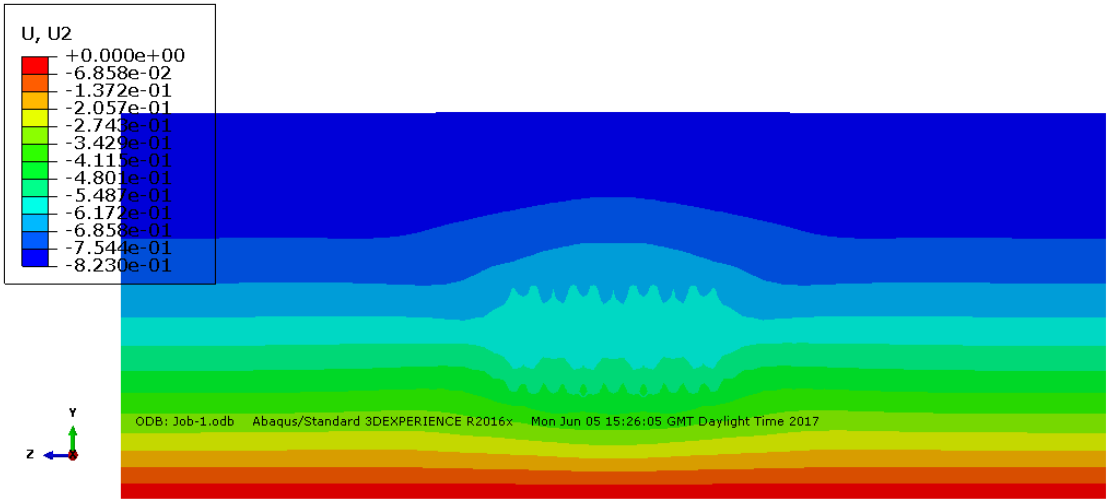

Figure 4-6 Phase-2: Soil Settlement

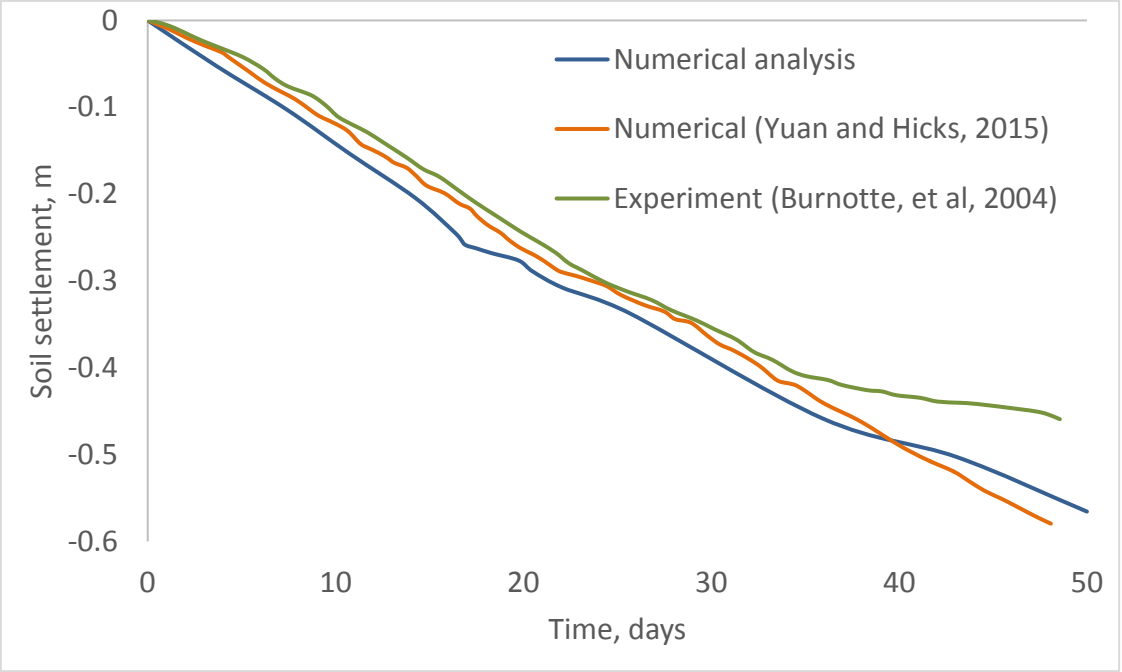

Figure 4-7 ABAQUS verification of coupled temperature-pore pressure element for electro-osmotic analysis

4.3 PHASE-3: EK Pipe-Soil Interaction Model

4.3.1 Test Series-1a

The test series describes the electro-osmotic consolidation of a small scale model to determine the behaviour of the EK treatment of soft clay soil. This phase gives the test of transient analyses in which soil is treated for 6-hours and 12-hours at 10V.

4.3.1.1 Electro-Osmotic Flow Behaviour

The electro-osmotic flow process for model series-1a is described in Figure 4-8 and Figure 4-9. Nodal temperature (N11) from the result shown in Figure 4-8 mimic the voltage (V). The flow originates from the anode to cathodes with the anode at the pipe bottom and the cathodes at the top. By conduction, voltage is passed from the anode to the soil and from the soil to water and then to the cathodes. Voltage flow is assumed to be mainly in the vertical direction and varies in the soil along the path of the circular pipe. Areas embedded with anodes have the same potential of 10V and consequently decrease as it moves towards the

cathodes. The spacing between anodes and cathodes is approximately 0.07m for model series-1a as shown in Figure 4-9. This spacing creates the potential gradient $i_e = \frac{\partial \emptyset}{\partial x}$ in Table 2-1. The gradient gives the driving force for the voltage and pore water u_e to flow from the soil.

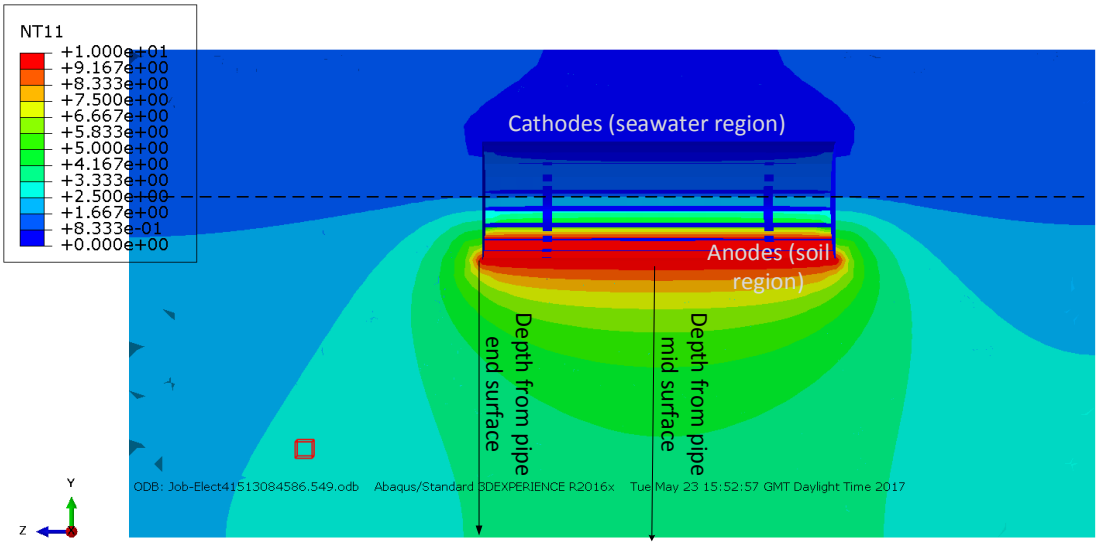

Figure 4-8 Series-1a: Contour plot showing a section view of electrical field distribution during the electro-osmotic flow process

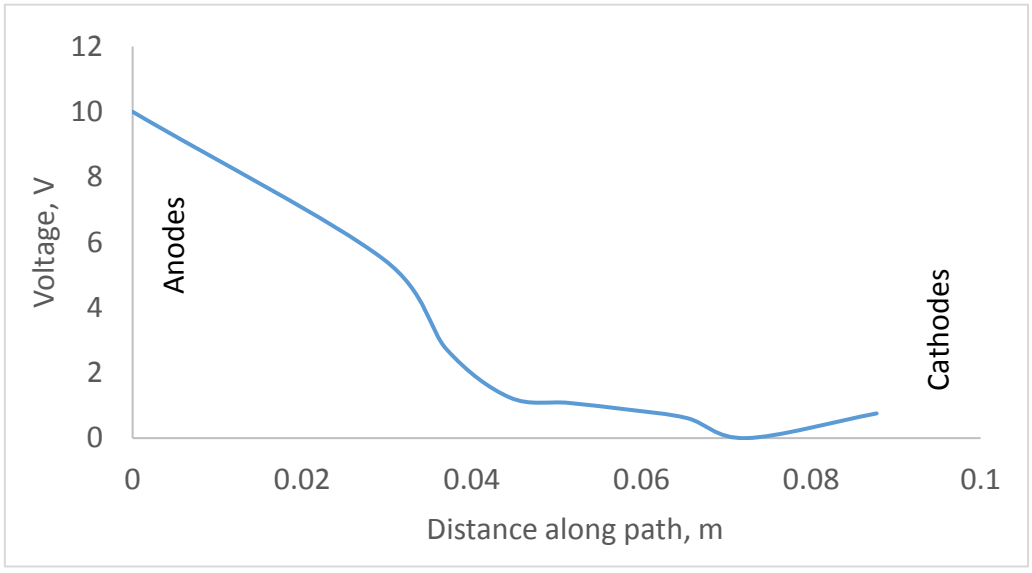

Figure 4-9 Series-1a: ABAQUS electrical field flow behaviour

During a higher voltage concentration at the anodes, the flow is observed to move towards the cathodes as the concentration reduces. The effect of treatment is

more effective at the anodes area. Results in Figure 4-9 shows the voltage at the cathode is approximately zero at 0.07m point, however, the further increase in voltage at this point to 0.76V explains that the excess pore water has drained into the water body due to cathode embedment in it. The removal of pore water from the soil leads to the soil settlement and consolidation. The resultant effect of the electro-osmotic consolidation on pipe-soil interaction is shown further in the dynamic analyses of series-2a.

4.3.1.2 EK Area of Influence

The region of influence is determined based on the electrical field distribution on the soil. The influence due to the electro-osmotic consolidation of the soil is seen to spread to a depth below the pipe mid surface as earlier shown in Figure 4-8 and to a distance along the soil horizontal surface. This is based on assumption that the potential at the soil surface is less than at the anodes. The loss in voltage away from the anode can also be attributed to the surroundings. Figure 4-10 shows that the EK influenced in the soil extended to a depth of about 0.2m. The greater influence is experienced at a depth from the pipe mid surface than from the pipe end surface. A voltage difference up to 0.43V is experienced within these two areas. This trend is also noticed at the soil horizontal surface.

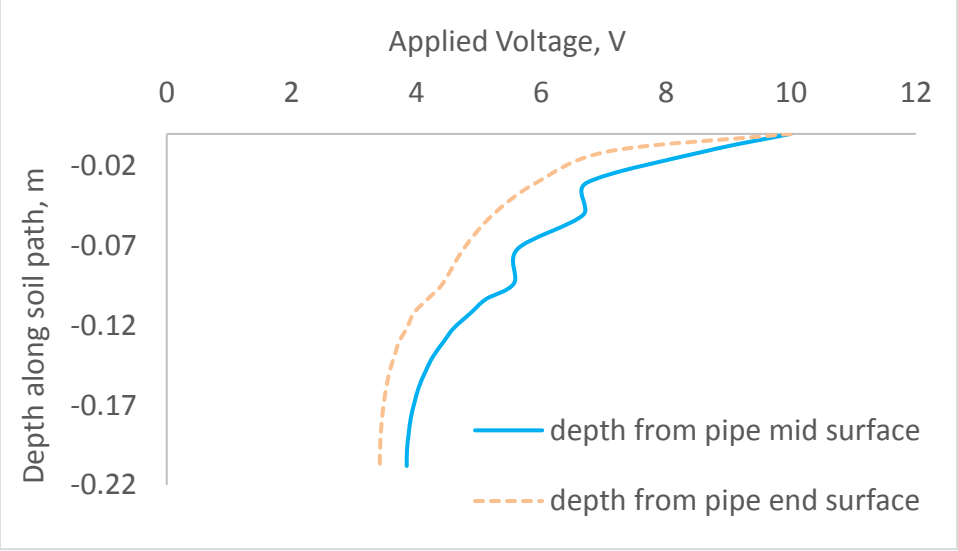

Figure 4-10 Series-1a area influence by electrical field distribution from pipe invert surface

4.3.1.3 Soil Pore Water Pressure

The spacing between anodes and cathodes is approximately 0.07m as shown in Figure 4-9. The potential gradient created within this space served as the driving force for the voltage and pore water u_e to flow from the soil. An observation from the 12-hours treatment time indicated a gradual build-up of negative pore water pressure mainly near the pipe invert perimeter is observed as shown in Figure 4-11. The effect is noticed to a depth of 0.12m as shown in Figure 4-12 due to the electro-osmotic influence being greater within this region.

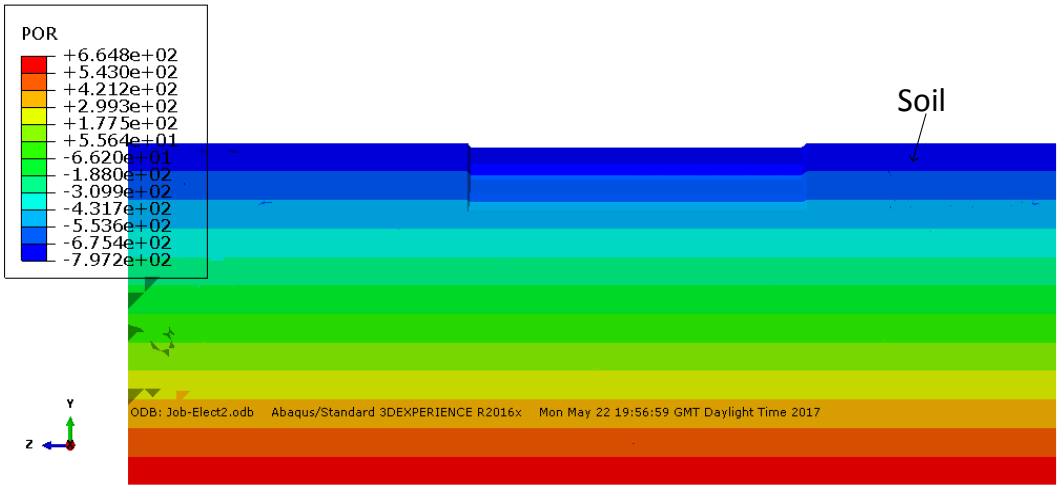

Figure 4-11 Series-1a Contour Plot of pore water pressure distribution within the soil

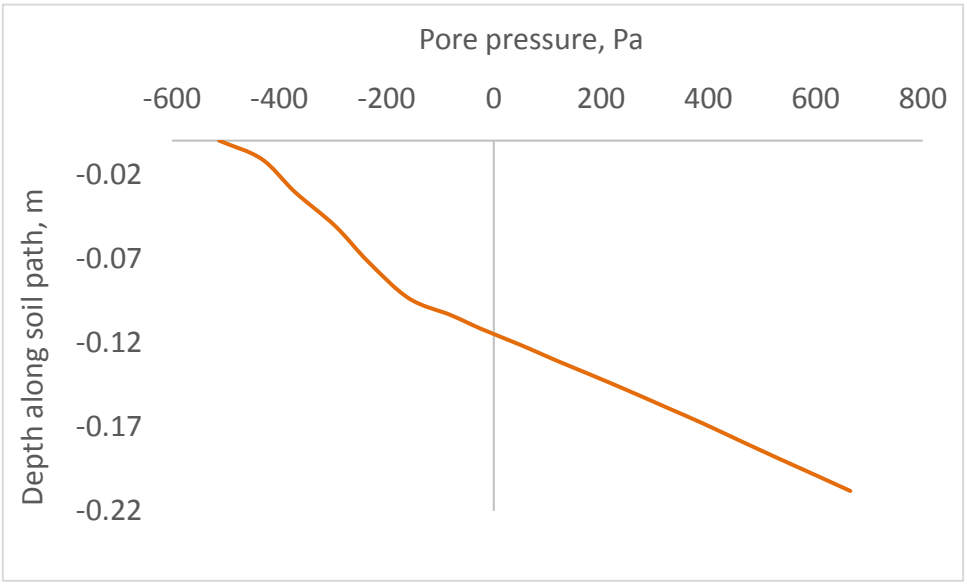

Figure 4-12 Series-1a pore water pressure distribution within the soil

A relationship between the pore water pressure and the soil void ratio is described in Figure 4-13. The void ratio of 1.5 shows a steady decrease with a decrease in the positive pore pressure. At a depth of 0.12m, as shown in Figure 4-12, a decrease in the positive pore pressure resulted in the build-up of negative pore pressure. The void ratio continuously shows a decrease as the negative pore pressure increases. The build-up of negative pore pressure has set up a capillary action with a resulting expulsion of water from the soil void.

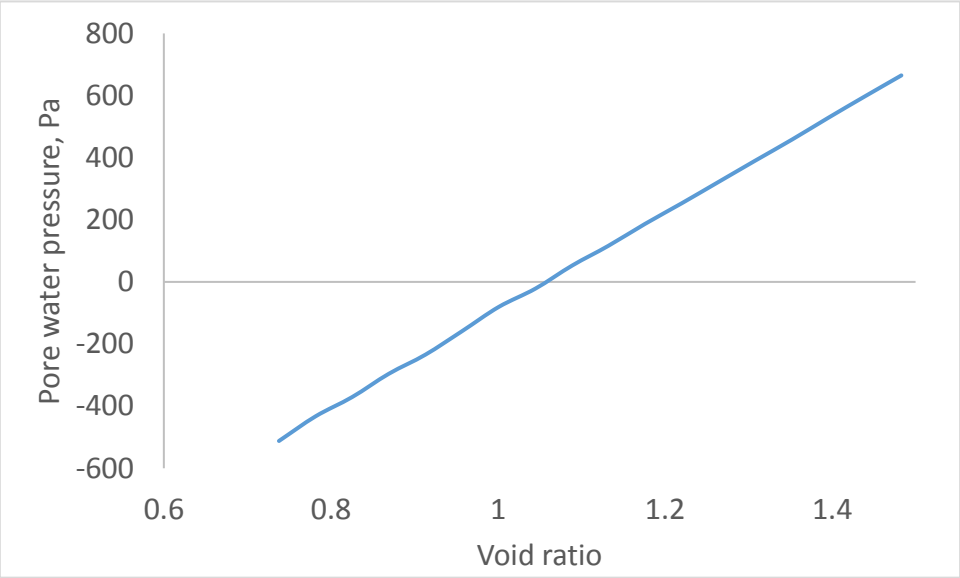

Figure 4-13 Series-1a: effect of pore water pressure dissipation on soil void ratio

The electro-osmotic process is not affected in all of the soil regions, which may lead to flow reversal after the soil treatments time. However, Lo et al. [57] observed that soil hardening progresses after electrical power is cut-off. This behaviour is attributed to an ion diffusion process still taking place in the soil and can be permanent.

4.3.1.4 Soil Effective Stress

As the pore water pressure is dissipated, soil settlement takes place simultaneously. This consolidation process leads to decrease in the soil void and as a result, the effective stress of the soil increases as shown in Figure 4-14. The stress is more effective directly below the pipe invert perimeter due to the voltage concentration within the anode region.

Figure 4-14 Series-1a: EK effect of soil void ratio on effective stress distribution within the soil

4.3.1.5 Soil Settlement

The soil experiences a vertical settlement of 1.826mm in Figure 4-15 and 4.215mm in Figure 4-16 after subjecting it to a treatment time of 6-hours and 12-hours respectively. This small decrease in the settlement is due to the area of influence when compared with the whole model. From equation 2-28, the pore water pressure $-\Delta u$ is proportional to the decrease in soil volume $\Delta\boldsymbol{\sigma}$. The dissipation of pore water pressure with a decrease in the soil void ratio leading to increase in soil effective stress is as expected.

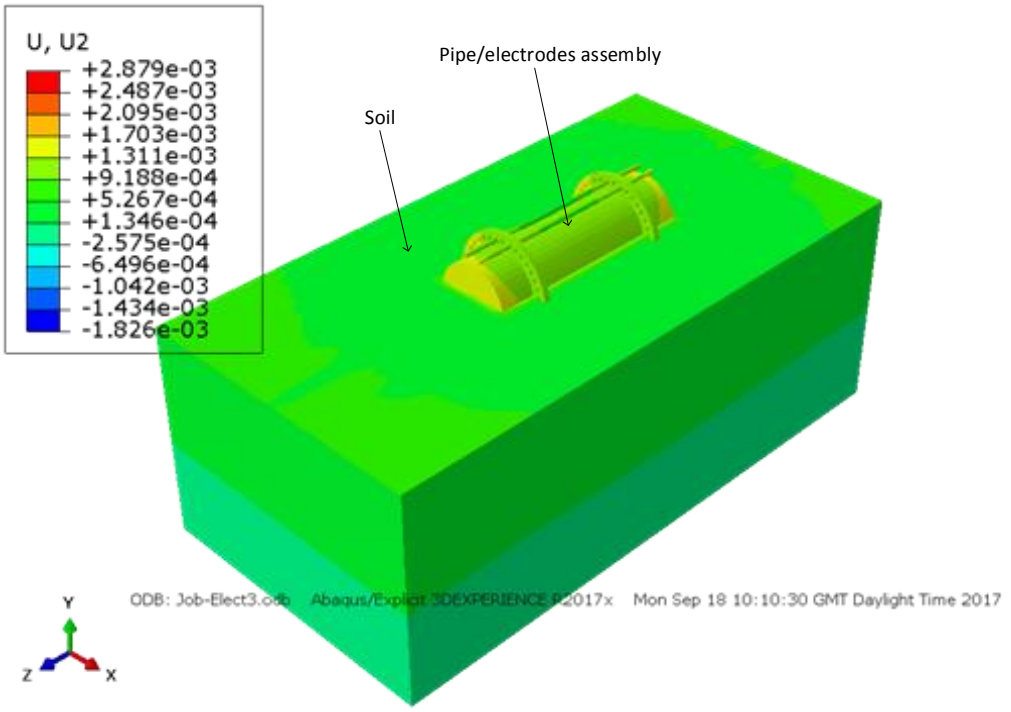

Figure 4-15 Series-1a: vertical soil settlement after 6-hours of treatment

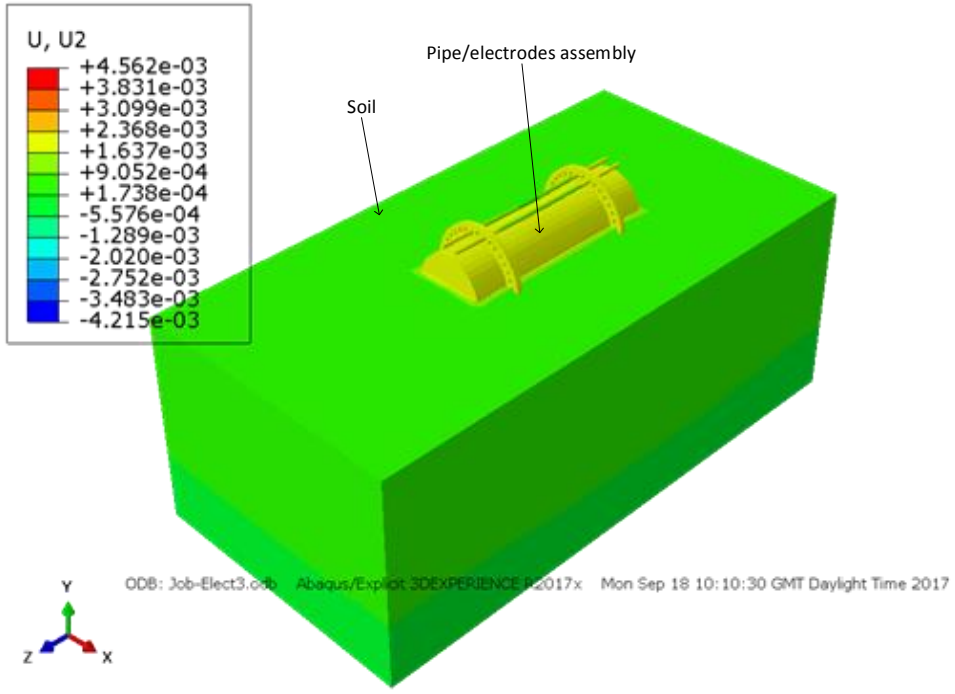

Figure 4-16 Series-1a: vertical soil settlement after 12-hours of treatment.

A little difference of 2.389mm in soil settlement between 6-hours and 12-hours is noticed. However, this difference could have a significant impact on the soil

strength as demonstrated in the dynamic analyses section 5.1 due to some activities not well captured by the ABAQUS tool discussed in subsequent sections.

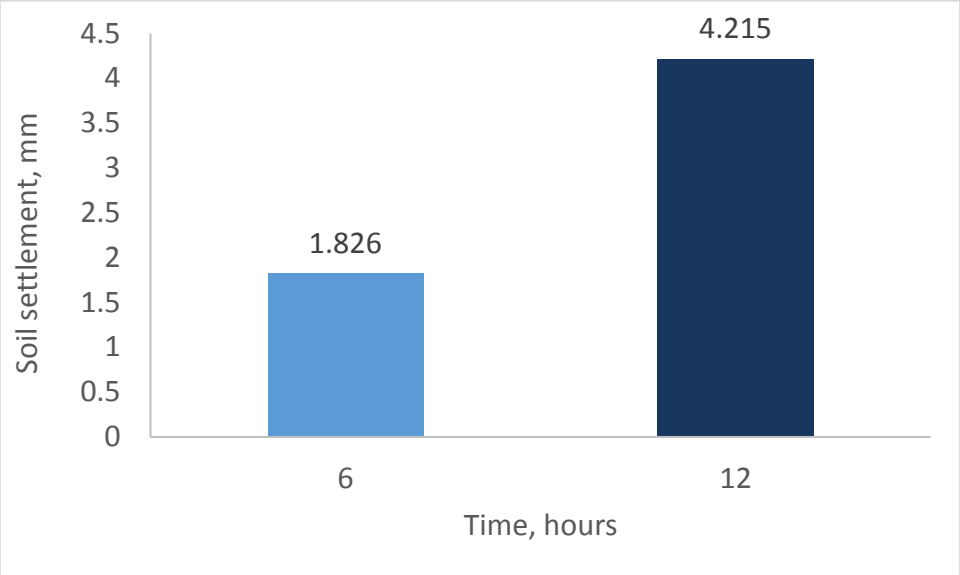

Figure 4-17 Series-1a: Vertical soil settlement

4.3.2 Test Series-2a

The flow behaviour of model series-2a is presented here. The nodal temperature (NT11) shown in Figure 4-18, mimics the voltage (V). The flow behaviour shows a similar trend with the model series-1a. The electrical field distribution from the anode to cathode is shown in Figure 4-18 and the flow behaviour below the pipe surface is also described in Figure 4-19. The distance of 0.19m between the anodes and cathodes, along the pipe surface, forms the effective voltage gradient as described in Figure 4-19. Assuming from the distance of 0.19m between the anode and cathode as described in Figure 4-19 a potential gradient of approximately 13V/m for the 2.5V and 132V/m for the 25V is developed. The greater the voltage, the higher the gradient for the same distance in consideration.

Areas embedded with anodes have the same potential of 10V and consequently decreases to below 2V around the cathode areas as the excess pore pressure is drained into the water. The flow shows a steady decrease in voltage up to point

0.1m and then maintain a steady state of 1.7V. The behaviour at this point is attributed to flow from the soil region into the seawater region. The flow distribution beside soil surface is shown in Appendix E.1.

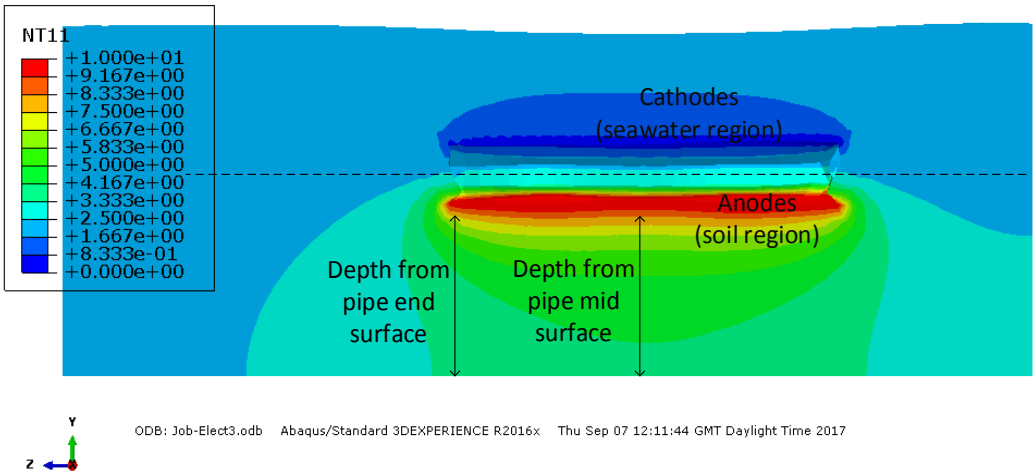

Figure 4-18 Series-2a: Contour plot showing a section view of electrical field distribution during the electro-osmotic flow process

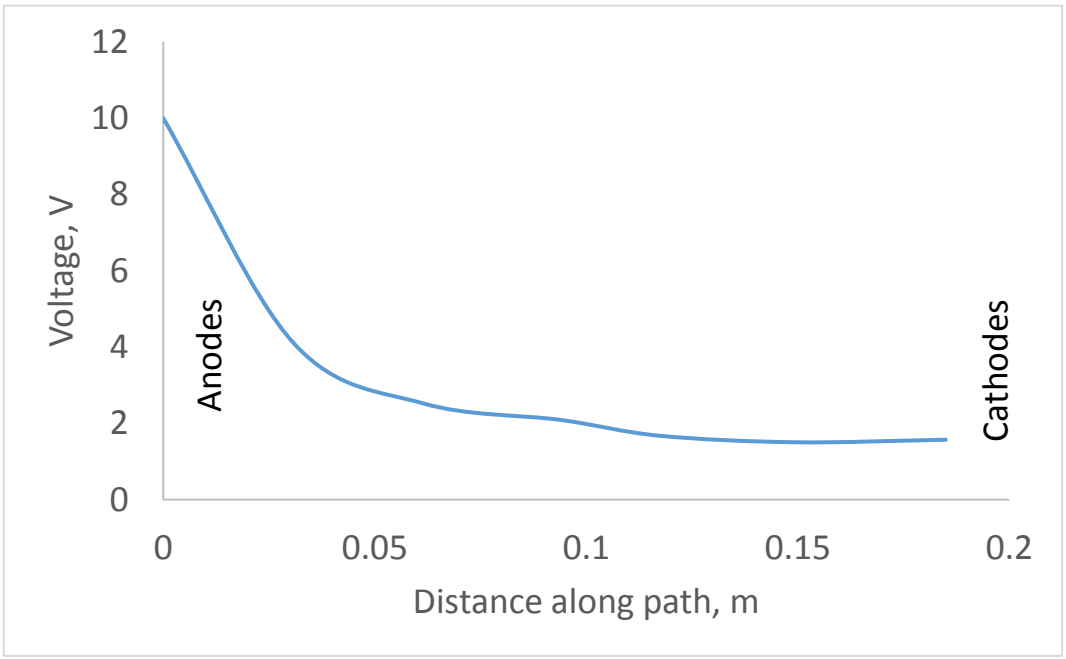

Figure 4-19 series-2a: ABAQUS electrical field distribution during the electro-osmotic flow process

4.3.2.1 EK Area of Influence

The electrical field distribution on the soil determines the area of influence. The area of influence due to EK soil treatment spread to a depth below the pipe as the potential at the soil surface is assumed to be less than the anodes. Figure 4-20 shows that the EK influenced in the soil extended to a depth of about 0.25m. The greater influence is experienced from the mid-surface of pipe than from ends surface. The flow on each of the surface shows a continuous decrease in flow concentration with depth. The midpoint of the pipe shows a decrease in the flow concentration to less than 4.1V while the endpoint decreases to 3.5V. A voltage difference up to 0.6V is experienced within these areas. The voltage is more concentrated within the centre surface of the pipe than at the ends point of the pipe surface. This can be attributed to the enclosure, as the end surface of the pipe has least resistance to flow than at the midpoint.

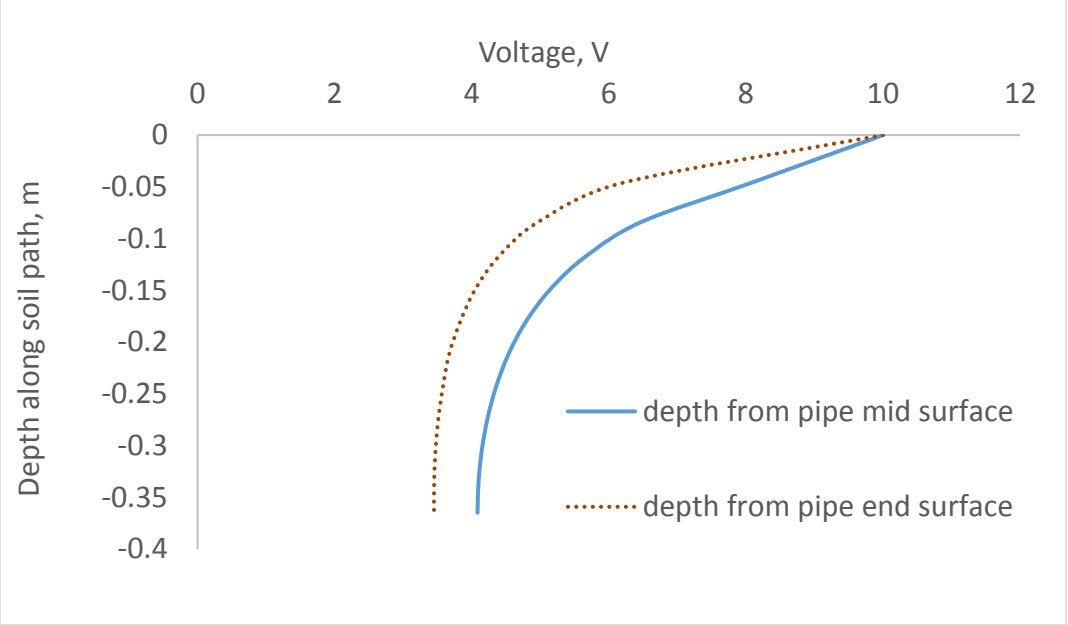

Figure 4-20 Series-2a: area influence by electrical field flow from pipe invert surface

4.3.2.2 Soil Pore Water Pressure

The voltage gradient $i_e = \frac{\partial \theta}{\partial x}$ in Table 2-1, created due to the spacing of 0.19m between the anodes and cathodes as show in Figure 4-19, has been the driving

force for the voltage and pore water $u_{e,}$ dissipated from the soil. The positive pore water pressure is experienced within the soil and shows gradual a decrease as it move towards the cathode as shown in Figure 4-21.

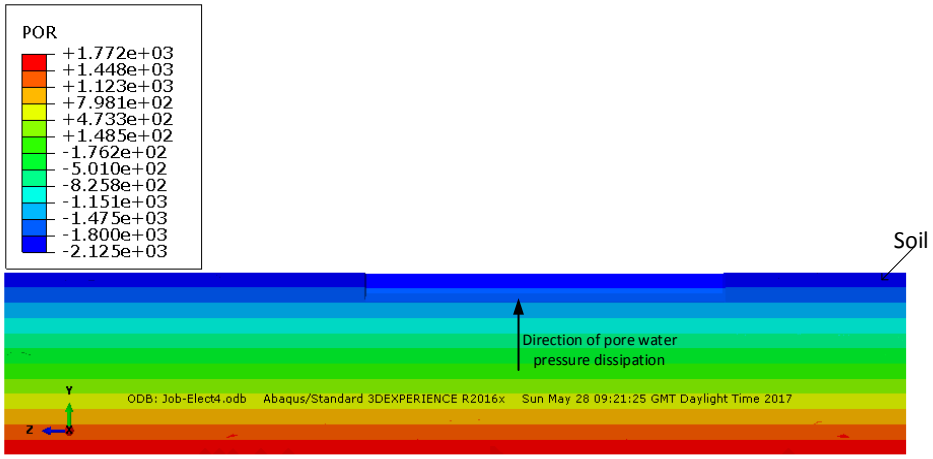

Figure 4-21 Series-2a: contour plot showing a section view of pore pressure distribution within the soil

The dissipation of positive pore water pressure from the soil void led to decrease in the soil void ratio from 1.5 to 0.79 as shown in Figure 4-22. The positive pore water pressure decreases and tends to be negative mainly around the anode region to a depth of 0.24m as shown Figure 4-23.

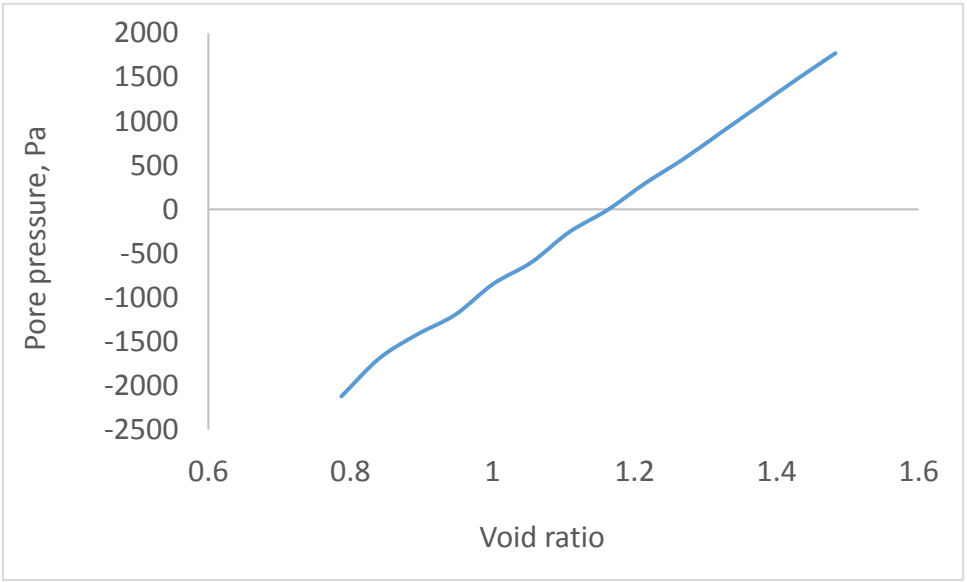

Figure 4-22 Series-2a: effect of pore water pressure dissipation on soil void ratio

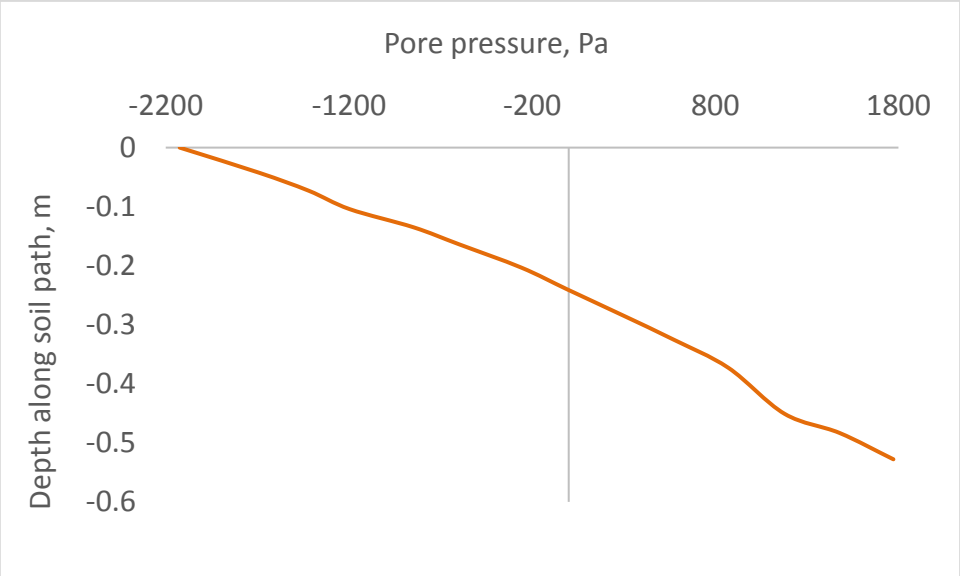

Figure 4-23 Series-2a: pore water pressure distribution within the soil

4.3.2.3 Soil Effective Stress Distribution

The build-up of negative pore water pressure resulted from the expulsion of pore water from the soil void. This process led to the decrease in the void volume. The resultant decrease in soil volume accounted for the increase in soil effective stress as shown in Figure 4-26. The soil effective stress distribution in Figure 4-25 indicated steady increase within the pipe invert perimeter from a depth of 0.1m. The vertical effective stress is affected by its closeness to the treatment zone near the anode and the settlement of the soil due to its own weight. This signifies an improvement in the soil strength near the treatment zone. As the depth increase, the effective stress is also noticed to increase, this behaviour can be attributed to the soil properties which indicates higher strength gradient with depth than the upper layer.

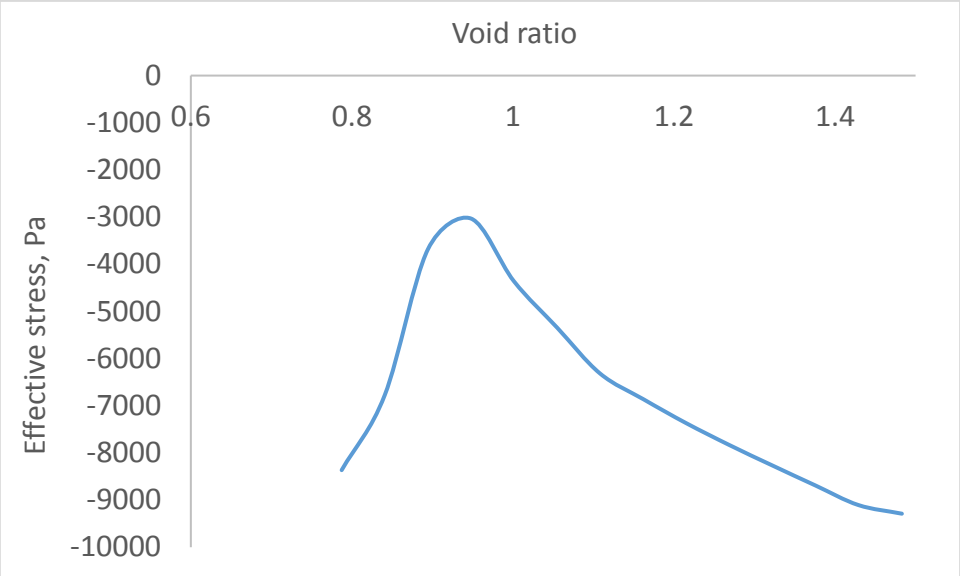

Figure 4-24 Series-2a: effect of vertical effective stress on soil void ratio

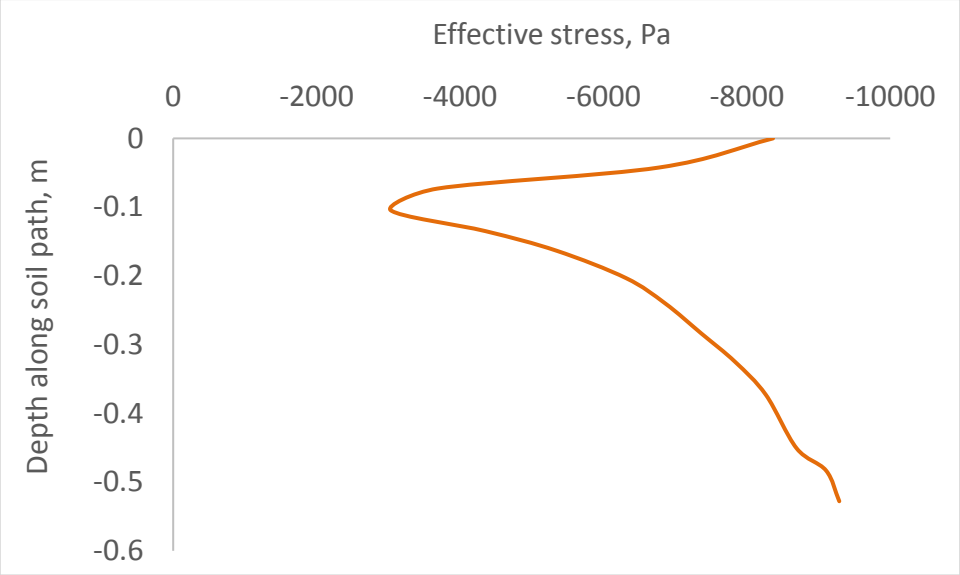

Figure 4-25 Series-2a: EK effect on soil effective stress distribution within the soil

4.3.2.4 Soil Settlement

4.3.2.4.1 Steady State Analysis

Soil settlement occurs due to the removal of pore water from the soil. The soil experiences a maximum vertical settlement of 18.72mm after subjecting it to a steady state consolidation process as shown in Figure 4-26. At some points, the soil experiences a swelling due to the initial pipe penetration and the resultant

settlement is also felt within other regions as shown in the contour plot of Figure 4-26. The settlement is experienced more besides the pipe surface. Further behaviour within and long the soil surface is shown in Appendix E.3. The resultant effects of the electro-osmosis on pipe-soil interactions are discussed further in the dynamic analyses, series-2b in section 5.2.

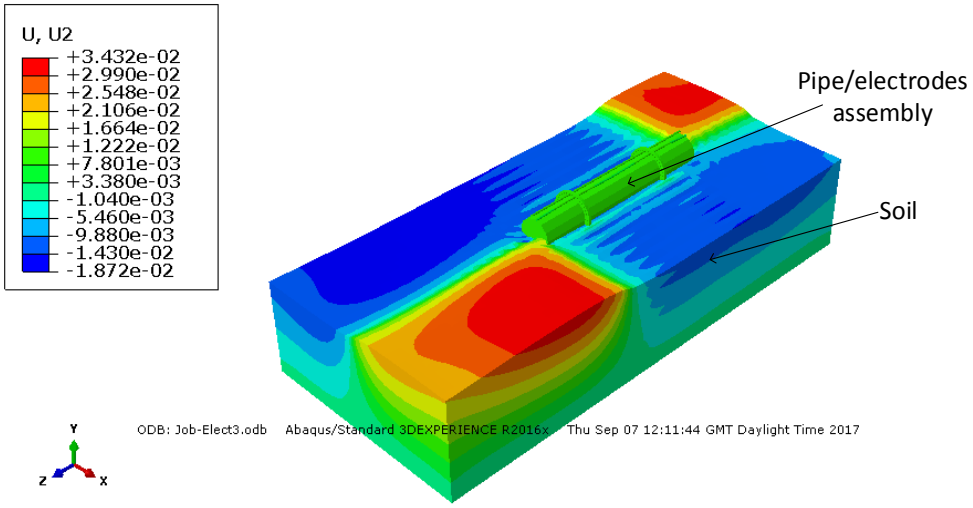

Figure 4-26 Series-2a: contour plot showing a section view of vertical soil settlement distribution within the soil

As discussed in test series-1, the higher voltage concentration at the anodes allows for the flow to move towards the cathodes being the surface the lower concentration. Figure 4-19 shows the flow behaviour to be more effective at a distance of 0.19m from anodes to cathodes areas. The effect of treatment does not span through all the soil region. A small area is being affected when compared with the whole model. However, as given by Lo et al [57], the continues iron diffusion after treatment allows for soil consolidation to continue, which is considered to be a permeant process. This may take care of the potential flow reversal, which has not been captured in this study and may be a factor to be considered in further studies. The reduction in the soil void is due to the dissipation of pore water pressure from the soil which led to the increase in effective stress experienced in the soil as given in Figure 4-25. This phenomenon has been given in equation 2-28.

4.3.2.4.2 Steady State: Effect of Voltage Variation

A steady-state analysis with voltage variation is also indicated in Figure 4-27. Applied voltages of 2.5V to 25V were tested, results indicate a gradual settlement of the soil with an increase in voltage. The least settlement can be noticed for the 2.5V with the highest settlement for the 25V.

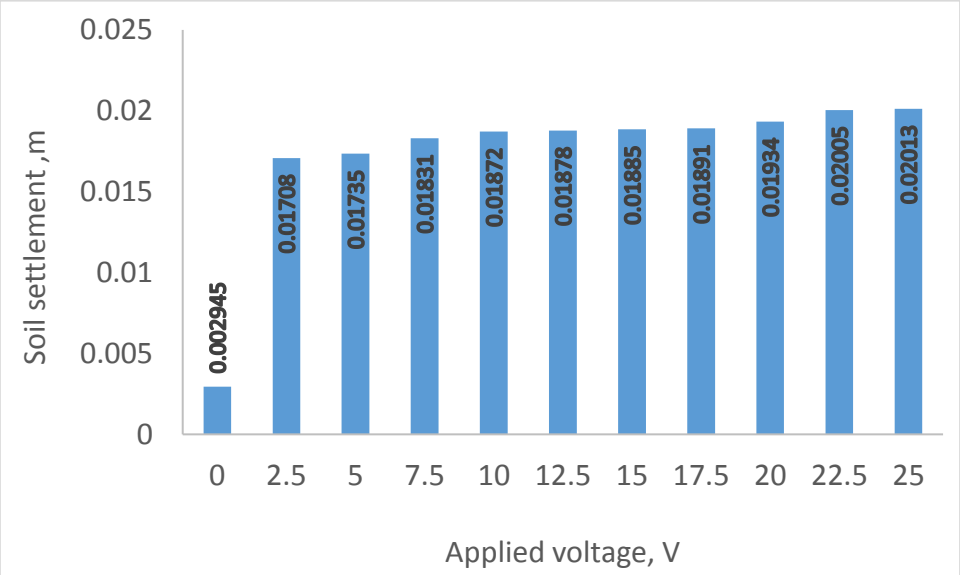

Figure 4-27 Series-2a: Steady State analysis showing the effect on soil settlement due to voltage variation

4.3.2.4.3 Transient Analyses: Effect of Treatment Time

The results from Figure 4-28 indicated the effect of soil settlement due to treatment time. A voltage of 10V is applied through for all treatment time. The soil indicates a progressive settlement of 5.28mm for 6 hours, 9.72mm for 12 hours, and 13.28mm for 24 hours. From Figure 4-28, a 3.5% increase in a settlement between 6-hours and 12-hours, and 18% between 6-hours and 24-hours is observed. The significant increase with time underscores the importance of treatment time to soil consolidation. The greater time taking, allows iron diffusion to be more effective aimed at the hardening of the soil with greater impact on the soil strength.

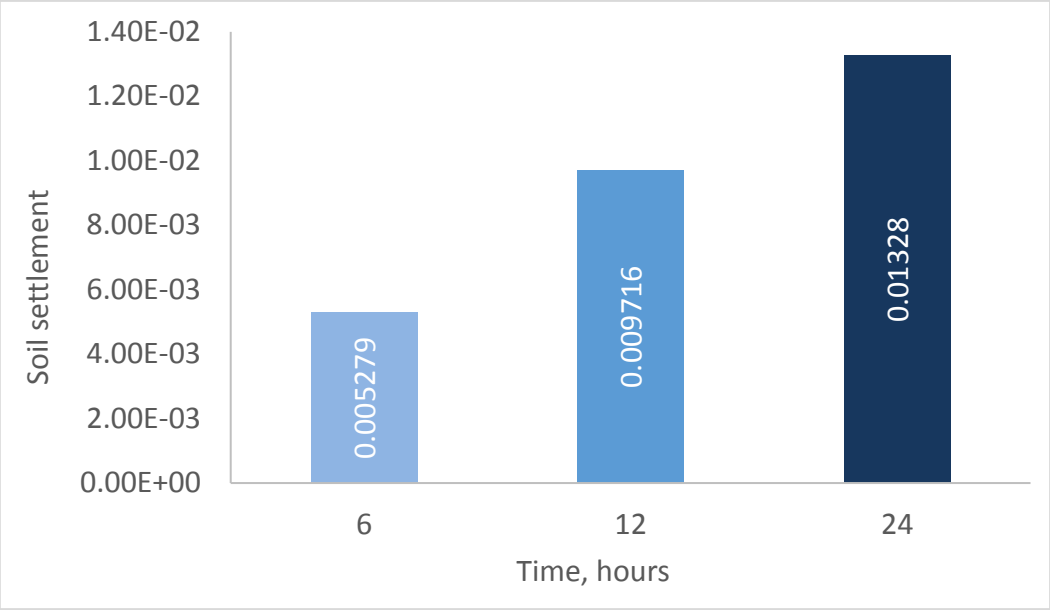

Figure 4-28 Series-2a: effect of treatment time on soil settlement

4.3.2.4.4 Transient Analyses: Effect of Voltage Variation

The effect of voltage variation on soil settlement is presented. The results as shown in Figure 4-29 indicates soil settlement is affected by variation in the applied voltage. The soil settlement shows a slight increase from 2.5V to 25V. This is attributed to small area being affected by the soil when compared with the whole soil dimensions. This behaviour indicates the feasibility of using a lower voltage to give approximately same effect as with higher voltage with consideration to treatment time as previously shown in Figure 4-28. Although the soil settlement experience is of a little fraction when compares with the increasing voltages, this is enough to cause significant changes in the soil strength as discussed further in the dynamic analyses section.

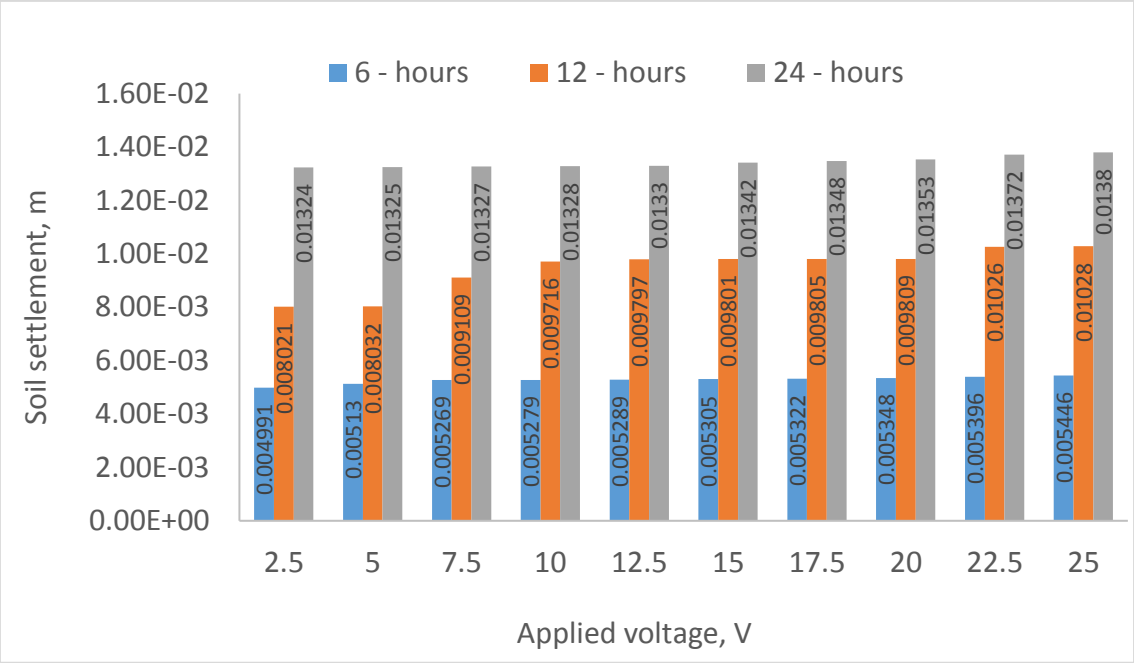

Figure 4-29 Series-2a: transient analysis showing the effect on soil settlement due to voltage variation

4.3.2.5 Mohr-Coulomb Plasticity Model with Coupled Temperature Displacement Element

A steady-state analysis using the Mohr-Coulomb plasticity model, with the adoption of coupled temperature-displacement element is tested with an applied voltage of 10V. The Mohr-Coulomb model is based on total stress analyses with the pore water pressure and void ratio not captured using coupled temperature displacement element and procedure in ABAQUS tool. The result as given in Figure 4-30 shows a very small displacement of 0.03058mm against the 18.72mm noticed from the effective stress model in Figure 4-26. This indicates a significant limitation of the procedures for soil consolidation analyses. However, the dynamic analyses using this procedure shows an interesting result when the EK and non-EK analyses were compared. Details on this can be found in the subsequent section 5.2.3.

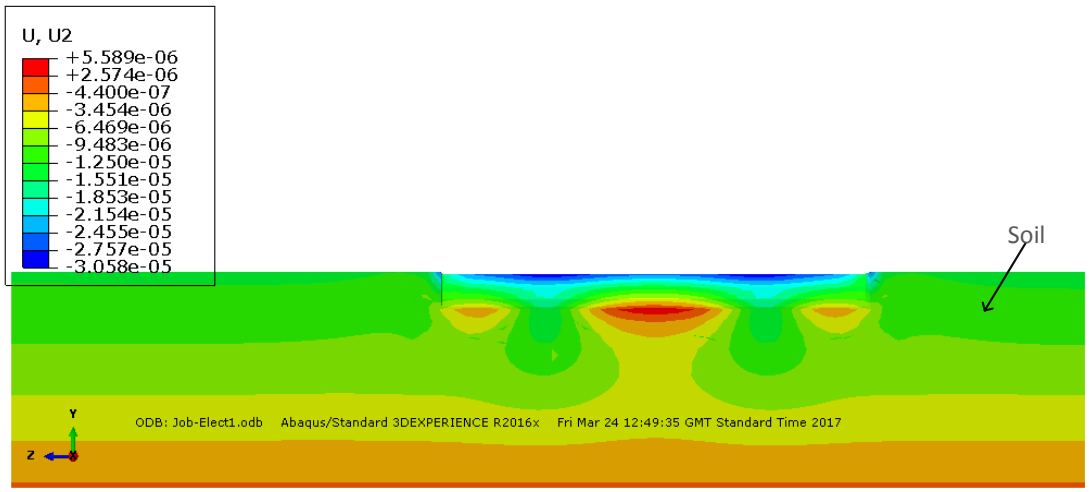

Figure 4-30 Series-2a: soil settlement using Mohr-Coulomb model with CTD element

4.3.3 Test Series-3a

4.3.3.1 Flow Behaviour

Properties of the soil due to the EK effect in model series-3 exhibit similar behaviour as discussed in model series-1 and 2. A steady-state analysis is considered for this study. Electrical field distribution within the soil is shown in Figure 4-31 and Figure 4-32. As described in previous analyses the nodal temperature (NT11) in Figure 4-31 mimic the voltage flow (V). The flow can be seen to concentrate more at the anodes region and gradually dissipate toward the cathodes region. Figure 4-33 shows a similar trend with the model series-1a. The flow is more concentrated from the anodes towards the 0.52m point as it moves to the cathodes. At this point, the concentration of 9V tends to decrease to zero. However, at point 2.2m the voltage is noticed to increase to 1.6V, due to embedment of cathodes inside the seawater were drainage occurs.

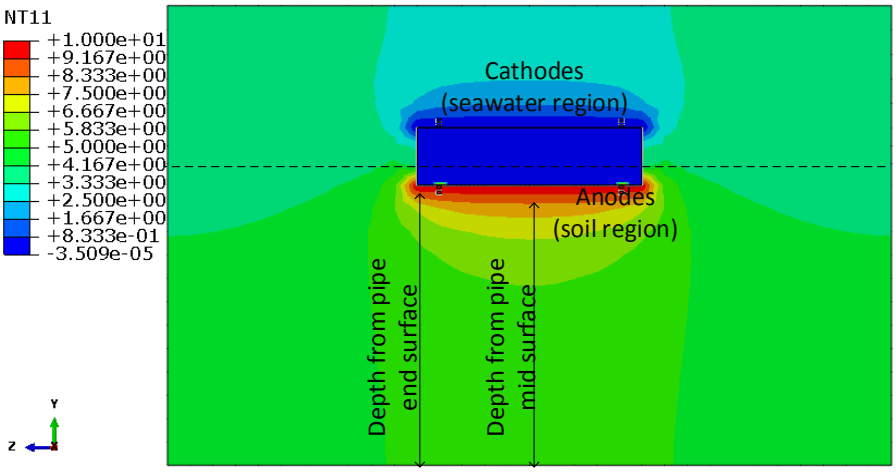

Figure 4-31 Series-3a: electrical field distribution

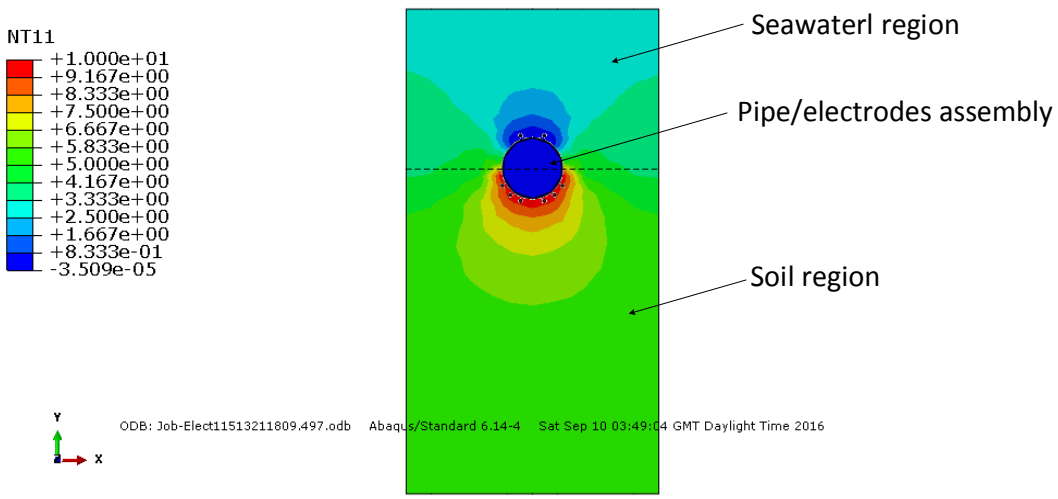

Figure 4-32 Series-3a: Electrical field distribution with depth and along the horizontal soil surface

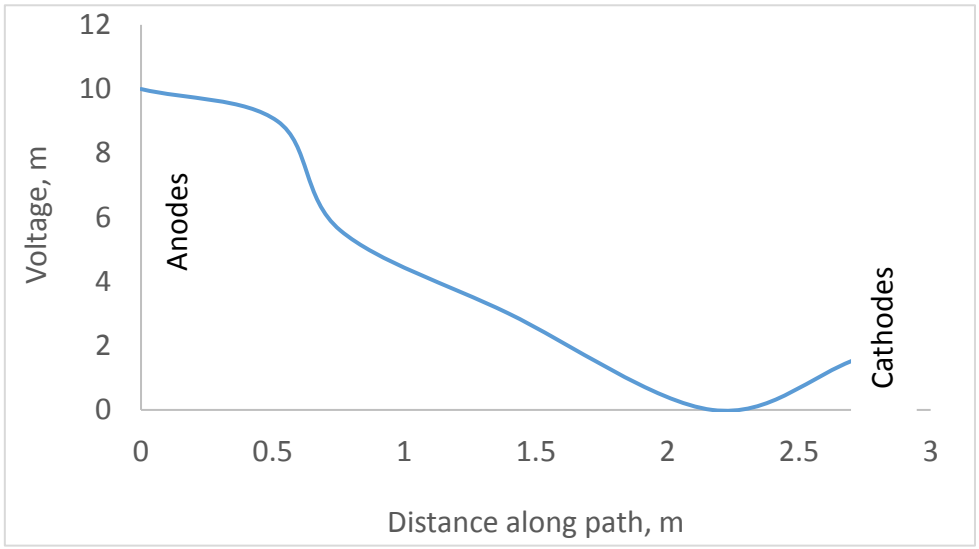

Figure 4-33 series-3a: ABAQUS pipe-soil interaction electro-osmotic flow behaviour

4.3.3.2 EK Area of Influence

The areas of influence of model series-3a is shown in Figure 4-31. Flow also is noticed towards soil horizontal surfaces and with depth as shown in Figure 4-32. As earlier stated, the flow towards other surfaces is due to zero potential assumed. The EK influenced extended to a 4.1m depth from the pipe bottom surface shown in Figure 4-34. As observed from the previous model, the influence is greater from the bottom mid-surface of pipe than from end surface of the pipe.

The flow on each of the surface shows a continuous decrease in flow concentration with depth. The midpoint of the pipe decrease in flow concentration to less than 5.2V while the pipe end surface decreases to 5.0V. A voltage difference up to 0.2V.

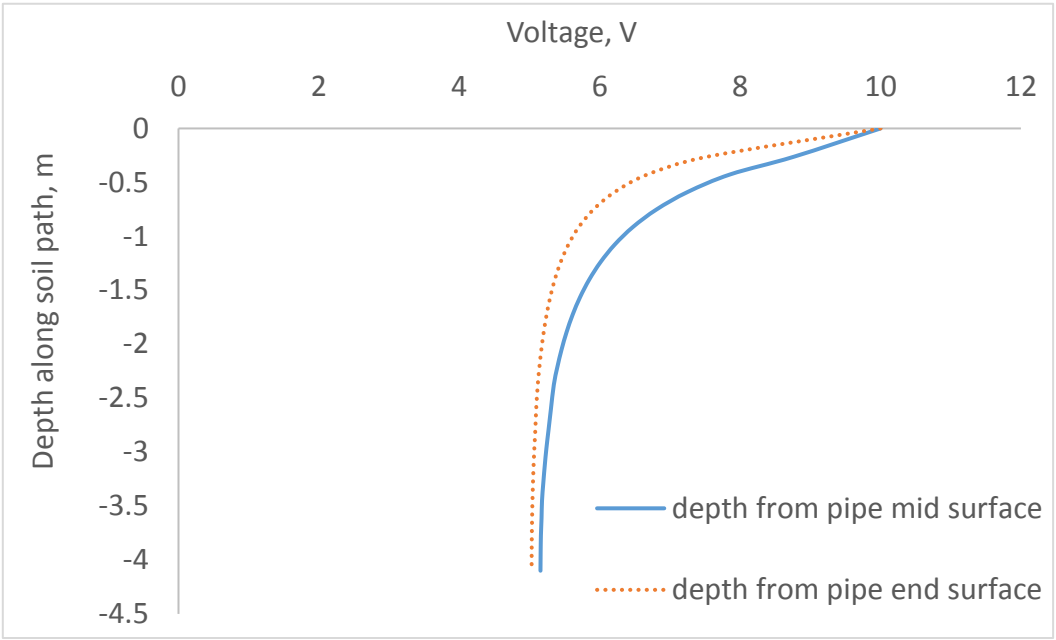

Figure 4-34 Series-3a: area influence by electrical field flow from pipe invert surface

4.3.3.3 Soil Pore Water Pressure Distribution

Pore water pressure in the soil shows a gradual reduction and tend to negative near the anode region as it drains towards the cathodes as shown in Figure 4-35. The dissipation of pore water pressure led to the gradual decrease in soil void ratio from its initial state of 3 to 1.554 shown in Figure 4-36. The largest decrease in the void ratio is experienced near the pipe surface due to its closeness to the EK region with a higher concentration of electrical field. As shown in Figure 4-37, the pore water pressure indicated a relatively constant state to a depth of 0.52m and a void ratio of 1.743. This depth effectively accounted for the soil settlement.

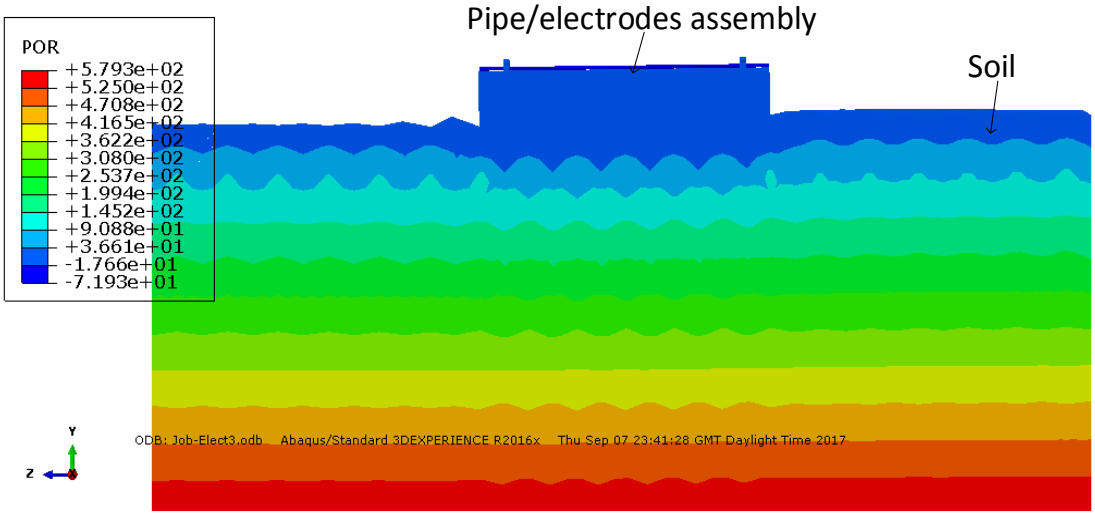

Figure 4-35 Series-3a: contour plot of model Pore pressure distribution due to EK effect

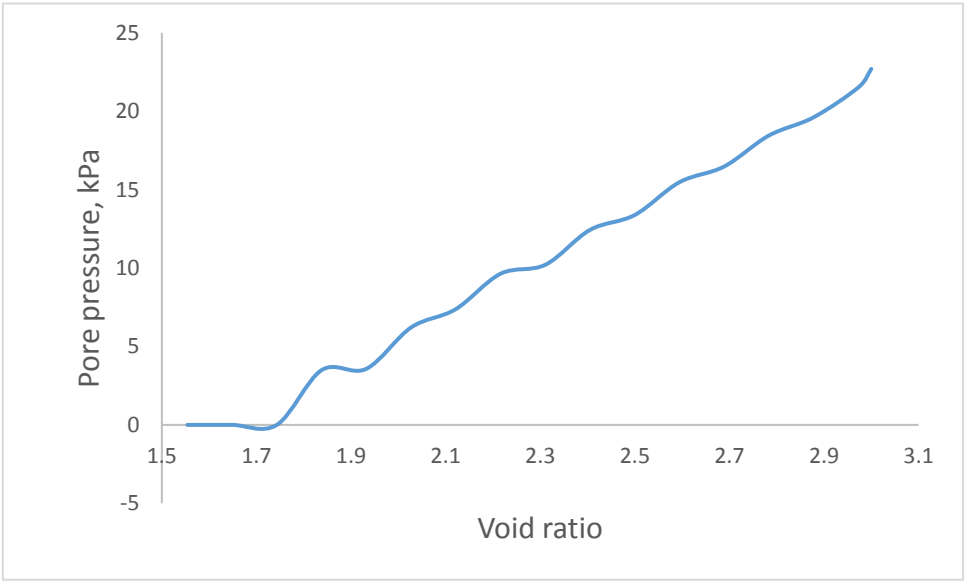

Figure 4-36 Series-3a: effect of pore water pressure dissipation on soil void ratio

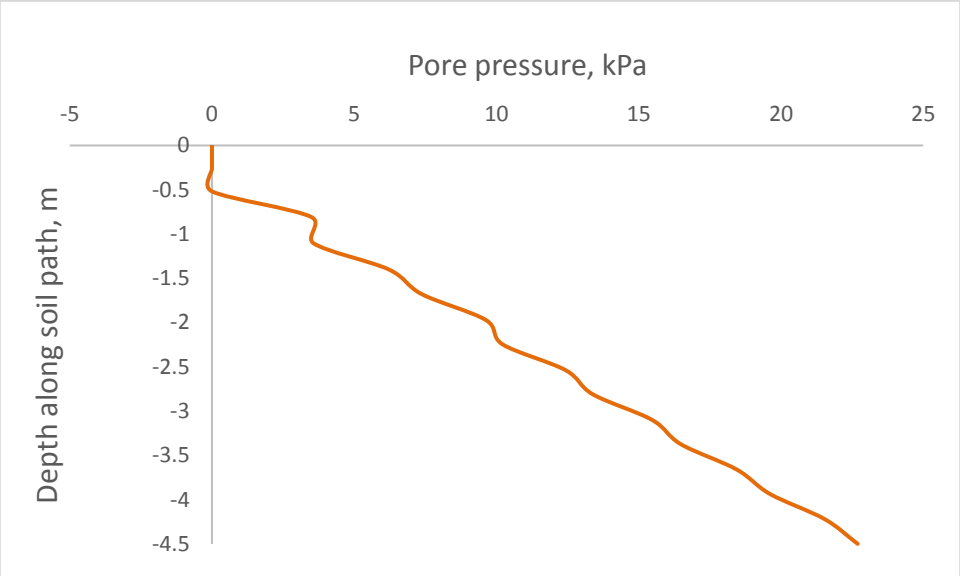

Figure 4-37 Series-3a: pore water pressure distribution within the soil

4.3.3.4 Soil Effective Stress Distribution

The effective stress distribution within the soil is shown in Figure 4-38. The stress away from the treatment areas shows a slight decrease at a void ratio of 3 to 1.84. At a void ratio of 1.84 to 1.554, the effective stress experiences an increase as it approaches the soil surface. This behaviour occurs from the soil depth of 0.8m close to the anodes as shown in Figure 4-39.

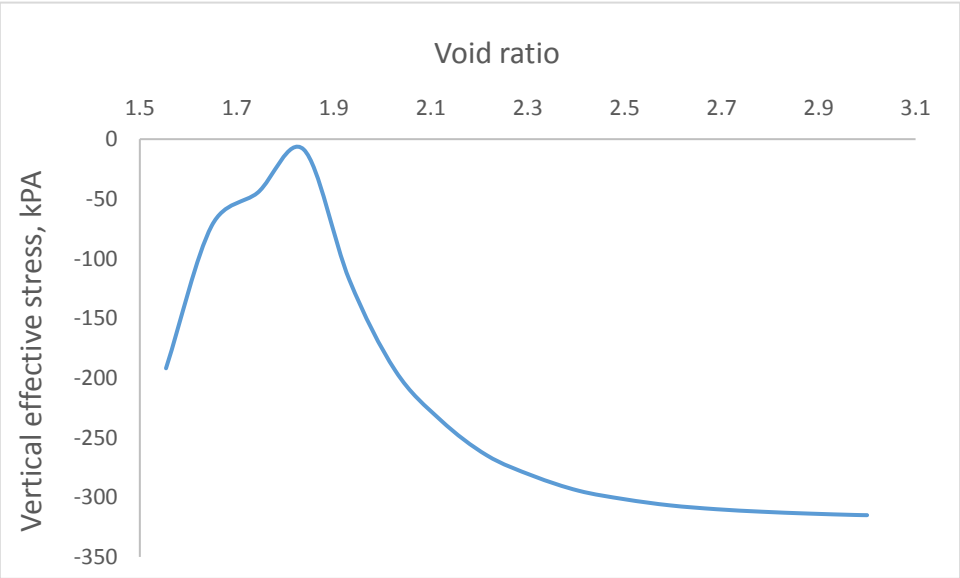

Figure 4-38 Series-3a: EK effect on soil effective stress and void ratio

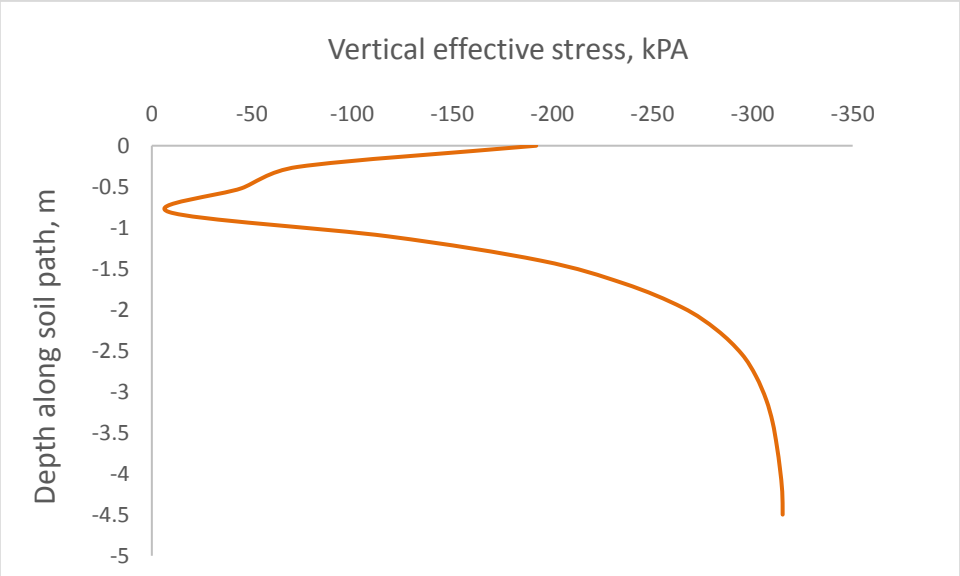

Figure 4-39 Series-3a: effective stress distribution along soil path

4.3.3.5 Soil Settlement

The contour plot of soil settlement is shown in Figure 4-40. Maximum soil settlement of 2.09mm has been achieved. The results are based on data obtained from small-scale modeling by Dutta et al. [102]. When scaled by a multiplier factor of 40, this represents the large-scale experiment by Dingle et al. [100]. In this case, a soil settlement of 83.6mm is achieved. This represents a settlement of 3.8% when compared with the average distance between anodes and cathodes of 2.2m. Further effects due to the EK soil consolidation are given in the dynamic analyses, series-3b in section 5.3.

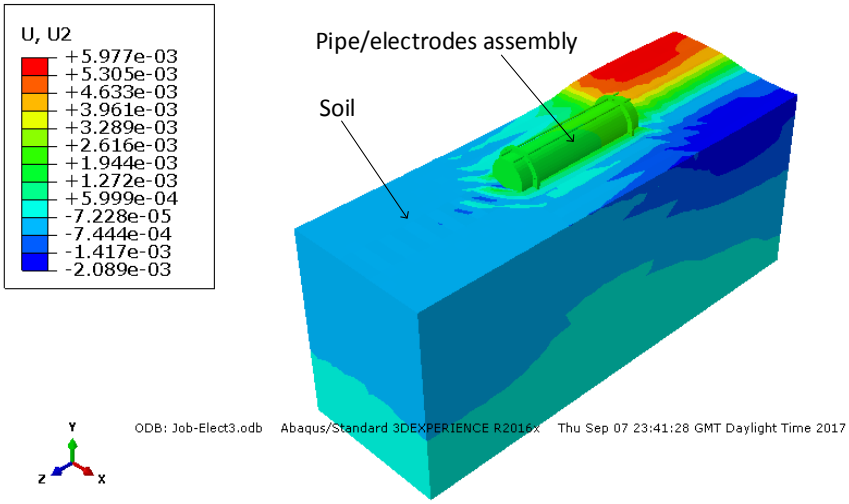

Figure 4-40 Series-3a: contour plot of soil settlement due to EK effect

4.4 Concluding Remarks

This chapter demonstrated the capabilities of the ABAQUS tool for electro-osmotic consolidation analyses as presented in phase-1 and phase-2. Results of the electro-osmotic consolidation process from phase-3 consist of series-1a, 2a, and 3a and for each, the soil behaviour is described. The applied voltage has been the driven force in the EK process. At the start of the analyses, the voltage tend to concentrate within the anodes and decrease with time towards the cathodes. The test demonstrated the effect of the applied voltage. The higher the applied voltage the higher the settlement of soil. This occurs due to higher ion migration resulting in the dissipation of pore water pressure. The time of treatment also plays an important role on the soil settlement. The magnitude of electrical field distribution within the soil depends on the electrodes configuration, electrodes and soil conductivity, types of soil and the applied voltage. The electrode material affect the pore water pressure dissipation and depends on its reaction with the soil minerals being encountered. Further research is required to ascertain these conditions for optimum performance in actual field condition.

From the obtained results, it is shown that the lower voltage can be compensated with a longer treatment time of the soil. The same applies to the numbers of the electrode being employed. The larger settlement occurs beside and below the pipe invert surfaces for all the test series of phase-3. These explained the

increase in soil strength with depth as described in the dynamic analyses. The expelling of the pore water pressure from the soil void led to the increase in soil effective stress. Other factors leading to pore water pressure dissipation from the soil is the electro-cementation [51] which has not been fully captured by ABAQUS tool. This occurs due to the breakdown of chemical particles release from the electrodes into the soil. The process depends strongly on the treatment time, the intensity of the electrical field and configuration of the electrodes. This process also accounts partly to the significant increase in the soil strength and the settlement being obtained.

CHAPTER 5: DYNAMIC PIPE-SOIL INTERACTION ASSESSMENT

The investigation of the dynamic analyses of the pipe-soil interaction is based on comparisons between non-EK and EK treated soil, which is presented in this section. Results obtained in series 1a, 2a and 3a are imported into the dynamic analyses of series 1b, 2b and 3b to assess the EK effect on the dynamic pipe-soil interaction.

5.1 Test Series-1b

The dynamic process in the series-b is a continuation from the electro-osmosis of series-1a. The analyses determine the effect on pipe displacement for both EK and non-EK processes due to vertical penetration and vertical pull-out.

5.1.1 Pipe Vertical Penetration

Results from the dynamic pipe-soil interactions in series-1b are presented in Figure 5-1. The pipe penetration into the soil shows a considerable improvement in the soil. The peak force developed in the soil due to EK when compared with non-EK effect, an increase is witnessed for both the 6- hours and 12-hours treatment time respectively. A peak stress of 201Pa is developed for the non-EK process. At the 6-hour time, a peak stress of 383Pa is observed. A further treatment up to 12-hours produces a peak stress of 596Pa.

Comparing the result with Eton [58] in Figure 5-1, the behaviour of the peak and residual stress for the non-EK and EK processes show a similar trend. However, for the numerical analyses, the residual stress for both the 6-hours and 12-hours period indicates decrease at a penetration depth of 88mm and 92mm respectively. This can be attributed to the region of influence. The residual stress has been an influencing factor as it is the dominant stress experienced.

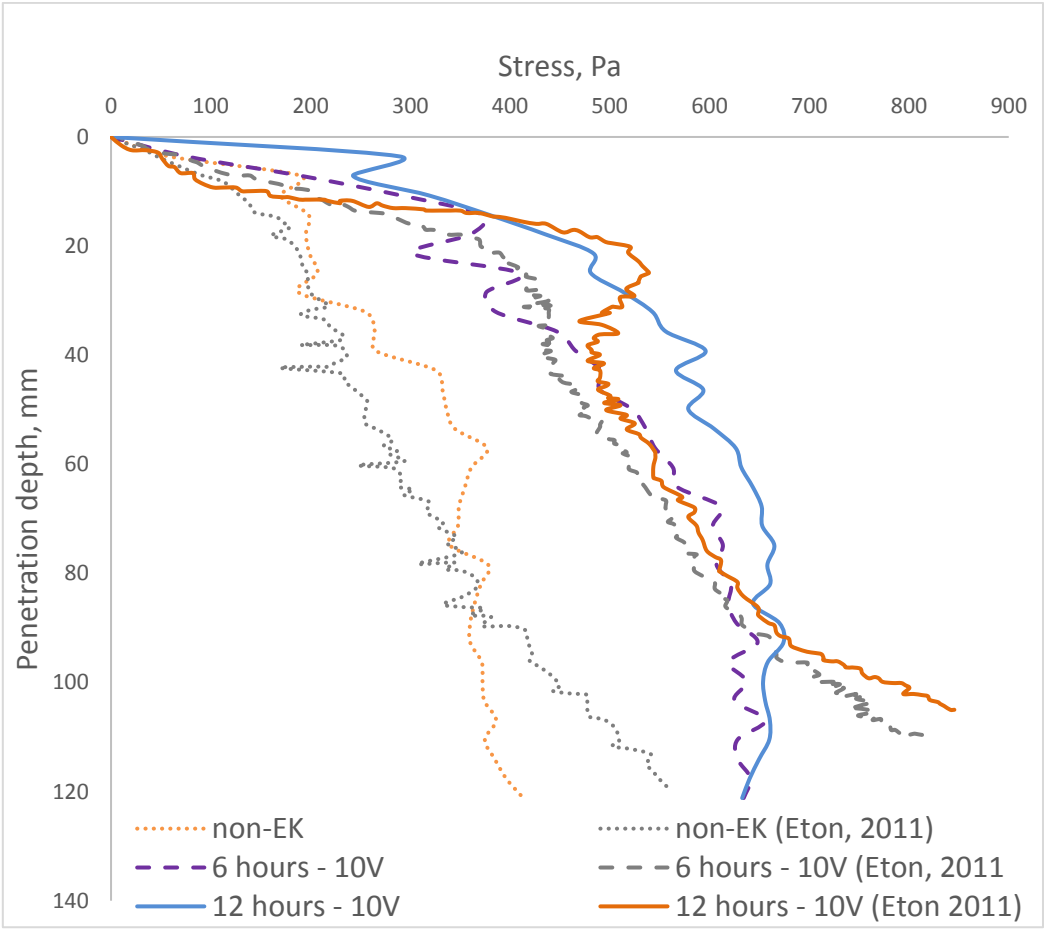

Figure 5-1 Series-1b: stresses enveloped in soil due to pipe vertical penetration.

The numerical results as shown in Figure 5-2 represent 91% and 197% increase in peak stress for the 6-hours and 12-hours respectively. The over 100% increase in the peak stress between the 6-hours and 12-hours is due to the soil consolidation.

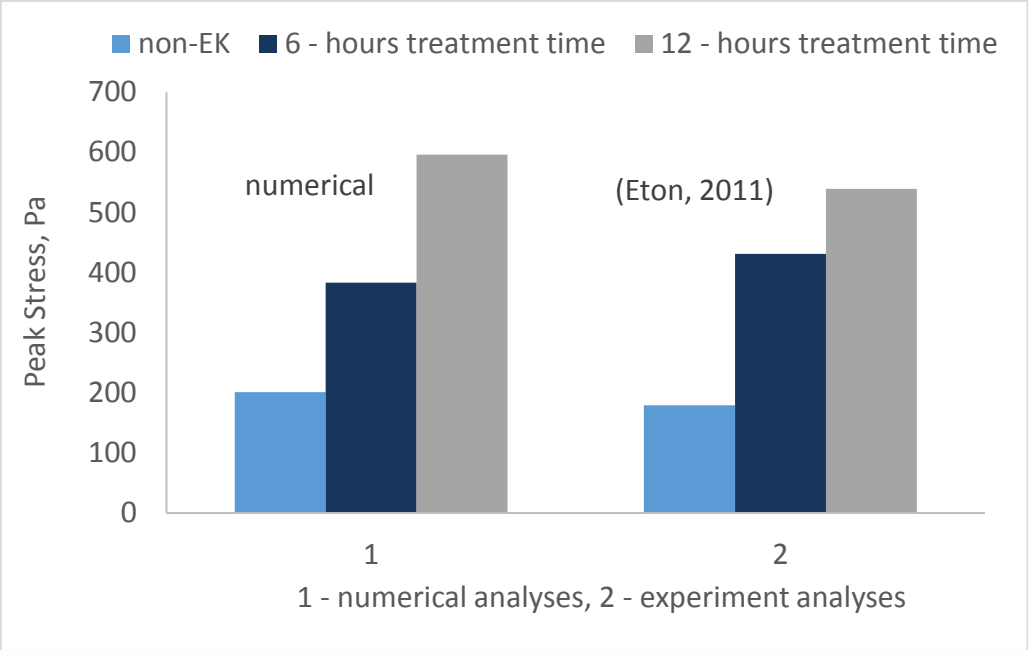

Figure 5-2 Series-1b: comparison of breakout stresses between non-EK and EK and experimental result

5.1.2 Vertical Pull-out

After the treatment time of 12 hours, the pipe was pulled out from the soil and the resulting pull-out force was observed for both the EK and non-EK tests as shown in Figure 5-3. For the non-EK test, a peak (breakout) force of 1.7N with a high stiffness tangent occurs to a distance of 0.95mm before rapidly decayed to a residual force of 0.43N at a distance of 6.8mm. At this point, the residual force decayed slowly. The EK test, however, shows a peak force of 4.65N with a high stiffness tangent which breaks out at a distance of 2.45mm. At this point, the peak pull-out force maintains a steady state to a distance of 4.83mm before rapidly decaying to the residual force of 1.38N at a distance of 12mm. The rapid decay is attributed to pipe movement away from the treatment area and the soil.

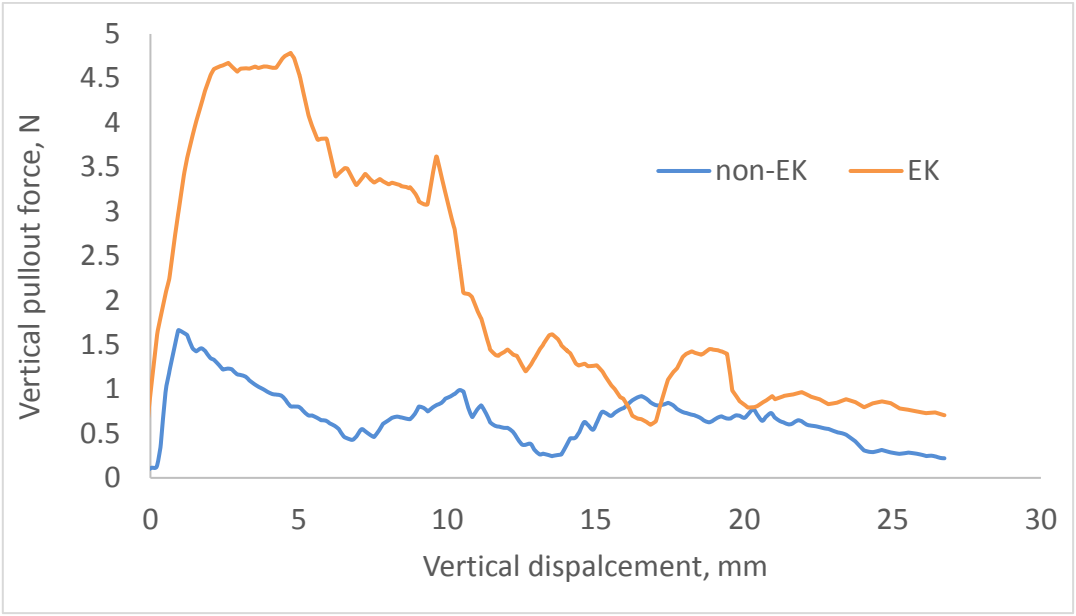

Figure 5-3 Series-1b: forces developed due to pipe vertical pull-out

The force required to remove the pipe from the soil is determined by the soil strength. Results in Figure 5-4 shows an increase of 174% in the peak pull-out force due to the EK effect when compared with the non-EK treated soil.

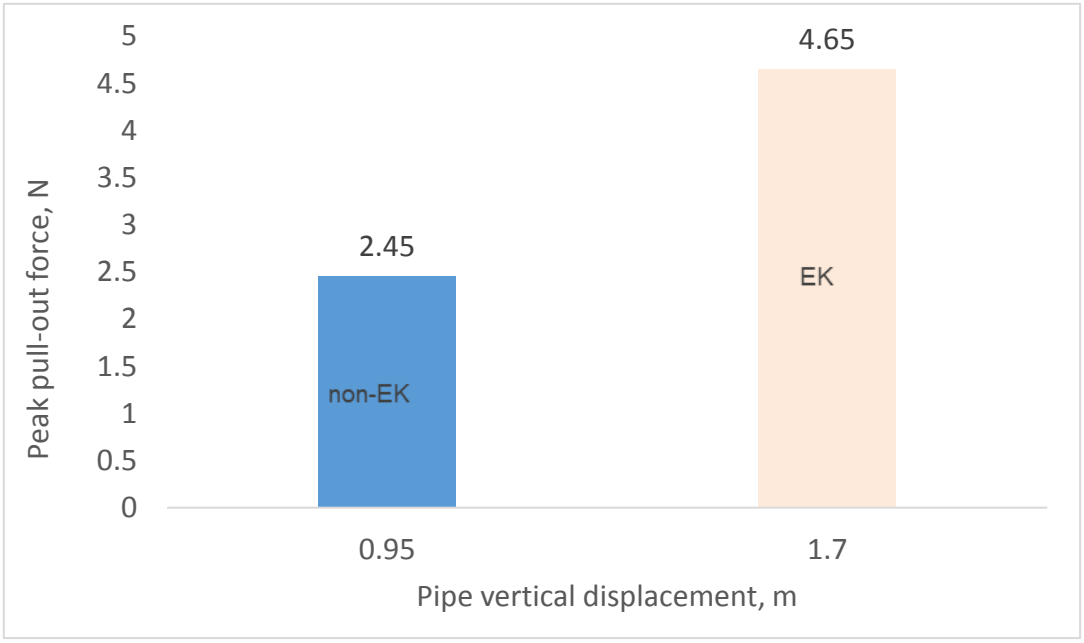

Figure 5-4 Series-1b: non-EK vs EK vertical breakout force

5.2 Test Series-2b

Series-2b indicates results due to soil settlement with variation in voltage, time, and forces developed due to axial pulling of the pipeline. Results from steady-state analyses in vertical, axial and lateral directions are also presented.

5.2.1 Steady State Analysis

5.2.1.1 Effect on Pipe Vertical Penetration

Pipeline vertical penetration behaviour is shown in Figure 5-5. Being a WIP pipe, the formation of heave around the pipe surface is minimal. A greater penetration force and behaviour may be experienced for a PIP than WIP pipe due to the formation of heave within the soil perimeter. Heave formation increases the pipe contact area with a resulting increase in resistance to displacement. However, as initially stated in previous sections, the WIP pipe is employed to allow for anodes-soil contact. The comparison of non-EK and EK processes under the same condition as shown in Figure 5-8 defines the effect electro-osmotic consolidation have on pipe displacement. The penetration velocity of the pipeline as described in Figure 5-6 indicates slight fluctuations with depth.

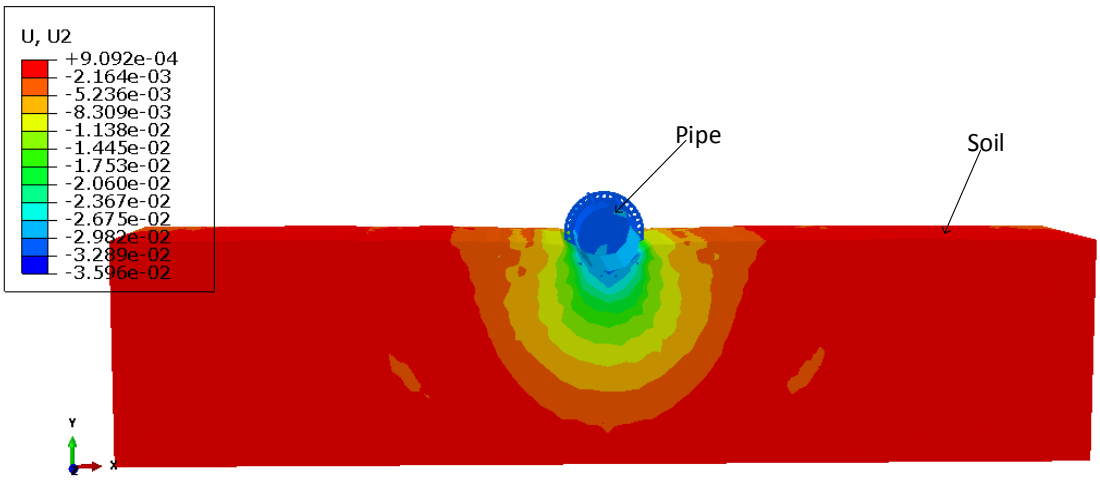

Figure 5-5 section view showing a contour plot of pipe vertical penetration

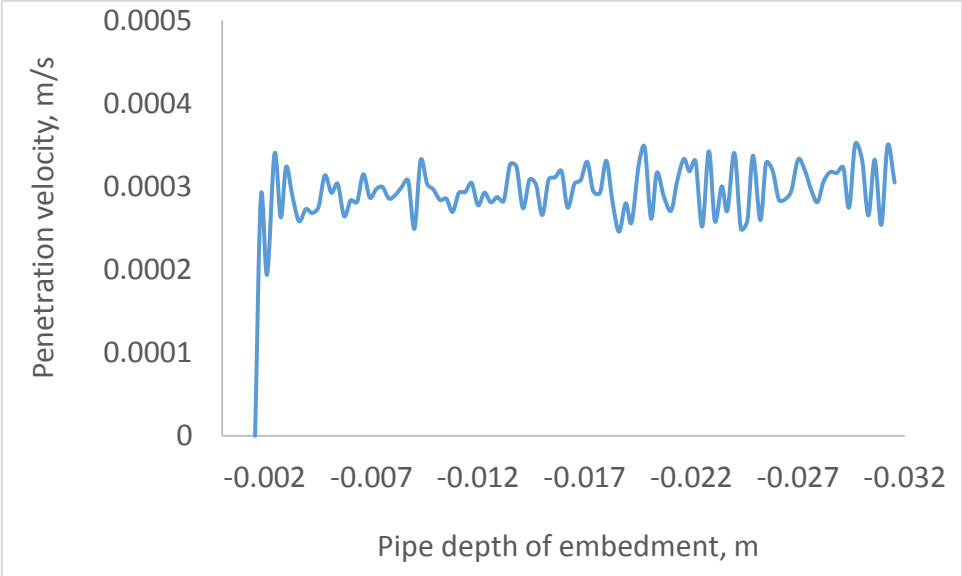

Figure 5-6 Pipe penetration velocity with depth

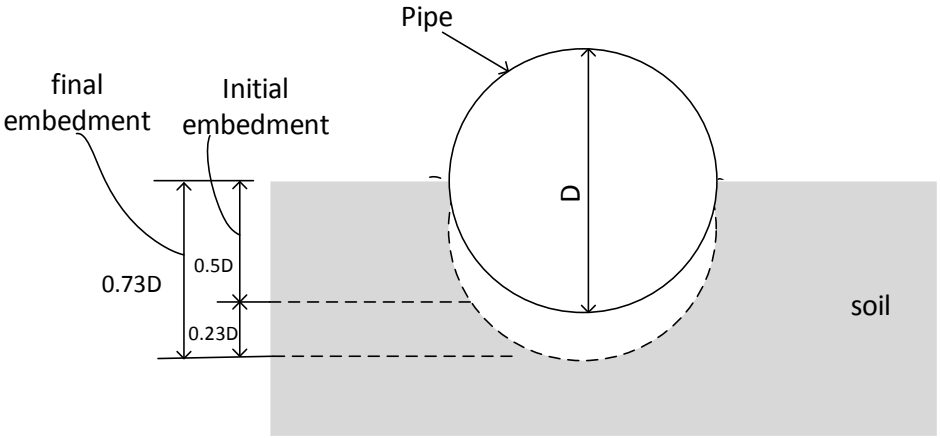

Figure 5-7 Description of pipe embedment due to vertical penetration

Figure 5-7 shows the initial and final position of the pipe embedment at 0.5D and 0.73D respectively. The reaction of the pipeline due to vertical penetration into the soil is shown in Figure 5-8. The penetration behaviour shows a gradual increase in resistance with embedment of the pipe. For the non-EK process, the penetration force increases to 79N before breaking at a depth 0.083m (z/D = 0.64) while the EK process shows an increase of 160N before breaking at 0.081m (z/D = 0.62). The pipe vertical penetration indicates approximately over 103% increase in the penetration force due to EK treatment of soil.

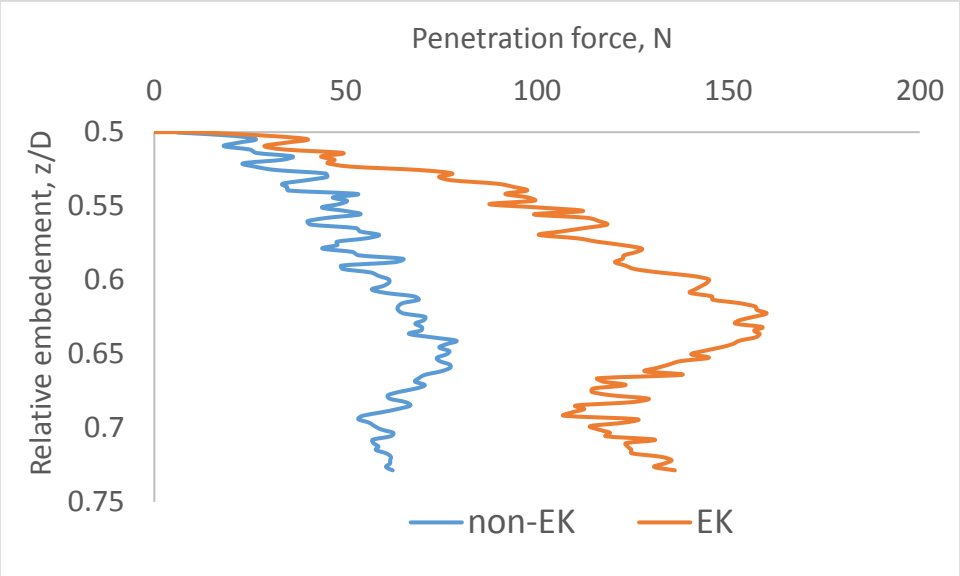

Figure 5-8 Series-2b: forces developed due to pipe vertical penetration with depth

5.2.1.2 Effect on Pipe Axial Displacement

The pipeline shows axial displacement with uniform velocity. At the initial embedded depth of 0.065m (0.5D), the pipe experiences gradual penetration to the final embedment of 0.1m (0.77D) as described in Figure 5-9 and Figure 5-10. The embedded depth increase as the pipe moves away from the EK treated zone. The force-displacement behaviour is described further in Figure 5-11.

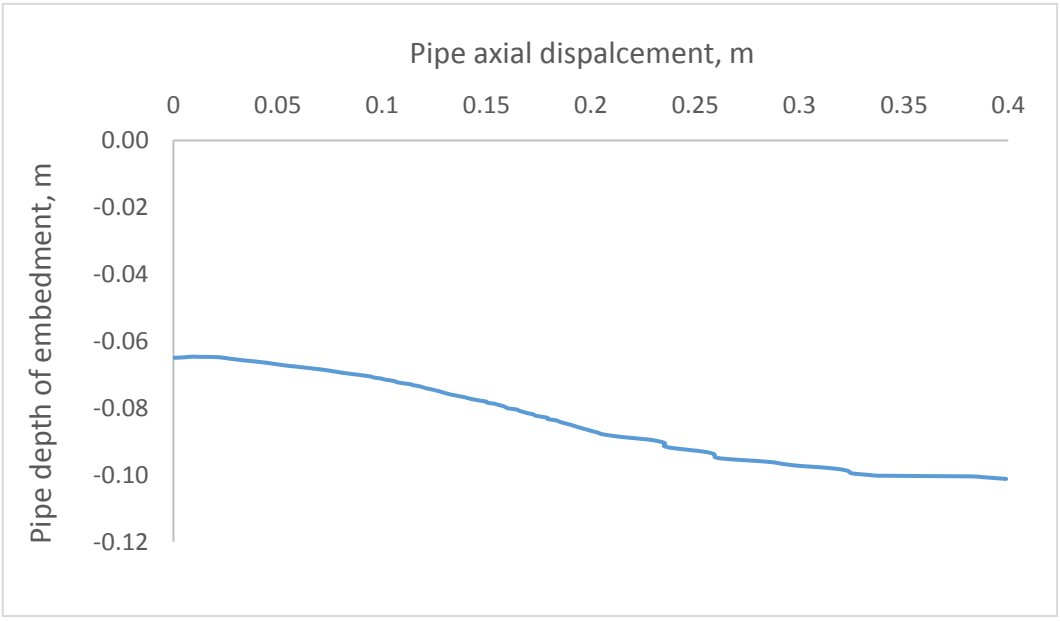

Figure 5-9 Embedment of the pipe due to axial displacement

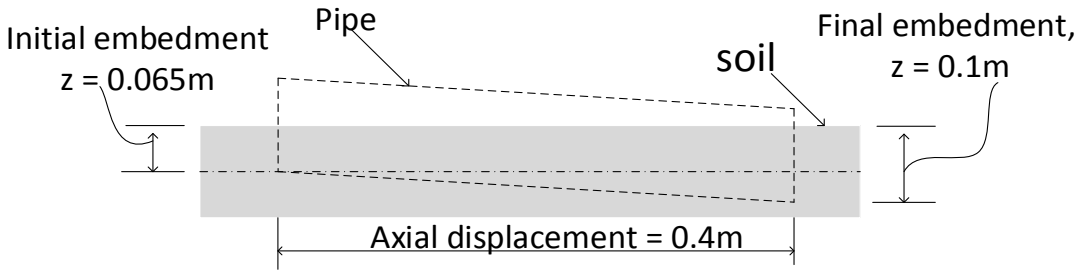

Figure 5-10 Description of pipe position due to axial displacement

Axial tests of the pipe-soil interaction were executed on non-EK and EK treated soil under same conditions. Results obtained were compared with experiments performed by Eton [58]. From Figure 5-11, the non-EK treated soil experiences high initial stiffness tangent which gradually reduces towards the breakout (peak) force of 93N at distance of 19mm, greater than 63N obtained by Eton [58]. At the peak resistance, the breakout force rapidly decayed to a residual force. However, the EK treated soil, experiences a peak force of 207N at distance of 37mm, more than 182N obtained by Eton [58]. The dominant resistance is the residual force, steadily experienced throughout the duration of pipe displacement. Hence, this determines the behaviour of the pipe displacement due to the effective force.

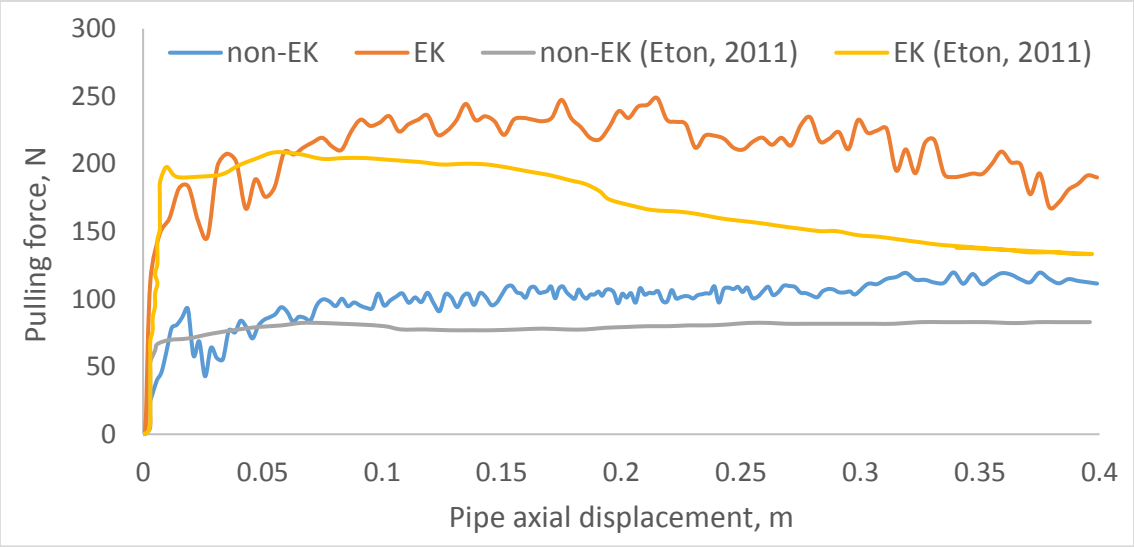

Figure 5-11 Series-2b: EK effect on axial pipe displacement

A comparison between EK and non-EK treated soil for the axial displacement of pipe; a 123% increase in the breakout force is achieved as shown in Figure 5-12.

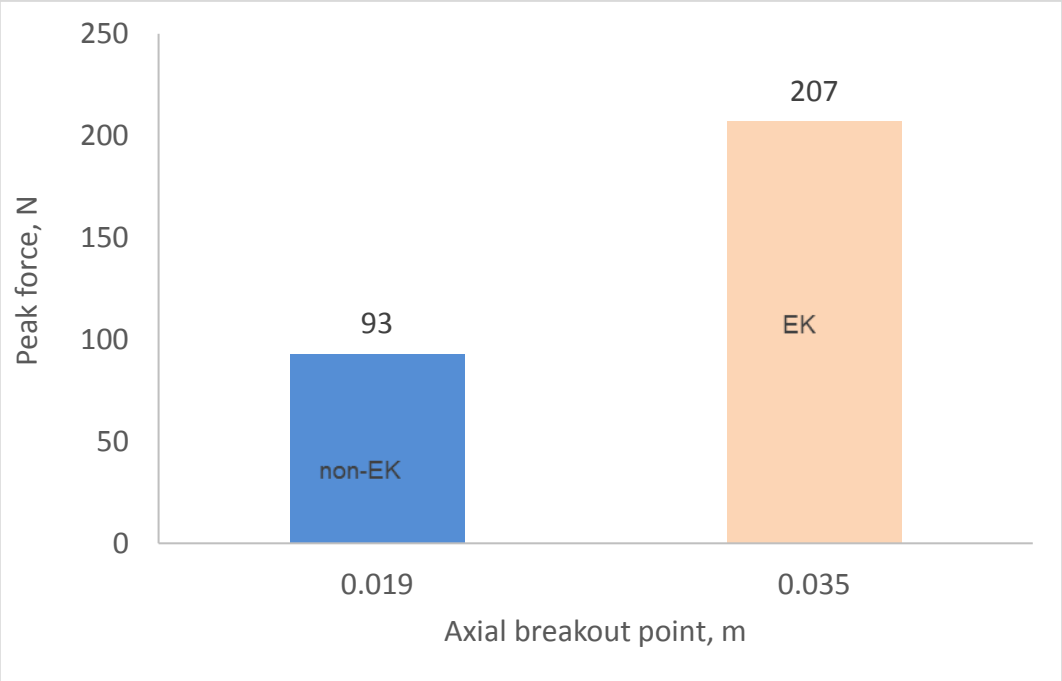

Figure 5-12 Series-2b: non-EK vs EK axial breakout force

5.2.1.3 Effect on Pipe Lateral Displacement

The pipe displaces laterally with uniform velocity. The lateral displacement account for the pipe final embedment at 0.146m (1.12D) from its initial WIP position are shown in Figure 5-13 and Figure 5-14. The pipe embedment indicates increase as the lateral displacement moves away from the treatment zone. The resultant effect on resistance developed against pipe displacement is shown in Figure 5-15.

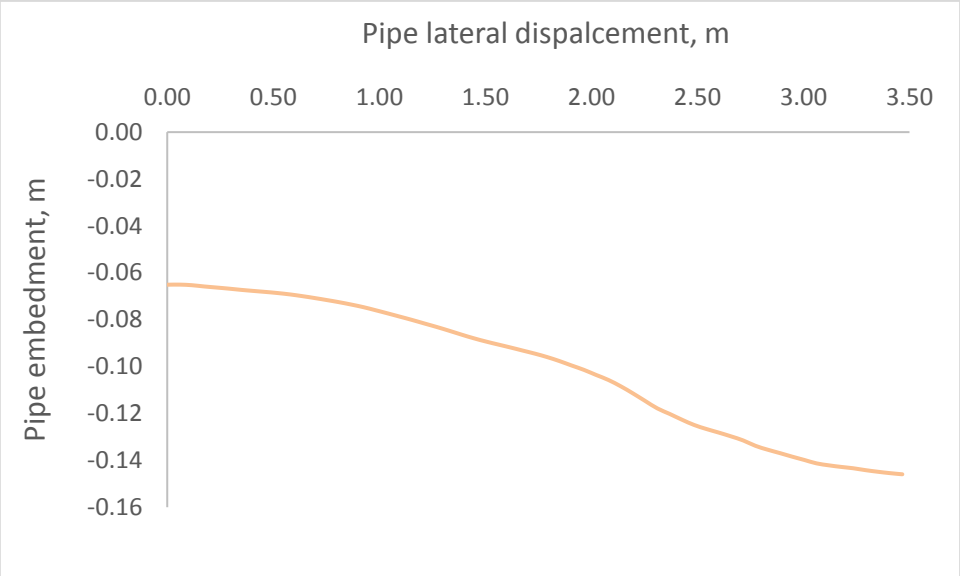

Figure 5-13 Embedment of the pipe due to lateral displacement

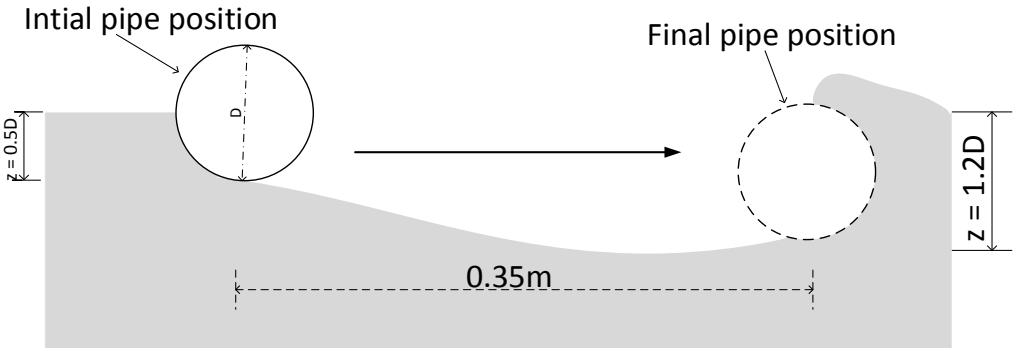

Figure 5-14 Description of pipe position due to lateral displacement

The lateral displacement of the pipe on both non-EK and EK treated soil and the corresponding resistance is shown in Figure 5-15. Results obtained were compared with an experiment performed by Eton [58]. The behavoiur shows a similar trend with the axial pipe displacement discussed in section 5.2.1.2. A comparing between the numerical and the experimental result shown in Figure 5-15, the numerical model indicates a higher peak force of 11% for the EK treated soil than the experiment.

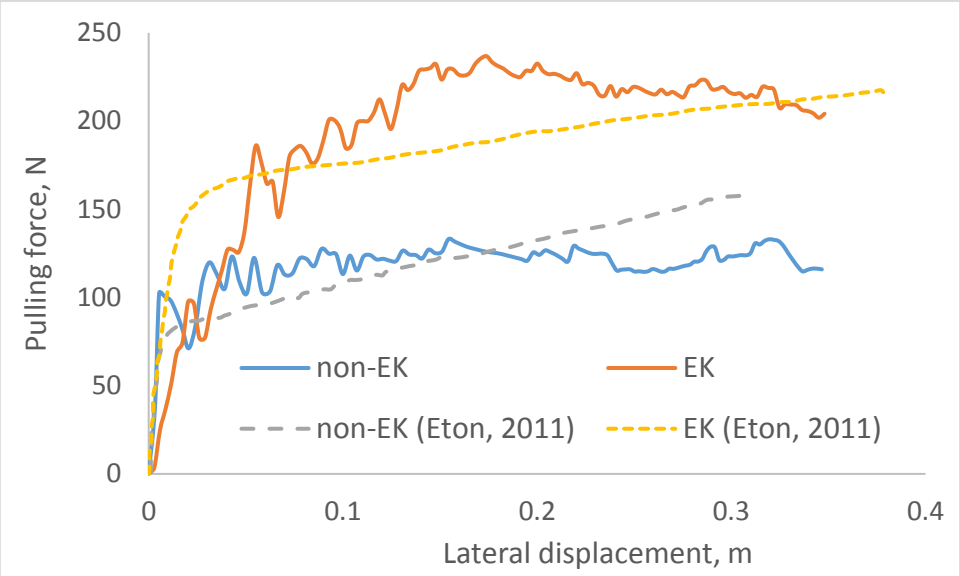

Figure 5-15 EK Series-2b: effect on lateral pipe displacement

Figure 5-15 shows a breakout force of 103N occurs at a distance of 5mm for the non-EK treated soil which is greater than 81N obtained from the experiment and 186N for the EK treated soil at 55mm greater than 168N obtained from the experiment. A comparison between EK and non-EK shows over 81% increase in the soil resistance as shown in Figure 5-16. While the experimental result in Figure 5-11 shows continues increase in the residual force with displacement, the numerical result indicates constant residual force as required. This may be attributed to physical conditions during the experiment which tends to alter some of the soil mechanical properties.

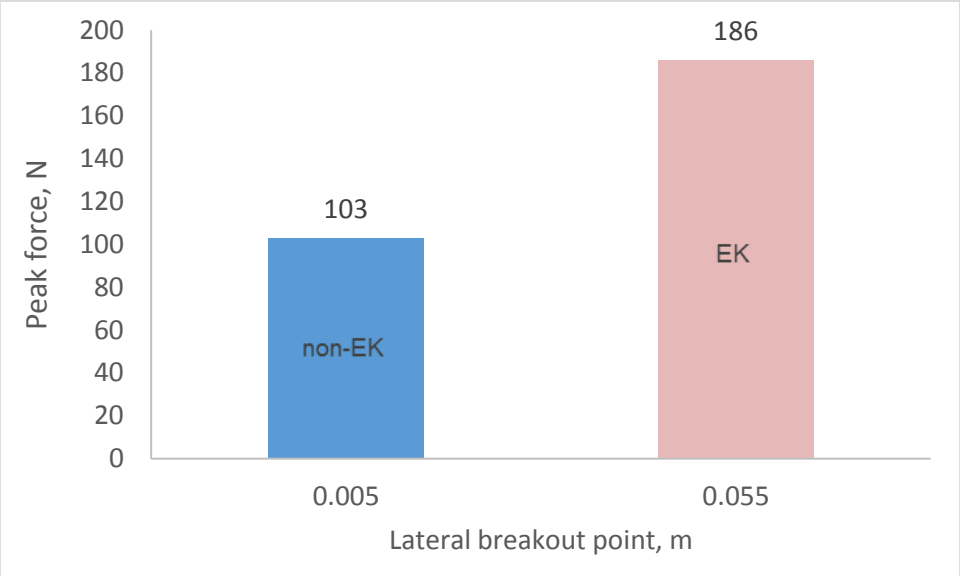

Figure 5-16 Series-2b: non-EK vs EK lateral breakout force

5.2.2 Transient Analyses

5.2.2.1 Effect of Treatment Time

The resultant effect on pipeline displacement in the axial direction due to treatment time is shown in Figure 5-17. The axial pulling force developed indicates the influence in which the duration of treatment will have on soil consolidation. The soil undergoes a treatment times of 6, 12, and 24 hours at a constant voltage of 10V. As the treatment time increases, the soil settlement also increases as discussed in section 4.3.2.4.3. Due to the soil settlement, the axial pulling force required to pull the pipeline increases with the treatment time. This signifies an improvement in the soil strength. The pulling force for each of the treatment time is characterized by a peak force and a residual force behaviour as discussed in section 5.2.1.2. As given in Figure 5-17 the peak force generated increases from 93N for the non-EK treated soil to 143N, 146N, and 148N for 6 hours, 12 hours, and 24 hours for the EK treated soil respectively.

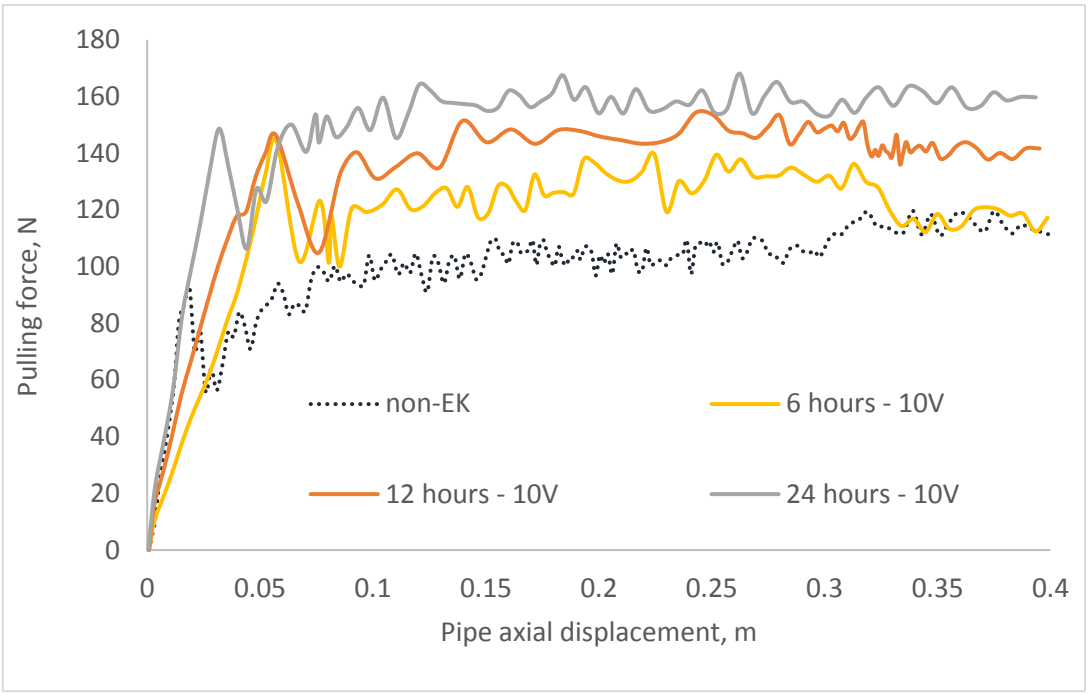

Figure 5-17 Series-2b: effect of EK on pipe axial displacement with time variation

Comparing the EK process for the varying time as shown in Figure 5-18, the soil indicated an increase in the peak (breakout) force of 54%, 57%, and 59% for the 6-hours, 12-hours, and 24-hours treatment time respectively.

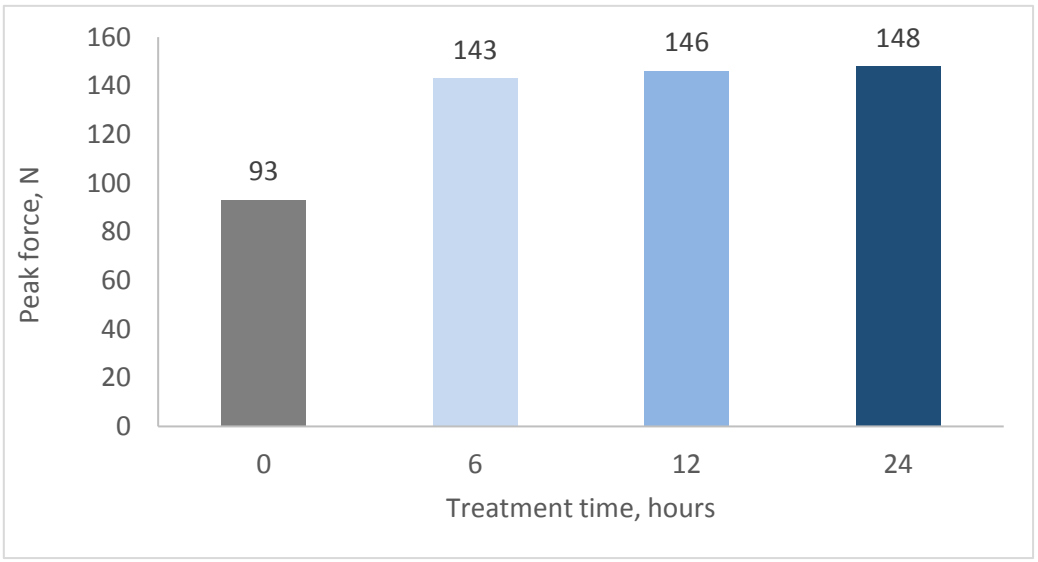

Figure 5-18 Series-2b: breakout forces developed with treatment time

5.2.2.2 Effect of Voltage Variation

5.2.2.2.1 Varying Voltages at Treatment Time of 6-Hours

The axial pulling force developed as shown in Figure 5-19 indicated the significance of increasing voltage on soil settlement. The force required to pull the pipeline increases with increasing voltage due to improvement in soil strength because of the soil settlement described in Figure 4-29. The soil undergoes a treatment time of 6 hours with the voltage increasing from 0 to 12.5V. The pulling force is characterized by peak force and a residual force behaviour discussed in section 5.1.2. As indicated in Figure 5-19, the peak force for 0V (non-EK) is 93N however, as the voltage is applied, the peak force increases to 136N, 143N and 144N for 7.5V, 10V and 12.5V respectively.

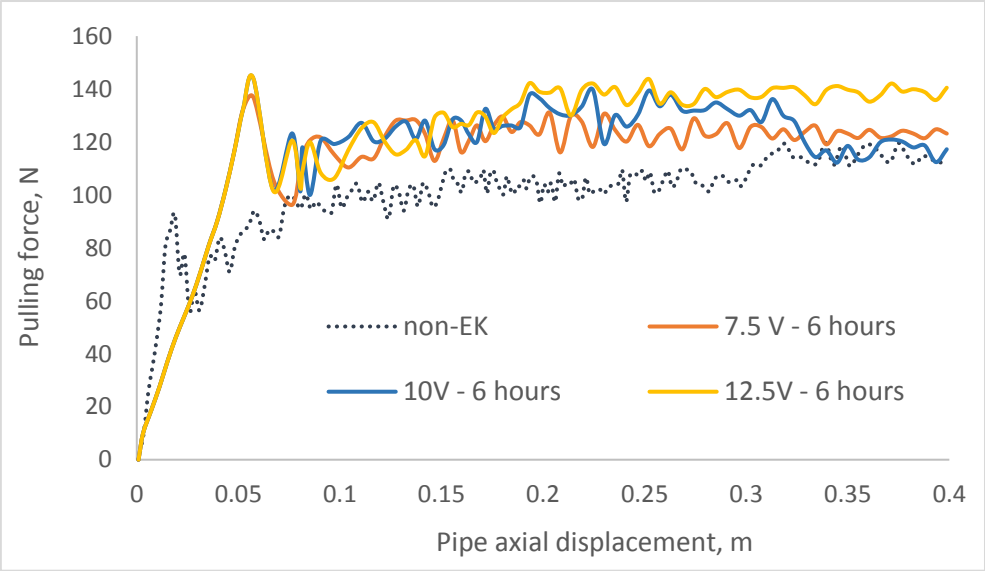

Figure 5-19 Series-2b: effect of soil settlement on pipe axial displacement with voltage variation at 6 hours

Comparisons between the EK and non-EK (zero voltage) as shown in Figure 5-20; there is a 46%, 54%, and 55% increases in the peak force for the 7.5V, 10V, and 12.5V respectively.

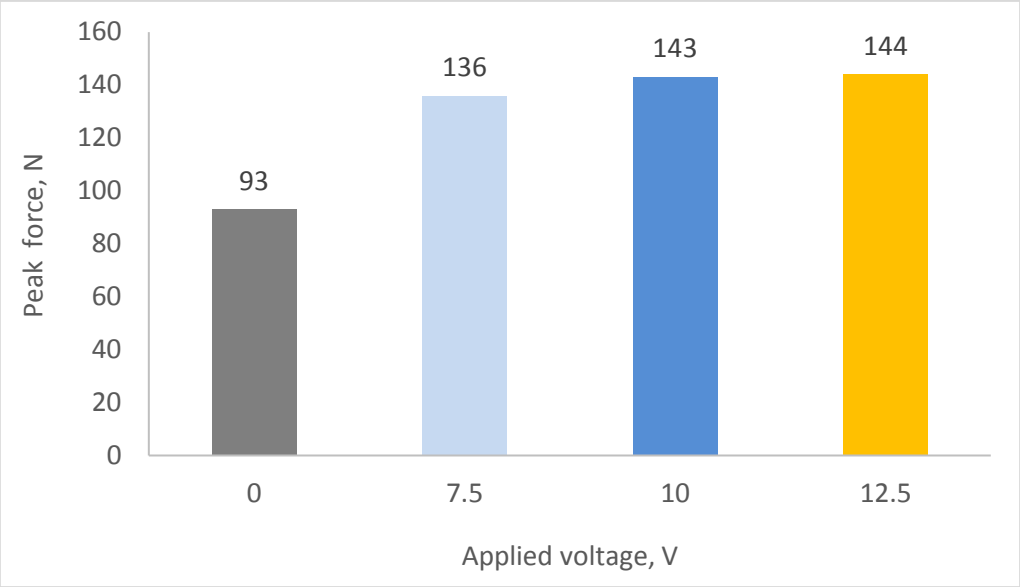

Figure 5-20 Series-2b: breakout forces with voltage variation at 6 hours treatment time

5.2.2.2.2 Varying Voltages at Treatment Time of 12-Hours

Further subjecting of the soil to a treatment time of 12 hours and varying the voltage from 2.5 to 12.5V, the soil indicates a further improvement in the peak and residual force as shown in Figure 5-21. Similar behaviours as previously described in section 5.1.2 were observed. Figure 5-22 indicates a peak force of 96N at 0V, as the voltage is applied, the peak force increases to 143N, 143N and 145N, 146N and 146.6N for 2.5V, 5V, 7.5V, 10V and 12.2V respectively.

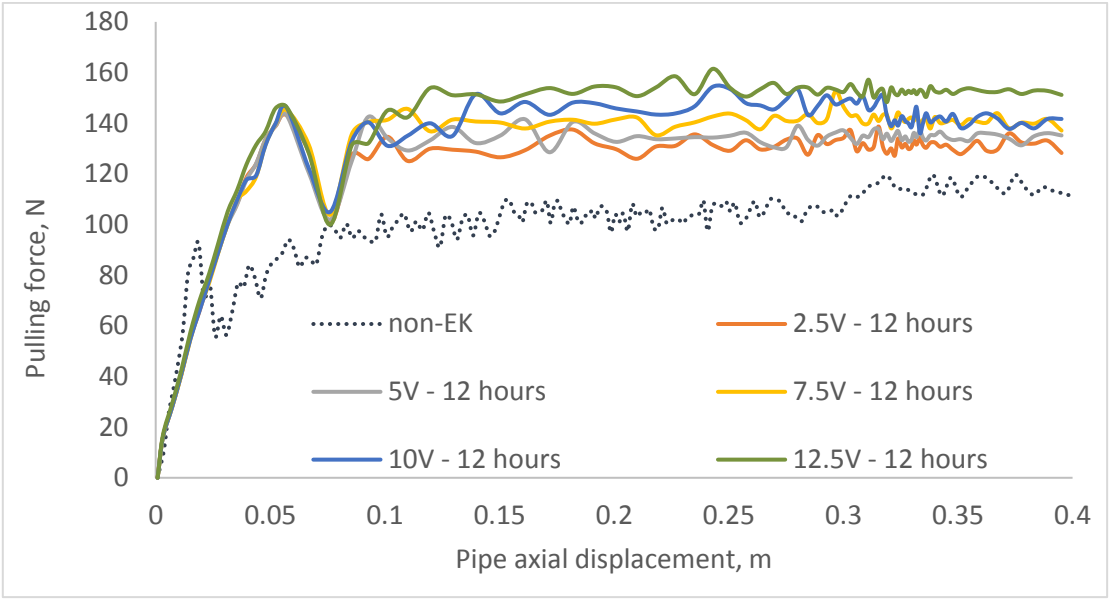

Figure 5-21 Series-2b: effect of soil settlement on pipe axial displacement with voltage variation at 12 hours

Comparisons with the non-EK treated soil as shown in Figure 5-22 indicates 54% increase in the axial pulling force for the 2.5 and 5V. The subsequent increase in voltage shows little increase with significant impact on the residual forces.

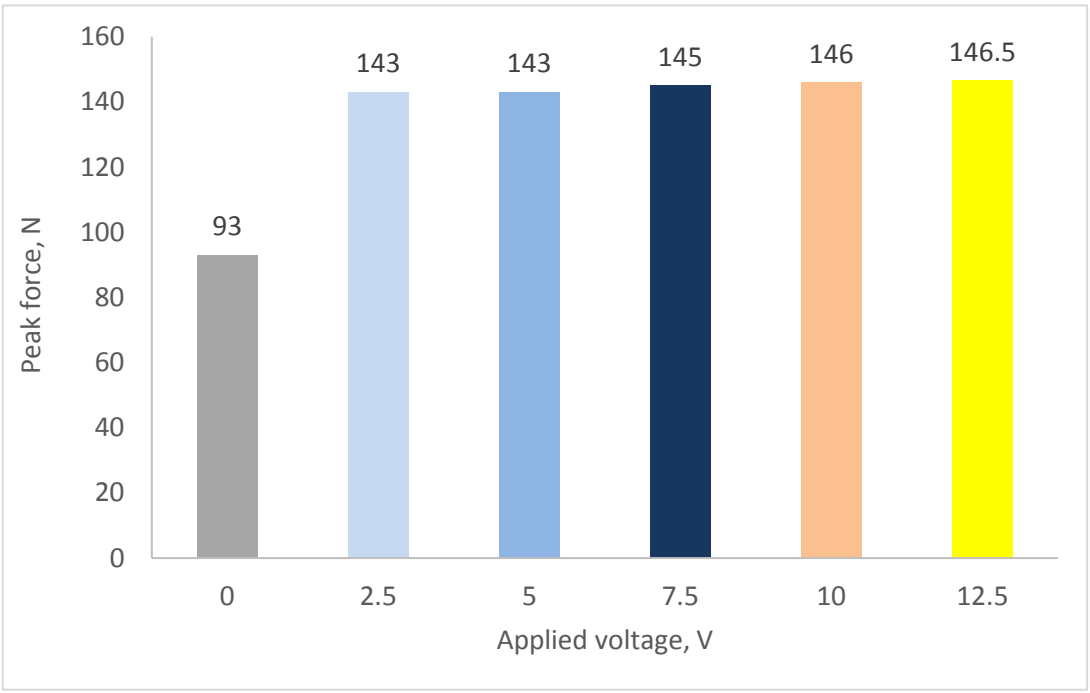

Figure 5-22 Series-2b breakout forces with voltage variation at 12 hours treatment time

5.2.3 Mohr-Coulomb Plasticity Model Test Results

Results obtained from the dynamic analysis using the Mohr-Coulomb soil model are shown in this section. Dynamic analysis of the pipe was executed on both the non-EK and EK process.

5.2.3.1 Effect on Axial Displacement

The axial test of the pipe-soil interaction executed on non-EK and EK treated soil under same conditions is presented here. Results obtained were compared with experiments performed by Eton [58]. From Figure 5-23, the non-EK treated soil experiences a high initial stiffness tangent which gradually reduces towards the breakout (peak) force of 93N which is greater than 63N obtained by Eton [58]. At the peak resistance, there is a brittle breakout force, which rapidly decayed and slowly rise to decay at a residual force. However, the EK treated soil experiences a breakout force of 167N which is less than the 182N obtained by Eton [58].

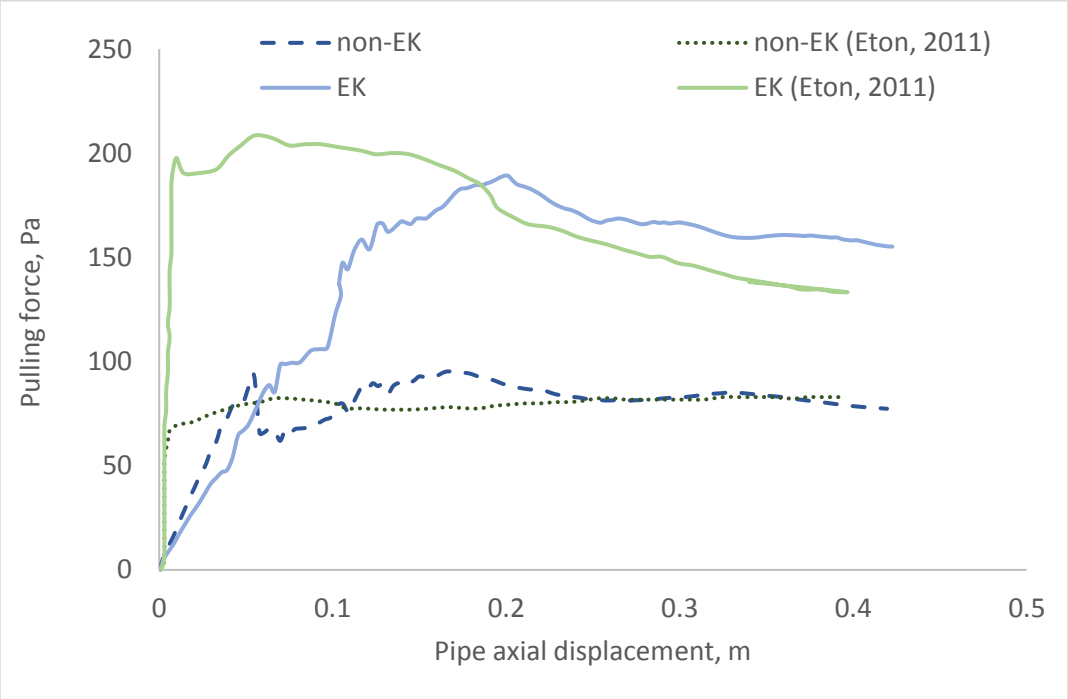

Figure 5-23 Series-2b: forces developed due to axial pipe displacement using Mohr-Coulomb plasticity model

Comparing the EK and non-EK treated soil, an 80% increase in the breakout force is achieved but less than the 190% increase obtained by Eton [58]. As discussed

in section 5.2.1.2., the dominant resistance is the residual force, which is steadily experienced throughout the duration of pipe displacement.

5.2.3.2 Variation with Numbers of Anodes

Tests were also conducted to determine the effect of varying numbers of anodes and their configurations around the pipe. Two, four, and six numbers of anodes were tested as shown in Figure 5-24. It can be observed that the axial pulling force increases with increase in the numbers of anodes. For each of the conditions, the axial resistance shortly experiences a higher breakout force for a few distances, this occurs across the section of pipe when it is about to move. The pipe displacement distance taking to achieve greatest peak force for EK treated soil is greater than that of non-EK treated soil, however, when compared with the same distance and point in time, it can be observed that both the peak and residual force for EK treated soil is always greater**.**

The numbers of anodes four and six show similarities in the residual force with variations in the breakout force, and as stated earlier, the residual force, in this case, determines the displacement behaviour. This gives a prospect of using fewer electrodes to achieve the same result. Electrode configuration may also be attributed to the force-displacement behaviour; this is an area left for further investigation. The breakout (peak) forces variation with numbers of anodes due to axial pulling test for the non-EK process shows an increase of 83N, 88N and 97N for 2, 4, 6 numbers of electrodes respectively. Similarly, for the EK process, an increase in peak force of 130N, 148N and 167N for 2, 4 and 6 numbers of anodes respectively are observed.

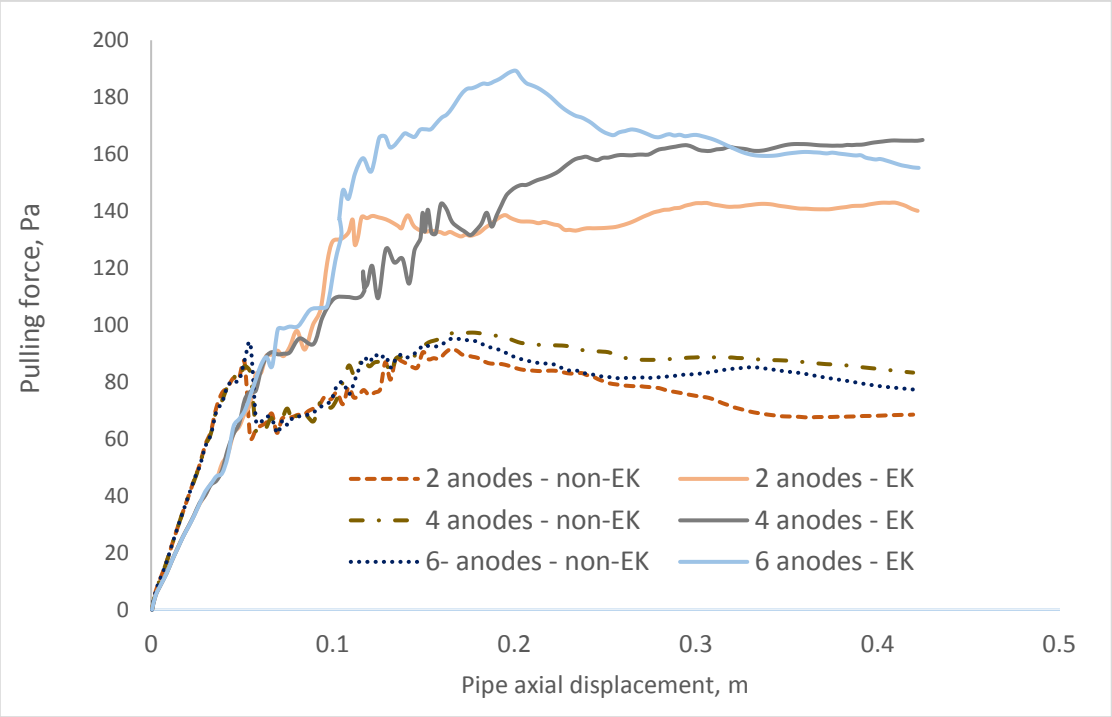

Figure 5-24 Series-2b: axial pulling effect with numbers of anodes using Mohr-Coulomb plasticity model

The increase in the peak force with increase in the numbers of the anode is shown in Figure 5-25. Comparing the EK with the non-EK process, an increase of 63%, 68%, and 80% is achieved for the 2, 4 and 6 numbers of anodes respectively. This behaviour indicates the significance of numbers of anodes in effecting the electro-osmosis process.

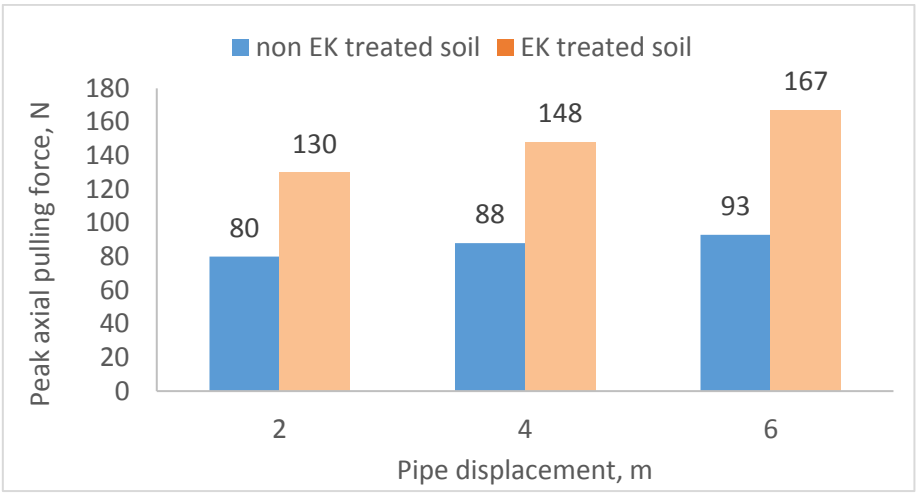

Figure 5-25 Series-2b: breakout forces vs numbers of anodes using the Mohr-Coulomb plasticity model

The improvement in the soil properties shown using the Mohr-Coulomb model indicate its possibilities for soil consolidation analyses except for its limitation at not capturing the pore water pressure and void ratio. This limitation leads to the very small settlement of the soil being observed. The model also indicates less force being obtained than the effective stress model as given in Figure 5-26. This gives credence to using the effective stress model and the couple temperature-pore pressure element to capture soil consolidation. The increase in resistance from the EK process using the Mohr-Coulomb model gives an indication of a little settlement to have a significant improvement in the soil properties.

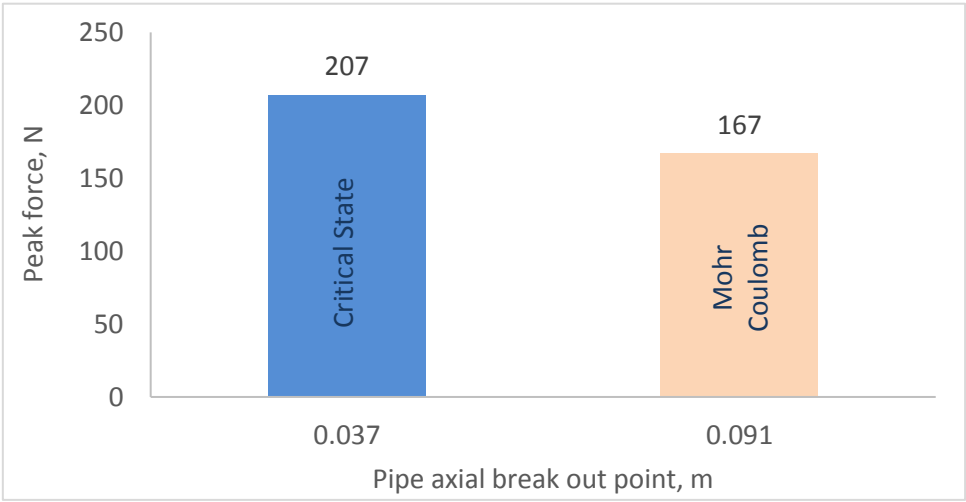

Figure 5-26 Comparison between Critical State and Mohr-Coulomb plasticity model

5.3 Test Series-3b

5.3.1 Effect on Pipe Vertical Penetration

The force-displacement reaction of the pipeline due to vertical penetration is shown in Figure 5-27. Results from the non-EK treated soil are compared with the non-EK experiment by Dingle et al. [100] and non-EK numerical analysis by Dutta et al. [102]. The penetration force shows a gradual increase with depth for all the processes. The EK process shows higher penetration force than the non-EK: approximately 95% increase is achieved.

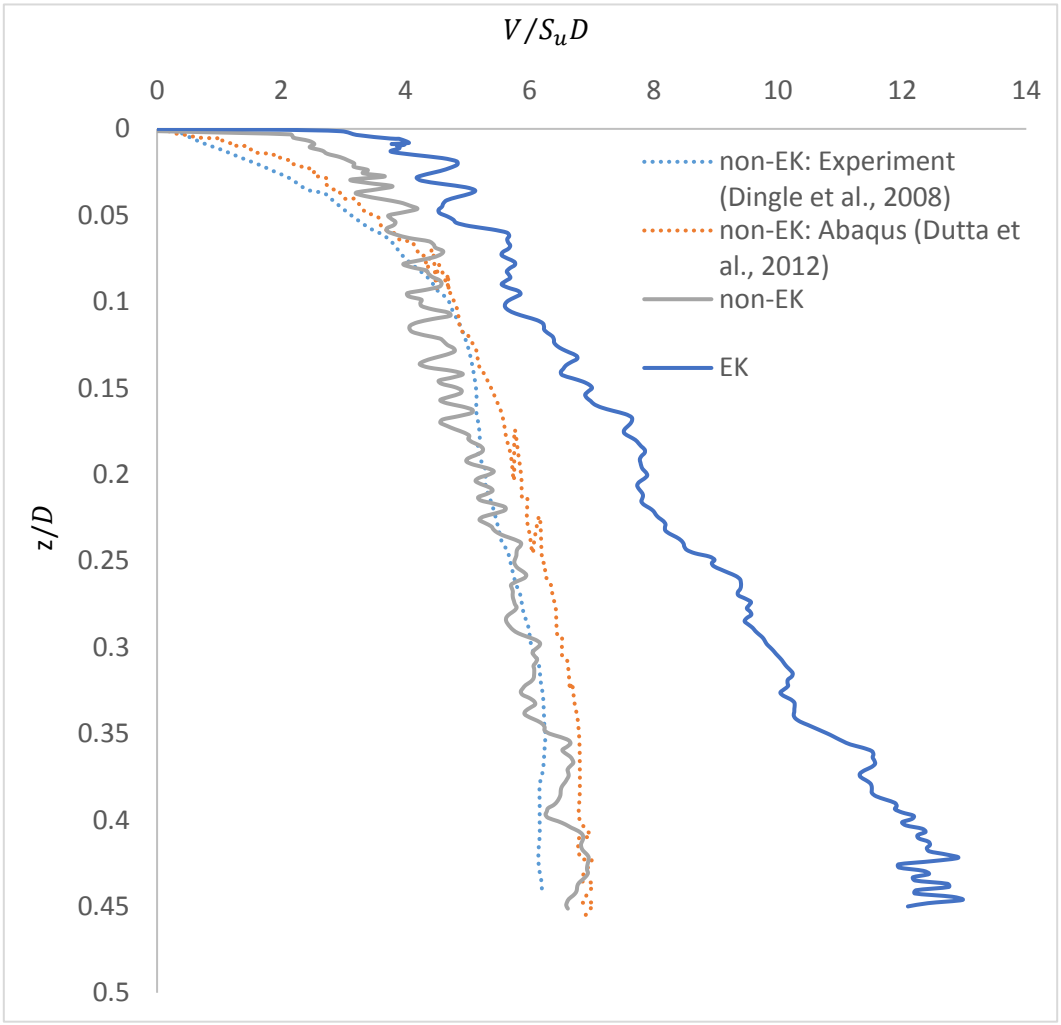

Figure 5-27 Series-3b: forces developed due to pipe vertical penetration

5.3.2 Effect on Pipe Axial Displacement

The pipeline is subjected to axial pulling as shown in Figure 5-28. Pipe displacement behaviour on non-EK treated soil shows a peak force of 5N at a distance of 0.06m. Further displacement of the pipe, the peak force slightly decayed to a residual force of 4.4N. This residual force maintained approximately steady state to a distance of 0.52m before gradually increases. The EK treated soil experiences a peak force of 12.9N, which breaks at 0.055m. Further displacement of the pipe shows a gradual increase in the residual force. This behaviour is attributed to the soil condition and the region influenced by the soil treatment.

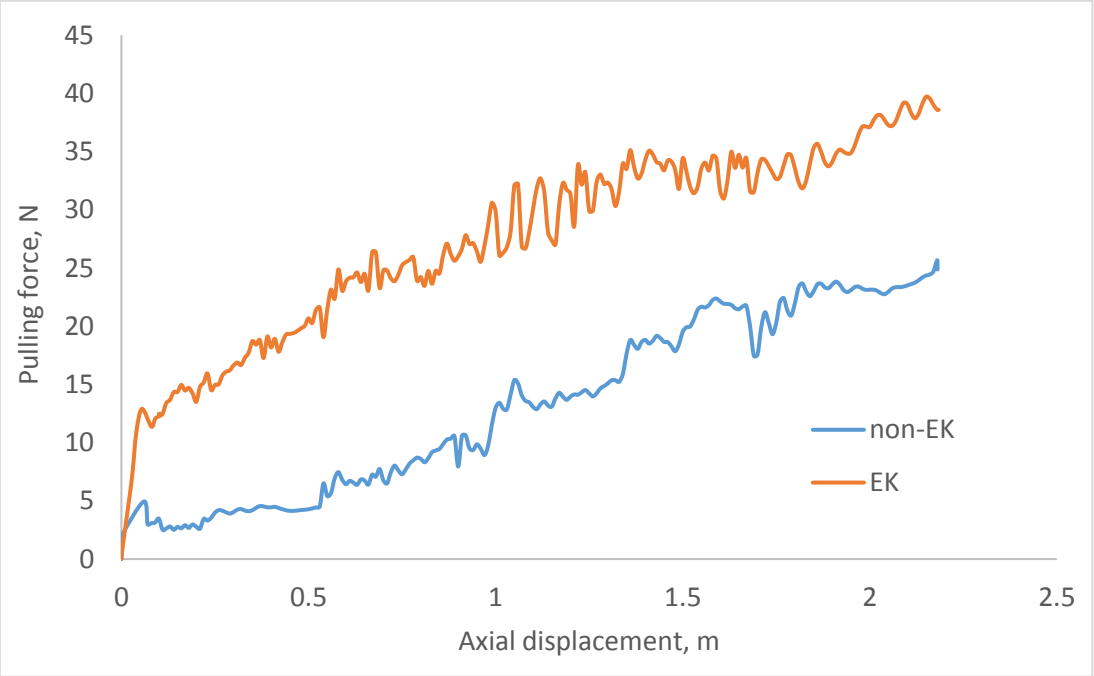

Figure 5-28 Series-3b: forces developed due to pipe axial displacement

A comparison of the axial displacement of the pipe between the EK and non-EK treated soil is as shown in Figure 5-29; a 158% increase in the breakout force is achieved. This increase in the axial pulling force due to EK effect indicates an improvement in the soil strength.

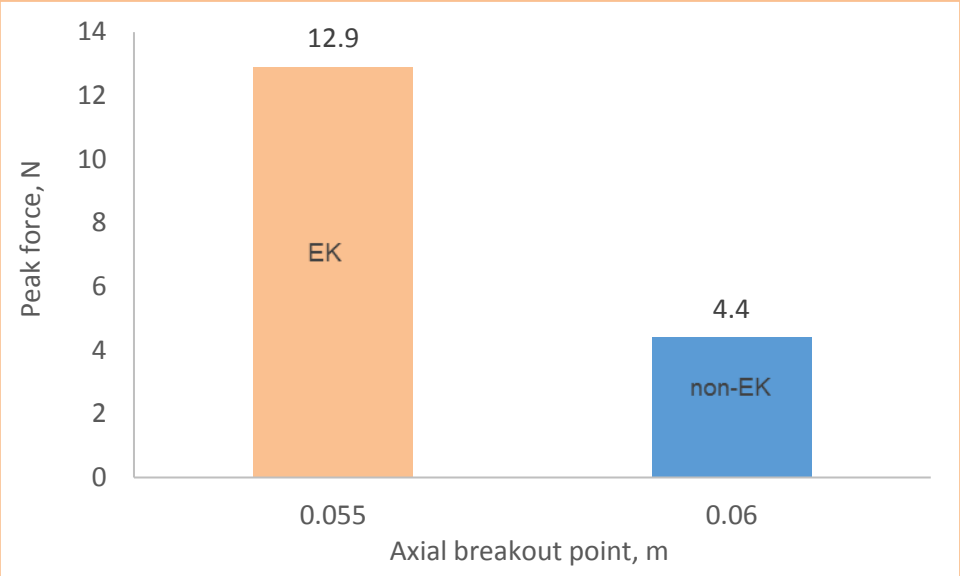

Figure 5-29 Series-3b: non-EK vs EK axial breakout force

5.3.3 Effect on Pipe Lateral Displacement

The lateral pulling test conducted and results shown in Figure 5-30. The peak force for the non-EK treated soil is 4.5N indicating higher stiffness, which breaks at 0.006m. The EK treated soil also shows higher stiffness tangent with the peak force of 11.5N which break at 0.1m. As the break out force is achieved, the residual force for both the EK and non-EK maintain a steady increase.

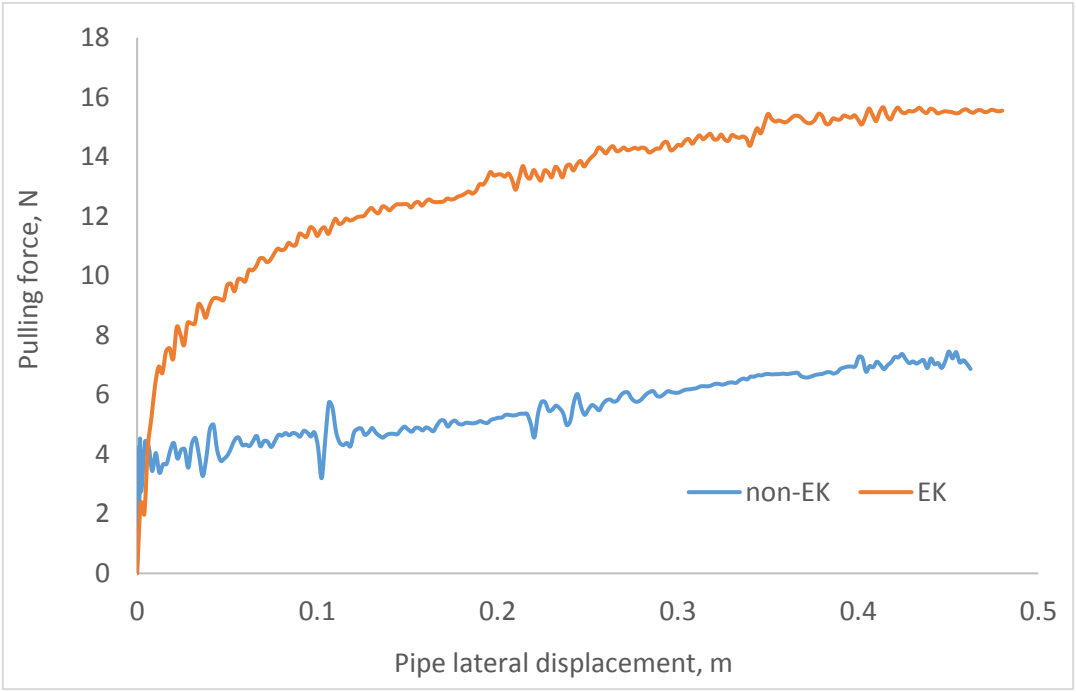

Figure 5-30 Series-3b: forces developed due to pipe lateral displacement

Comparing the EK with non-EK treated soil as shown in Figure 5-31, the lateral peak force due to the EK effect indicated over 156% increase.

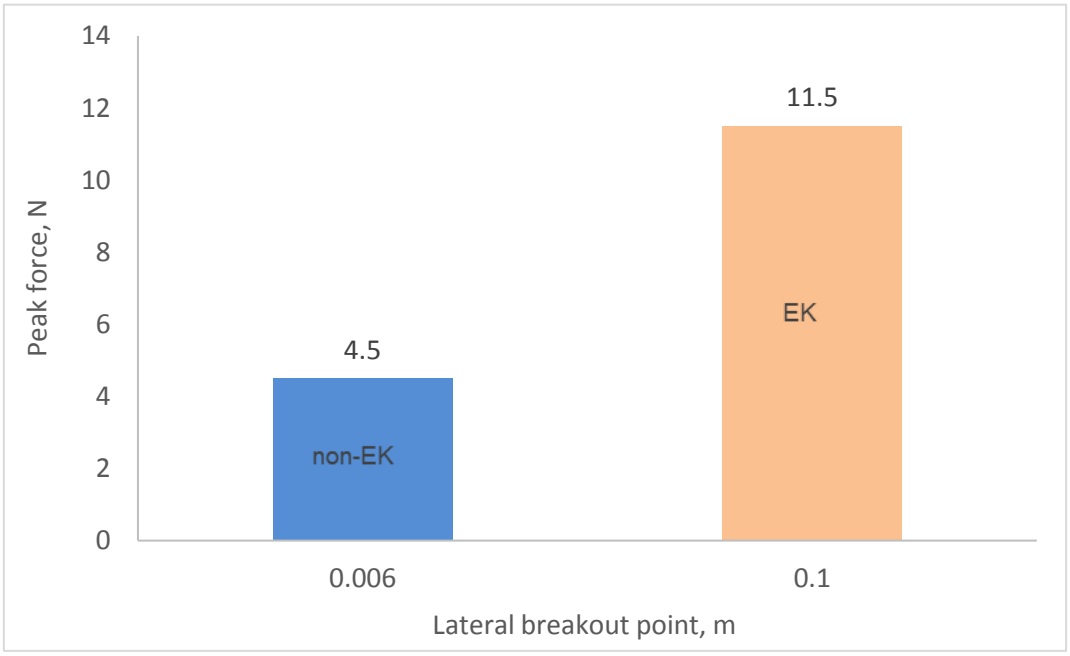

Figure 5-31 Series-3b: non-EK vs EK lateral breakout force

5.4 Field Application

A possible mitigation against pipeline displacement is to increase soil resistance [3–7]. The EK effect has the potential to significantly improve soil strength to serve as a possible mitigating measure. Shear box testing by White et al., (2012) demonstrated the process of increasing axial resistance due to cyclic hardening of soil. This involved pipe shearing on the soil and in the process excess pore water pressure is dissipated. The EK process when compared with soil hardening due to shearing and its own weight; EK process has an advantage in significantly reducing the time for soil consolidation to take place. Result obtained, indicated the influence of EK treatment on clay soil.

This new approach for mitigating against pipeline displacement can be incorporated into a new offshore pipeline design. It is recommended that the EK design should have electrodes attached to the pipeline or pre-installed at certain areas prior to pipeline installation depending on the field conditions and cost of operation. Assessment of the soil properties and the pipeline embedment during installation and in operating condition should be conducted. The assessment will help to determine the electrodes configuration and power requirement for each individual case. Assessment of electrochemical reactions with consideration to the insulation of pipeline and inline structures from interfering with the EK reaction should be a priority. Other areas of possible application are the underwater cables.

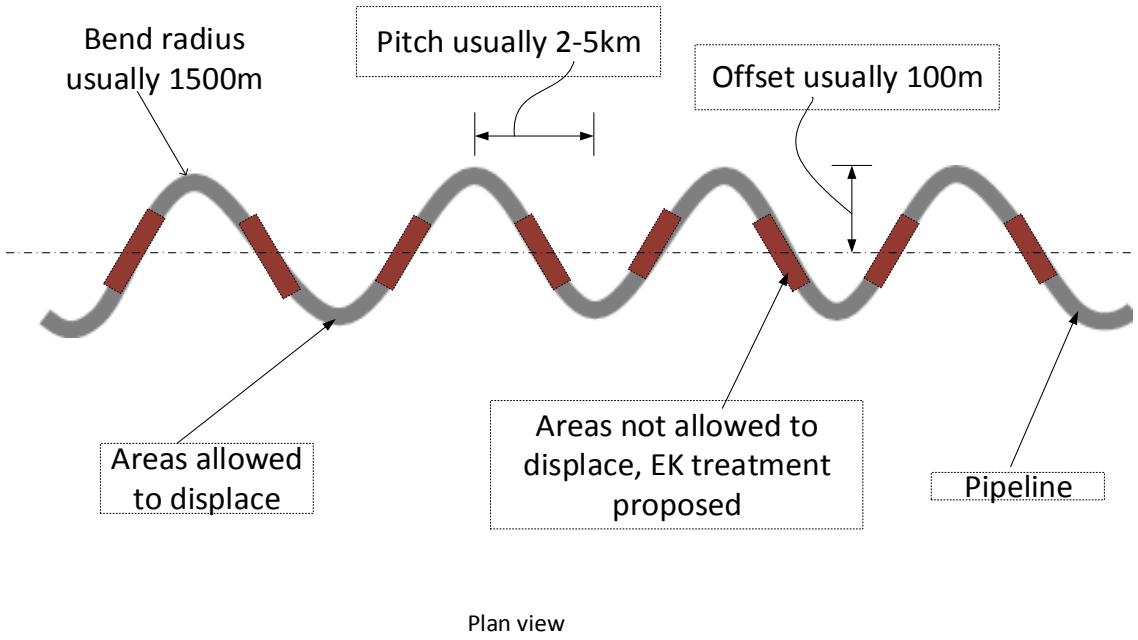

Figure 5-32 Snake Lay pipeline showing possible areas for EK treatment.

The Figure 5-32 shows a snake lay of the pipeline as given by Perinet and Simon [82]. This method helps to reduce axial displacement but with limitation in deep water due to uncertainties in lateral buckling control as stated by Rong et al. [7]. Eton [58] proposed the anchoring point as shown in Figure 5-32, of which pipeline is not allowed to move. In this case, these points can be mitigated with the EK process. Typically short pipeline with a length between 2-5km is usually being affected by pipeline walking [2]. The current subsea capabilities such as the umbilical cable may be used for power supply and control.

Due to the high saline environment, high power consumption will serve as disadvantage using the EK method. However, Eton [58] suggested that consolidation of a small volume of the soil during axial displacement of the pipeline is needed to increase significantly its resistance. This implies that lower power may be required than expected.

5.5 Concluding Remarks

The resultant effect of the electro-osmotic consolidation on dynamic pipe-soil interaction process on both EK and non-EK analyses were considered and results compared. Results from available experiments were also compared with these numerical models. Major areas in the dynamic analyses are the peak and residual forces generated due to the soil treatment. The resultant effect of pipe displacement in vertical axial and lateral direction was also demonstrated. EK treated soil when compared with the non-EK treated soil for both the peak and residual forces shows a significant increase.

Series-1b shows pipeline behaviour due to vertical penetration and pull-out force. The displacement of the pipeline in vertical direction indicates an increase in the soil strength by 91% for the 6 hours and 197% for the 12-hours treatment time. Vertical pulling of the pipeline out of the soil after a treatment time of 12 hours will require an applied force of over 174% from its initial state due to the increase in soil strength. Series-2b which is a large scale of series-1b shows the pipeline behaviour in vertical, axial and lateral directions, similarly, a significant increase in the soil strength is observed. The pipeline witness a 103% increase in the vertical penetration force, a 123% increase in the axial pulling force and an 81% increase in the lateral pulling force. The transient analyses of this large-scale model also indicate the effect of soil treatment time and voltages. The duration of treatment has a significant impact on the soil strength with greater considerations to the applied voltage. Series-3b also described the pipeline behaviour in vertical, axial and lateral direction. A 95% increase in the vertical penetration force, a 158% increase in the axial pulling force and a 156% increase in the lateral pulling for the pipeline are observed.

Strength profile for all the series also indicates linear increase with depth attributed to the soil properties and the EK effect. Comparison with experimental data also indicates similarities. Effective stress (Cam-Clay) and Mohr-Coulomb model were considered with the effective stress model showing good behaviour with regards to soil settlement. A gradual and slight increase in the resistance to pipe displacement is observed with increase in voltage. The time of treatment

greatly impact on the soil consolidation with greater resistance to pipe displacement being observed as the time of treatment increases. A slight increase in the force is also observed with increase in the numbers of electrodes. For better performance in service, the determination on the numbers of electrodes, applied voltage and the treatment time has a significant impact on the electro-osmotic consolidation of the soil to mitigate against pipeline displacement

CHAPTER 6: CONCLUSION

The main aim of this study is to investigate the EK effect on pipe-soil interaction and the major objectives have been achieved. A review of the electro-osmotic consolidation of clay soil, the pipe-soil interaction behaviour in vertical, axial and lateral directions and the current mitigation process against pipeline displacement were considered. The numerical investigation of the EK effect on pipe-soil interaction using the ABAQUS commercial software tool and its capabilities for the EK process have been demonstrated. Numerical models developed for the analyses and the procedures adopted were detailed in Chapter 3. Chapter 4 detailed the soil settlement due to electro-osmotic consolidation considering both transient and steady state.

The sensitivity of the electro-osmotic consolidation with variations in voltages is considered with consideration to numbers of electrode/electrodes configurations. Different spacing, numbers, and arrangement of the electrodes were also considered. Chapter 4 demonstrated the effectiveness of the EK process on the applied voltage, time of soil treatment and strength developed. The behaviour of the electrical field and pore water pressure within the soil leading to the decrease in the soils void ratio and increase in effective stress were demonstrated. Applied voltage significantly affects the consolidation process and the impact is greatly dependant on the duration of treatment.

The dynamic pipe-soil interactions were also conducted and their resultant effects determined. The behaviour of the pipe displacement for both the non-EK and EK process indicated a peak (breakout) and residual force. The peak force for each of the test series in axial directions indicates a rapid decay of the peak force at a short distance before it gradually decayed at the residual forces. The residual forces have been the dominant resistance during the pipe displacement for all of the test series in vertical, axial and lateral directions. The strength of the soil is determined for both EK and non-EK treated soil and the results obtained are then compared. Results indicate an increase in soil strength due to the EK treatment when compared with the non-EK. A comparison with field data also shows agreement with the current results.

As obtained in the consolidation assessment, the strength in the soil due to the vertical, axial and lateral displacement of the pipe also indicated increase with an increase in the consolidation time. This also applies to an increase in voltage. The soil settlement due to voltage increase is minimal when compared with an increase in time. In this case, the soil tends to show higher strength with increase in time than with an increase in voltage. Hence, a balance between treatment time and minimum applied voltage to achieve the same result should be established.

The considerable increase in soil strength due to the EK effect gives the feasibility of using the process to enhance pipeline stability and underscores the success of this study.

6.1 Research Novelty

The numerical modeling of this study successfully demonstrates the capabilities of the ABAQUS software tool using the coupled temperature-pore pressure element/procedure to mimic the coupled electrical-pore pressure for electro-osmotic consolidation analyses.

The numerical approach in this study considers the electro-osmotic consolidation along the tangential surface of the pipeline with varying voltages and time. Both steady-state and transient analyses were assessed.

The novelty also has been the successful incorporation of the dynamic pipe-soil interaction into the electro-osmotic consolidation to determine the behaviour of pipe displacement in vertical, axial and lateral directions. A significant increase in the soil resistance to pipeline displacement has been achieved with this concept.

This concept serves as a new approach for the stability of pipelines and could be attractive for the stability of dynamic cables laid on a seabed.

6.2 Study Significance

Industry requires a less conservative design approach and cost-saving measure with regard to capital expenditure by understanding the behaviour of pipe-soil interaction [3]. The EK process will lead to less requirement for complex and

expensive pipeline mitigation. This should also serve as a benchmark for further research on the stability of pipeline and other offshore structures.

6.3 Further Studies

Some areas that require further studies to have a better understanding of the EK effect on the pipe-soil interaction behaviours are stated below:

- considerations to cyclic loading, to determine if the higher shearing rate may cause additional pore pressure and cancel out the hardening effect as suggested by White et al [6]. It is not clear what the effect of this cyclic movement would be on the EK modified soil.
- Prediction of the full load-displacement response of pipeline through its operating life, by understanding the axial mobilization displacement and how much of it is recovered elastically when pipeline movement reverses. This is significant to pipeline design.
- Studies with other velocities and other stress conditions under pipe as pipeline displaces with varying velocities and loading conditions.
- Investigation of the numbers of electrode/electrode configurations, merit further research to have clarity on the optimum numbers of electrodes to minimize complexity and save cost.
- Area influenced by electrical field need further investigation to determine its effect with depth and the horizontal distance across the soil. This will determine the maximum distance to be affected and the strength developed with distance from the treatment zone.
- Application of EK process on the stability of subsea cables.
- Economic feasibility assessment in the subsea environment
- This test considers Kaolin clay only. The EK effect on different soil properties and the resultant behaviour should be considered and compared.
- Study on the electrochemical effect on pipeline due to the highly corrosive saline environment.

REFERENCES

[1] Perinet, D., and Frazer, I., 2006, “Mitigation Methods for Deepwater Pipeline Instability Induced by Pressure and Temperature Variations,” Proc. Offshore Technol. Conf., (17815–MS).

[2] Bruton, D., Bolton, M., Carr, M., and White, D., 2008, “Pipe-Soil Interaction during Lateral Buckling and Pipeline Walking — The SAFEBUCK JIP,” *Proceedings of Offshore Technology Conference*, Offshore Technology Conference, Houston, Texas, p. 20pp.

[3] Ballard, J. C., Brier, C. De, Stassen, K., and Jewell, R. a, 2013, “Observations of Pipe-Soil Response from in-Situ Measurements,” *Proc. Offshore Technology Conference*, Offshore Technology Conference, Houston, Texas, pp. 6–9.

[4] Smith, V., and Kaynia, A. M., 2015, “Pipe-Soil Interaction under Rapid Axial Loading,” Front. Offshore Geotech. III, pp. 978–1.

[5] Smith, V. B., and White, D. J., 2014, “OTC-24856-MS Volumetric Hardening in Axial Pipe Soil Interaction,” *Offshore Technology Conference - ASIA*, Offshore Technology Conference, Kuala Lumpur, Malaysia, pp. 1–11.

[6] White, D. J., Campbell, M. E., Boylan, N. P., and Bransby, M. F., 2012, “A New Framework For Axial Pipe-Soil Interaction, Illustrated By Shear Box Tests On Carbonate Soils,” *Proceedings of the 7th International Conference of Offshore Site Investigations and Geotechnics*, Society of Underwater Technology, London, pp. 379–387.

[7] Rong, H., Inglis, R., Bell, G., Huang, Z., Chan, R., and Kenny, J. P., 2009, “Evaluation and Mitigation of Axial Walking with a Focus on Deep Water Flowlines,” *Proc. Offshore Technol. Conf., Houston, TX, OTC 19862*, Offshore Technology Conference, Houston, Texas, pp. 1–10.

[8] Mitchell, J. K., and Soga, K., 2005, *Soil Composition and Engineering*

Properties, John Wiley & Sons.

[9] Micic, S., Shang, J. Q., and Lo, K. Y., 2002, “Electrokinetic Strengthening of Marine Clay Adjacent to Offshore Foundations,” Int. J. Offshore Polar Eng., **12**(1), pp. 64–73.

[10] Rittirong, A., and Shang, J. Q., 2008, “Numerical Analysis for Electro-Osmotic Consolidation in Two-Dimensional Electric Field,” Eighteenth Int. Offshore Polar Eng. Conf., **8**, pp. 566–572.

[11] Staff, J., 1998, “In-Situ Casing Consolidation by Electrokinetic Methods,” Pet. Technol., **50**(02), pp. 51–53.

[12] Ghoi, H. S., 1995, “Expansion Analysis of Offshore Pipelines Close to Restraints.Pdf,” *Proceedings of the Fifth International Offshore and Polar Engineering Conference*, International Society of Offshore and Polar Engineers, Hague, Netherlands, pp. 81–88.

[13] Helwany, S., 2007, *Applied Soil Mechanics: With ABAQUS Applications. Sam*, John Wiley and Sons.

[14] Pichler, T., Pucker, T., Hamann, T., Henke, S., and Qiu, G., 2012, “High-Performance Abaqus Simulations in Soil Me- Chanics Reloaded – Chances and Frontiers,” 2012 SIMULIA Community Conf., pp. 1–30.

[15] Rosenak, S., 1963, *Soil Mechanics*, B. T. Batsford, London.

[16] Schofield, A., and Wroth, P., 1968, *Critical State Soil Mechanics*, McGraw-Hill, London.

[17] Parry, R. H. G., 1972, *Stress-Strain Behaviour of Soils*, G. T. Foulis and Co, Henley, England.

[18] Dassault Systèmes, 2014, *Abaqus Analysis User’s Guide*, Dassault Systèmes Simulia Corporation, RI, USA.

[19] Wall, S., 2010, “The History of Electrokinetic Phenomena,” Curr. Opin. Colloid Interface Sci., **15**(3), pp. 119–124.

[20] Airoldi, F., Jommi, C., Musso, G., and Paglino, E., 2009, “Influence of Calcite on the Electrokinetic Treatment of a Natural Clay,” J. Appl. Electrochem., **39**(11), pp. 2227–2237.

[21] Fourie, A. B., Johns, D. G., and Jones, C. F., 2007, “Dewatering of Mine Tailings Using Electrokinetic Geosynthetics,” Can. Geotech. J., **44**(2), pp. 160–172.

[22] Gabrieli, L., Jommi, C., Musso, G., and Romero, E., 2008, “Influence of Electroosmotic Treatment on the Hydro-Mechanical Behaviour of Clayey Silts: Preliminary Experimental Results,” J. Appl. Electrochem., **38**(7), pp. 1043–1051.

[23] Gray, D. H., 1970, “Electrochemical Hardening of Clay Soils,” Geotechnique, **20**(1), pp. 81–93.

[24] Lefebvre, G., and Burnotte, F., 2002, “Improvements of Electroosmotic Consolidation of Soft Clays by Minimizing Power Loss at Electrodes,” Can. Geotech. J., **39**(2), pp. 399–408.

[25] Lockhart, N. C., and Hart, G. H., 1988, “Electro-Osmotic Dewatering of Fine Suspensions: The Efficacy of Current Interruptions,” Dry. Technol., **6**(3), pp. 415–423.

[26] Shang, J. Q., and Lo, K. Y., 1997, “Electrokinetic Dewatering of a Phosphate Clay,” J. Hazard. Mater., **55**(1–3), pp. 117–133.

[27] Shang, J. Q., 1998, “Electroosmosis-Enhanced Preloading Consolidation via Vertical Drains,” Can. Geotech. J., **35**(3), pp. 491–499.

[28] Srinivasaraghavan, R., and Rajasekaran, G., 1994, “Electro-Osmotic Stabilization of Marine Clay with Chemical Piles,” Ocean Eng., **21**(2), pp. 207–219.

[29] Casagrande, L., 1949, “Electro-Osmosis in Soils,” Geotechnique, pp. 159–177.

[30] Casagrande, L., 1952, “Electro-Osmotic Stabilization of Soils,” J. Bost. Soc.

Civ. Eng., **39**(1), pp. 51–83.

[31] Chappell, B. A., and Burton, P. L., 1975, “Electro-Osmosis Applied to Unstable Embankment,” ASCE J Geotech Eng Div, **101**, pp. 733–740.

[32] Bjerrum, L., Moum, J., and Eide, O., 1967, “Application of Electro-Osmosis to a Foundation Problem in a Norwegian Quick Clay,” Géotechnique, **17**(3), pp. 214–235.

[33] Burnotte, F., Lefebvre, G., and Grondin, G., 2004, “A Case Record of Electroosmotic Consolidation of Soft Clay with Improved Soil–electrode Contact.,” Can. Geotech. J., **41**(6), pp. 1038–1053.

[34] Chew, S. H., Karunaratne, G. P., Kuma, V. M., Lim, L. H., Toh, M. L., and Hee, A. M., 2004, “A Field Trial for Soft Clay Consolidation Using Electric Vertical Drains,” Geotext. Geomembranes, **22**(1–2), pp. 17–35.

[35] Lo, K. Y., and Ho, K. S., 1991, “The Effects of Electroosmotic Field Treatment on the Soil Properties of a Soft Sensitive Clay,” Can. Geotech. J., **28**(October 1989), pp. 763–770.

[36] Yuan, J., and Hicks, M. A., 2015, “Numerical Analysis of Electro-Osmosis Consolidation: A Case Study,” Géotechnique Lett., **5**(July–September), pp. 147–152.

[37] Esrig, M., 1968, “Pore Pressures, Consolidation, and Electrokinetics,” J. Soil Mech. Found. Div., **Vol 94**(No SM4), p. 899−921.

[38] Su, J., and Wang, Z., 2003, “The Two-Dimensional Consolidation Theory of Electro-Osmosis,” Géotechnique, **Vol 53**(No 8), p. 759−763.

[39] Lewis, R. W., and Garner, R. W., 1972, “A Finite Element Solution of Coupled Electrokinetic and Hydrodynamic Flow in Porous Media,” Int. J. Numer. Methods Eng., **5**(1), pp. 41–55.

[40] Lewis, R. W., Majorana, C. E., and Schrefler, B. A., 1986, “A Coupled Finite Element Model for the Consolidation of Nonisothermal Elastoplastic Porous Media,” Transp. Porous Media, **1**(2), pp. 155–178.

[41] Lewis, R., and Humpheson, C., 1973, “Numerical Analysis of Electroosmotic Flow in Soils,” J. Soil Mech. Found. Div. ASCE, **Vol 95**(No 4), p. 603−616.

[42] Wan, T., and Mitchell, J., 1976, “Electro-Osmotic Consolidation of Soils,” J. Soil Mech. Found. Div. ASCE, **Vol 102,**(No GT5), p. 473−491.

[43] Tamagnini, C., Jommi, C., and Cattaneo, F., 2010, “A Model for Coupled Electro-Hydro-Mechanical Processes in Fine-Grained Soils Accounting for Gas Generation and Transport,” An. Acad. Bras. Cienc., **82**(1), pp. 169–193.

[44] Jeyakanthan, V., and Gnanendran, C. T., 2013, “Elastoplastic Numerical Approach for Predicting the Electro-Osmotic Consolidation Behaviour of Soft Clays,” Can. Geotech. J., **50**(12), pp. 1219–1235.

[45] Jeyakanthan, V., Gnanendran, C. T., and Lo, S.-C. R., 2011, “Laboratory Assessment of Electro-Osmotic Stabilization of Soft Clay,” Can. Geotech. J., **48**(12), pp. 1788–1802.

[46] Zhou, Y., Deng, A., and Wang, C., 2013, “Finite-Difference Model for One-Dimensional Electro-Osmotic Consolidation,” Comput. Geotech., **54**, pp. 152–165.

[47] Yuan, J., and Hicks, M. A., 2016, “Numerical Simulation of Elasto-Plastic Electro-Osmosis Consolidation at Large Strain,” Acta Geotech., **11**(1), pp. 127–143.

[48] Yuan, J., Hicks, M. a, and Jommi, C., 2015, “Large Strain Consolidation of Clays : Numerical Comparison between Evaporation and Electro-Osmosis Dewatering,” Comput. Methods Recent Adv. Geomech., (1990), pp. 1655–1660.

[49] Yuan, J., and Hicks, M., 2014, “Numerical Modelling of Electro-Osmosis Consolidation of Unsaturated Clay at Large Strain,” *Numerical Methods in Geotechnical Engineering*, pp. 1061–1066.

[50] Yuan, J., and Hicks, M. A., 2013, “Large Deformation Elastic Electro-Osmosis Consolidation of Clays,” Comput. Geotech., **54**, pp. 60–68.

[51] Micic, S., Shang, J. Q., and Lo, K. Y., 2003, “Electrocementation of a Marine Clay Induced by Electrokinetics,” Int. J. Offshore Polar Eng., **13**(4), pp. 308–315.

[52] HU, L., and WU, H., 2014, “Mathematical Model of Electro-Osmotic Consolidation for Soft Ground Improvement,” Géotechnique, **64**(2), pp. 155–164.

[53] Jones, C., and Glendinning, S., 2006, “Soil Consolidation and Strengthening Using Electrokinetic Geosynthetics–concepts and Analysis,” Geosynthetics, (2), pp. 411–414.

[54] Al-Hamdan, A. Z., and Reddy, K. R., 2008, “Electrokinetic Remediation Modeling Incorporating Geochemical Effects,” J. Geotech. Geoenvironmental Eng., **134**(January), pp. 91–105.

[55] Virkutyte, J., Sillanpaa, M., and Latostenmaa, P., 2002, “Electrokinetic Soil Remediation - Critical Overview,” Sci. Total Environ., **289**(1–3), pp. 97–121.

[56] Wu, H., Wu, W., and Hu, L., 2012, “Numerical Model of Electro-Osmotic Consolidation in Clay,” Géotechnique, **62**(6), pp. 537–541.

[57] Lo, K. Y., Micic, S., Shang, J. Q., Lee, Y. N., and Lee, S. W., 2001, “Electrokinetic Strengthening of a Marine Sediment Using Intermittent Current,” Can. Geotech. J., **38**(2), pp. 287–302.

[58] Eton, G. E., 2011, “Mitigation against Lateral Buckling and Axial Walking of Subsea Pipeline,” Doctor of Philosophy thesis, Institute of Resilient Infracstructure, School of Civil Engineering, University of Leeds.

[59] Mitchell, J. K., 1960, “Components of Pore Water Pressure and Their Engineering Significance,” Clays Clay Miner., **9**(1), pp. 162–184.

[60] Lo, K. Y., Micic, S., and Shang, J. Q., 1999, “Electrokinetic Strengthening

of Soft Marine Clays," *Proceedings of the Ninth (1999) International Offshore and Polar Engineering Conference*, International Society of Offshore and Polar Engineers, Brest, France, pp. 1–6.

[61] Micic, S., Lo, K. Y., and Shang, J. Q., 2004, "Increasing Load-Carrying Capacities of Offshore Foundations in Soft Clays," J. Pet. Technol., **56**(2), pp. 53–55.

[62] Segall, B. A., C. E. O'Bannon, C. E., and J. A. J. Matthias, J. A. J., 1980, "Electro-Osmosis Chemistry and Water Quality," J. Geotech. Eng. Div., **106**(10), pp. 1148–1152.

[63] Hansen, E. J., and Saouma, V. E., 1999, "Numerical Simulation of Reinforced Concrete Deterioration: Part II–steel Corrosion and Concrete Cracking," ACI Mater. J., **96**(3), pp. 331–338.

[64] Callister, W. D., and Rethwisch, D. G., 2014, *Materials Science and Engineering : An Introduction*, John Wiley & Sons.

[65] Cormie, P., McBride, J. M., McCaulley, G. O., Jensen, A., and Lidell, E., 2009, "The Influence of Body Mass on Calculation of Power during Lower-Body Resistance Exercises," J. Strength Cond. Res., **16**(4), pp. 1042–1049.

[66] Bruton, D. a S., and Carr, M., 2007, "'The Influence of Pipe-Soil Interaction on Lateral Buckling and Walking of Pipelines- the SAFEBUCK Jip,'" *International Offshore Site Investigation and Geotechnics Conference*, Society of Underwater Technology, London, pp. 11–13.

[67] Casola, F., El-chayeb, A., Greco, S., and Carlucci, A., 2011, "Characterization of Pipe Soil Interaction and Influence on HPHT Pipeline Design," Int. Soc. Offshore Polar Eng., **8**, pp. 111–121.

[68] Merifield, R., White, D. J., and Randolph, M. F., 2008, "The Ultimate Undrained Resistance of Partially Embedded Pipelines," Géotechnique, **58**(6), pp. 461–470.

[69] Aubeny, C. P., Shi, H., and Murff, J. D., 2005, “Collapse Loads for a Cylinder Embedded in Trench in Cohesive Soil,” Int. J. Geomech., **5**(4), pp. 320–325.

[70] Merifield, R. S., White, D. J., and Randolph, M. F., 2009, “Effect of Surface Heave on Response of Partially Embedded Pipelines on Clay,” J. Geotech. Geoenvironmental Eng., **135**(6), pp. 819–829.

[71] Muthukrishnan, S., Kodikara, J., and Rajeev, P., 2011, “Numerical Modelling of Undrained Vertical Load- Displacement Behaviour of Offshore Pipeline Using Coupled Analysis,” *2011 Pan-Am CGS Geotechnical Conference*, pp. 1–8.

[72] Randolph, M. F., and White, D. J., 2008, “Pipeline Embedment in Deep Water: Processes and Quantitative Assessment,” *Proceedings of Offshore Technology Conference (OTC)*, Offshore Technology Conference, Houston, Texas, pp. 1–16.

[73] Ballard, J., and Falepin, H., 2009, “Towards More Advanced Pipe-Soil Interaction Models in Finite Element Pipeline Analysis,” *Proceedings of the SUT Annual Conference*, Society of Underwater Technology, Perth, Western Australia, pp. 1–5.

[74] Westgate, Z. J., Randolph, M. F., White, D. J., and Li, S., 2010, “The Influence of Sea State on As-Laid Pipeline Embedment: A Case Study,” Appl. Ocean Res., **32**(3), pp. 321–331.

[75] Oliphant, J., and Maconochie, A., 2006, “Axial Pipeline-Soil Interaction,” *International Society of Offshore and Polar Engineers*, International Society of Offshore and Polar Engineers, San Francisco, California, USA, pp. 100–107.

[76] Randolph, M. F., and House, A. R., 2001, “The Complementary Roles of Physical and Computational Modelling,” Int. J. Phys. Model. Geotech., **1**(1), pp. 1–8.

[77] Profound Technologies, 2014, “Pipeline Walking,”

http://pipelinewalking.com, p.1 [Online]. Available: http://pipelinewalking.com. [Accessed: 21-Oct-2014].

[78] Carr, M., Sinclair, F., and Bruton, D., 2008, “Pipeline Walking--Understanding the Field Layout Challenges and Analytical Solutions Developed for the Safebuck JIP,” SPE Proj. Facil. Constr., **3**(3), pp. 1–9.

[79] Carneiro, D., and Castelo, A., 2011, “Walking Analyses of HP/HT Pipelines with Sliding End Structures Using Different FE Models,” *Rio Pipeline 2011*, Rio Pipeline Conference & Exposition, Rio de Janeiro, Brazil, pp. 1–11.

[80] Bruton, D. A. S., and Carr, M., 2011, “Overview of the SAFEBUCK JIP,” *Proceedings of Offshore Technology Conference*, Offshore Technology Conference, Houston, Texas, pp. 2–5.

[81] Bruton, D. A. S., Sinclair, F., and Carr, M., 2010, “OTC 20750 Lessons Learned From Observing Walking of Pipelines with Lateral Buckles , Including New Driving Mechanisms and Updated Analysis Models,” *Proceedings of Offshore Technology Conference*, Offshore Technology Conference, Houston, Texas, pp. 1–12.

[82] Perinet, D., and Simon, J., 2011, “Lateral Buckling and Pipeline Walking Mitigation in Deep Water,” Offshore Technol. Conf., (May), pp. 2–5.

[83] Thusyanthan, I., Mesmar, S., Robert, D., Wang, J., and Haigh, S. K., 2011, “Upheaval Buckling Assessment Based on Pipeline Features,” *Offshore Technology Conference*, Offshore Technology Conference, Houston, Texas, pp. 2–5.

[84] Bruton, D., Boreas, A., White, D., and Langford, T., 2009, “Techniques for the Assessment of Pipe-Soil Interaction Forces for Future Deepwater Developments,” *Offshore Technology Conference*, Offshore Technology Conference, Houston, Texas, pp. 1–12.

[85] Yew, C. C., 2013, “SliPIPE-New Pipeline Expansion Concept,” p. 1 [Online]. Available: http://www.dnv.com/industry/oil_gas/publications/updates/pipeline_update

/2013/01_2013/SliPIPE__new_pipeline_expansion_concept.asp. [Accessed: 10-Oct-2014].

[86] Bai, Q., and Bai, Y., 2014, “Lateral Buckling and Pipeline Walking,” *Subsea Pipeline Design, Analysis, and Installation*, pp. 221–253.

[87] Bruton, D., White, D. J., and Cheuk, C. Y., 2006, “‘Pipe/Soil Interaction Behavior during Lateral Buckling, Including Large-Amplitude Cyclic Displacement Tests by the Safebuck JIP,’” *Offshore Technology Conference*, pp. 1–10.

[88] Altaee, A., and Fellenius, B. H., 1996, “Finite Element Modeling of Lateral Pipeline-Soil Interaction,” *114th International Conference on Offshore Mechanics and Arctic Engineering, OMAE 96*, Florence, Italy, pp. 283–300.

[89] O’Rourke, T. D., and Trautmann, C. H., 1985, “Lateral Force-Displacement of Buried Pipe Response,” J. Geotech. Eng., **111**(9), pp. 1077–1092.

[90] Hill, A., White, D. J., Bruton, D. A. S., Langford, T., Meyer, V., Jewell, R. A., and Ballard, J.-C., 2012, “A New Framework for Axial Pipe-Soil Resistance, Illustrated by a Range of Marine Clay Datasets,” *Proceedings of the International Conference on Offshore Site Investigation and Geotechnics*, Society of Underwater Technology, London, pp. 367–377.

[91] White, D. J., and Cathie, D. N., 2011, *Geotechnics for Subsea Pipelines*.

[92] Boylan, N. P., and White, D., 2014, “OTC-25398-MS Seabed Friction On Carbonate Soils : Physical Modelling of Axial Pipe-Soil Friction,” *Proceedings of Offshore Technology Conference (OTC)*, Offshore Technology Conference (OTC), Houston, Texas, pp. 1–16.

[93] Ansari, Y., Kouretzis, G. P., and Sheng, D., 2014, “An Effective Stress Analysis of Partially Embedded Offshore Pipelines: Vertical Penetration and Axial Walking,” Comput. Geotech., **58**(May), pp. 69–80.

[94] Vermeer, P., A., and Verruijt, A., 1981, “An Accuracy Condition for Consolidation by Finite Elements,” Int. J. Numer. Anal. Methods Geomech.,

5(January), pp. 1–14.

[95] Bergado, D. T., Sasanakul, I., and Horpibulsuk, S., 2003, “Electro-Osmotic Consolidation of Soft Bangkok Clay Using Copper and Carbon Electrodes with PVD,” Geotech. Test. J., **26**(3), pp. 277–288.

[96] Mohamedelhassan, E., and Shang, J. Q., 2001, “Effects of Electrode Materials and Current Intermittence in Electro-Osmosis,” Proc. Inst. Civ. Eng. - Gr. Improv., **5**(1), pp. 3–11.

[97] Xie, L., and Shang, C., 2006, “Effects of Copper and Palladium on the Reduction of Bromate by Fe(0),” Chemosphere, **64**(6), pp. 919–930.

[98] Gourvenec, S. M., and White, D. J., 2010, “Elastic Solutions for Consolidation Around Seabed Pipelines,” *Otc*, pp. 3–6.

[99] Krost, K., Gourvenec, S. M., and White, D. J., 2011, “Consolidation around Partially Embedded Seabed Pipelines,” Géotechnique, **61**(2), pp. 167–173.

[100] Dingle, H. R. C., White, D. J., and Gaudin, C., 2008, “Mechanisms of Pipe Embedment and Lateral Breakout on Soft Clay,” Can. Geotech. J., **45**(5), pp. 636–652.

[101] Engineering Toolbox, 2015, “Conductivity of Some Common Materials and Gases,” http://www.engineeringtoolbox.com/thermal-conductivity-d_429.html [Online]. Available: http://www.engineeringtoolbox.com/thermal-conductivity-d_429.html. [Accessed: 02-Mar-2015].

[102] Dutta, S., Hawlader, B., and Phillips, R., 2014, “Finite Element Modeling of Partially Embedded Pipelines in Clay Seabed Using Coupled Eulerian-Lagrangian Method,” Can. Geotech. J., **72**(February 2014), pp. 1–15.

APPENDICES

Appendix A **Mesh sensitivity Analysis**

A.1 Test Series-1a, 1b

Table A-1 Mesh convergence: test series-1

Element Sizes				Number of elements				Total numbers of elements	Mises Stress, MPa
Soil	Pipe	Electrodes	Rings	Soil	Pipe	Electrodes	Rings		
0.015	0.004	0.001	0.0008	38290	3594	6468	14910	123448	2.828E+01
0.0145	0.004	0.001	0.0008	44863	3594	6468	14910	130021	2.84E+01
0.014	0.004	0.001	0.0008	51721	3594	6468	14910	136879	2.84E+01
0.0135	0.004	0.001	0.0008	55571	3594	6468	14910	140729	2.85E+01
0.013	0.004	0.001	0.0008	61469	3594	6468	14910	146627	2.86E+01
0.0125	0.004	0.001	0.0008	65463	3594	6468	14910	150620	2.86E+01
0.012	0.004	0.001	0.0008	76099	3594	6468	14910	161257	2.86E+01

A.2 Test Series-2a, 2b

Table A-2 Mesh convergence test series-2

Element Sizes				Number of elements				Total numbers of elements	Stress, MPa
Soil	Pipe	Electrodes	Rings	Soil	Pipe	Electrodes	Rings		
0.04	0.04	0.035	0.0025	141301	680	6750	14201	224383	30.5383
0.039	0.04	0.035	0.0025	153778	680	6750	14201	236860	30.6186
0.038	0.04	0.035	0.0025	156732	680	6750	14201	239814	30.6314
0.037	0.04	0.035	0.0025	162625	680	6750	14210	245707	30.3707
0.036	0.04	0.035	0.0025	178361	680	6750	14201	261443	30.9243
0.035	0.04	0.035	0.0025	195893	680	6750	14201	278295	32.1129
0.034	0.04	0.035	0.0025	205018	680	6750	14201	288100	31.0518
0.033	0.04	0.035	0.0025	222140	680	6750	14201	305222	32.1322
0.032	0.04	0.035	0.0025	229666	680	6750	14210	312748	32.1648
0.031	0.04	0.035	0.0025	274357	680	6750	14201	357439	32.2639
0.03	0.04	0.035	0.0025	281144	680	6750	14201	364226	32.3626
0.029	0.04	0.035	0.0025	329393	680	6750	14201	412475	32.4875

Table A-3 Mesh convergence test series-2: Mohr-Coulomb model with CTD elements

Element Sizes				Number of elements				Total numbers of elements	Stress, MPa
Soil	Pipe	Electrodes	Rings	Soil	Pipe	Electrodes	Rings		
0.038	0.038	0.034	0.0025	27469	352	33600	12904	74325	21.8217
0.037	0.038	0.034	0.0025	28501	352	33600	12904	75357	22.0323
0.036	0.038	0.034	0.0025	32351	352	33600	12904	79207	21.2229
0.035	0.038	0.034	0.0025	34093	352	33600	12904	80949	21.0353
0.034	0.038	0.034	0.0025	38292	352	33600	12904	85148	21.7285
0.033	0.038	0.034	0.0025	42372	352	33600	12904	89228	21.3062
0.032	0.038	0.034	0.0025	43768	352	33600	12904	90624	22.1839
0.031	0.038	0.034	0.0025	49075	352	33600	12904	95931	22.8771
0.03	0.038	0.034	0.0025	55150	352	33600	12904	102006	22.7354
0.029	0.038	0.034	0.0025	64568	352	33600	12904	111424	22.6396
0.028	0.038	0.034	0.0025	68064	352	33600	12904	114920	22.8843
0.027	0.038	0.034	0.0025	79680	352	33600	12904	126536	22.9759

A.3 Test Series-3a, 3b

Table A-4 Mesh convergence test series-3

Element Sizes				Number of elements				Numbers of elements	Stress, MPa
Soil	Pipe	Electrodes	Rings	Soil	Pipe	Electrodes	Rings		
0.012	0.012	0.001	0.0008	19235	1880	3027	11570	68471	1.3174
0.01	0.012	0.001	0.0008	31946	1880	3027	11570	81182	1.3977
0.009	0.012	0.001	0.0008	40395	1880	3027	11570	89631	1.3198
0.0085	0.012	0.001	0.0008	47141	1880	3027	11570	96377	1.4832
0.008	0.012	0.001	0.0008	56438	1880	3027	11570	105674	1.4407
0.0075	0.012	0.001	0.0008	67951	1880	3027	11570	117187	1.4829
0.007	0.012	0.001	0.0008	82328	1880	3027	11570	131564	1.4861
0.0065	0.012	0.001	0.0008	103169	1880	3027	11570	152405	1.4871

Appendix B **PHASE-1: ABAQUS Heat Transfer, Electrical, and Chemical Flow Verification**

Figure B-1 Phase-1: ABAQUS Flow behaviour of chloride diffusion cracking of concrete

Appendix C **PHASE-2: ABAQUS Temperature-Pore Pressure Elements Verification**

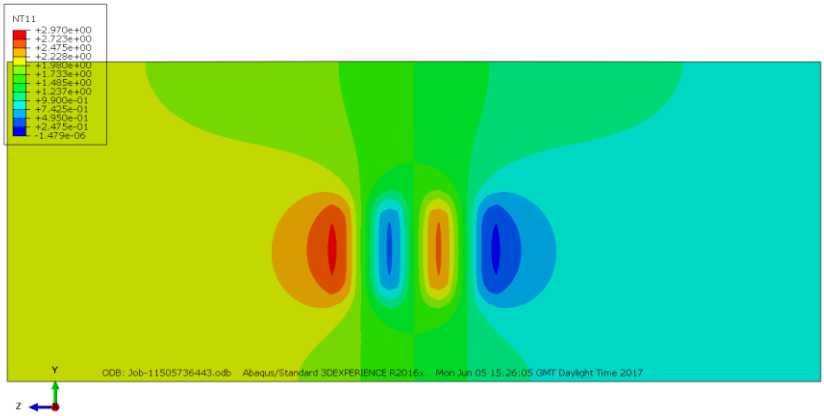

Figure C-1 Phase-2: electrical field distribution

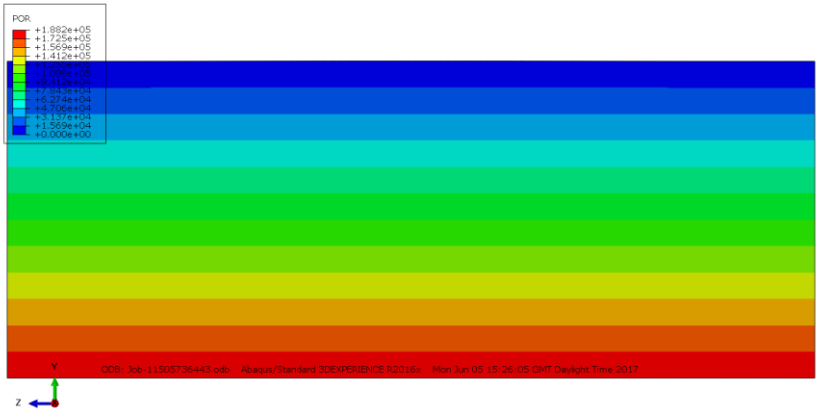

Figure C-2 Phase-2: pore water pressure distribution

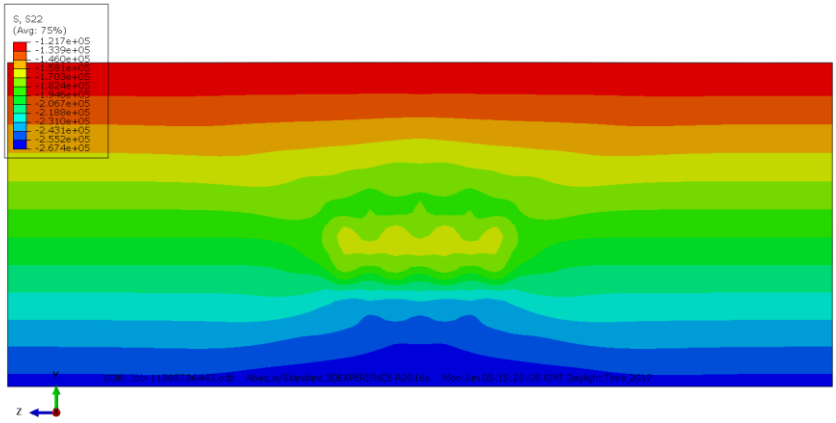

Figure C-3 Phase-2: effective stress distribution

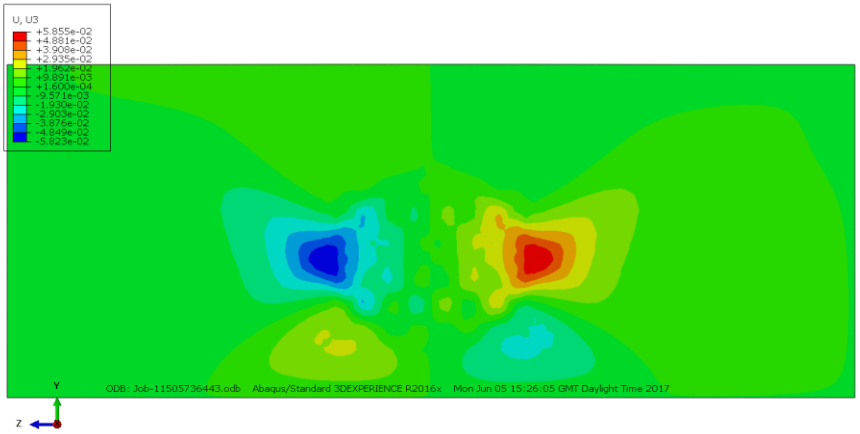

Figure C-4 contour plot showing a section view of horizontal soil settlement distribution within the soil

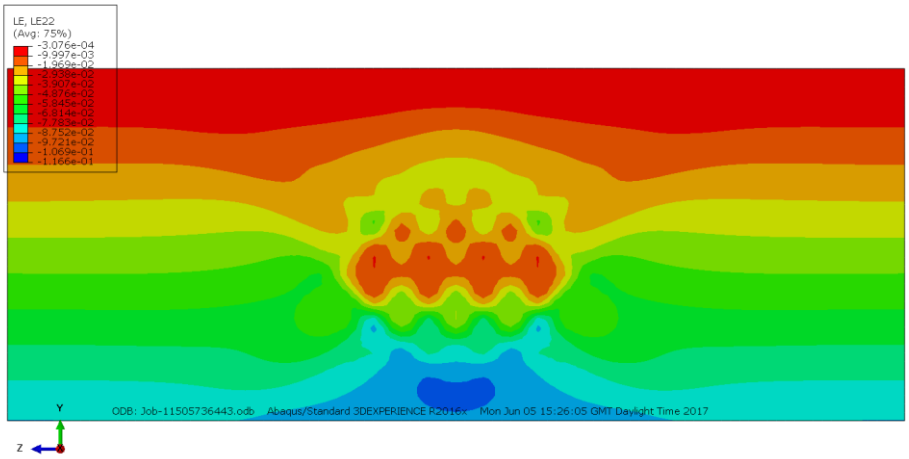

Figure C-5 Phase-2: contour plot of Soil Strain distribution

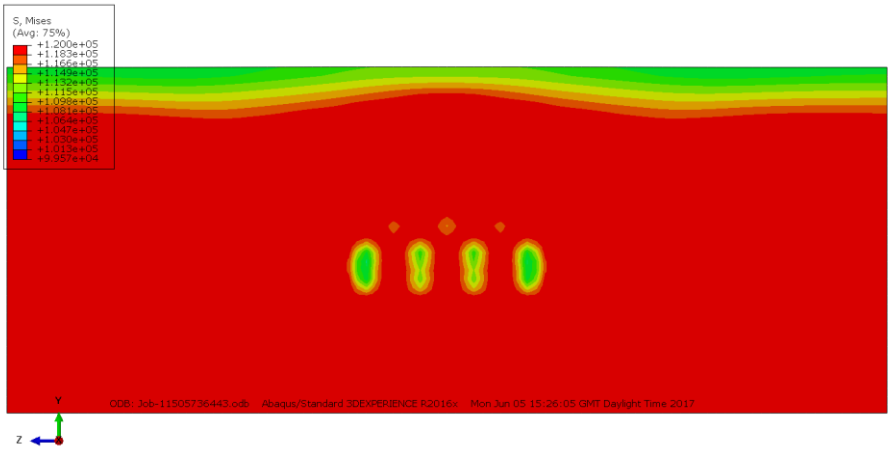

Figure C-6 Phase-2: Mises stress distribution

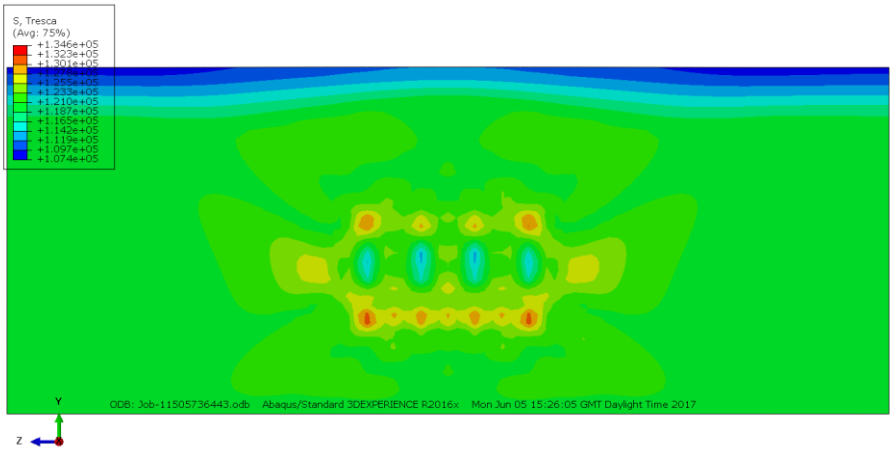

Figure C-7 Phase-2: Tresca stress distribution

Appendix D **PHASE-3: Series-1**

D.1 Electrical Field Distribution

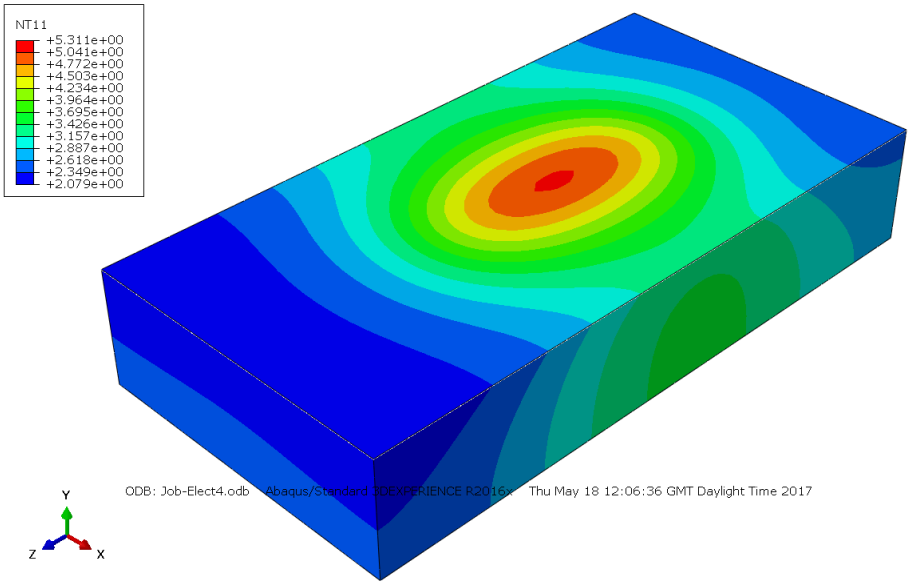

Figure D-1 Series-1a: section view of electrical field flow behaviour along soil horizontal surface

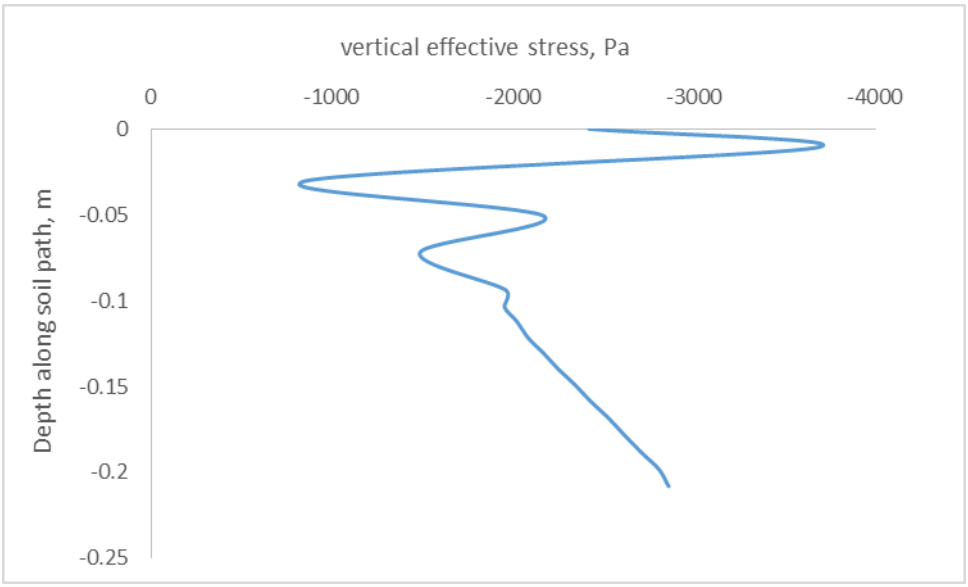

Figure D-2 Series-1a: effective stress distribution with depth

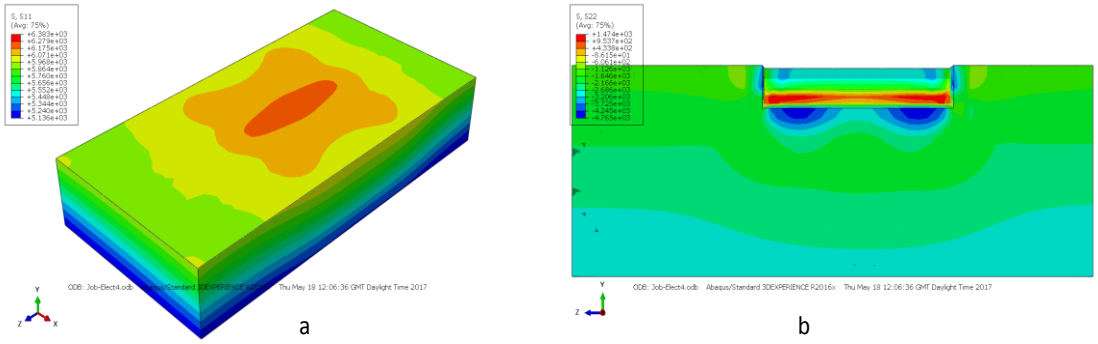

Figure D-3 Series-1a: (a). Section view of horizontal effective stress, (b). Section view of vertical effective stress behaviour

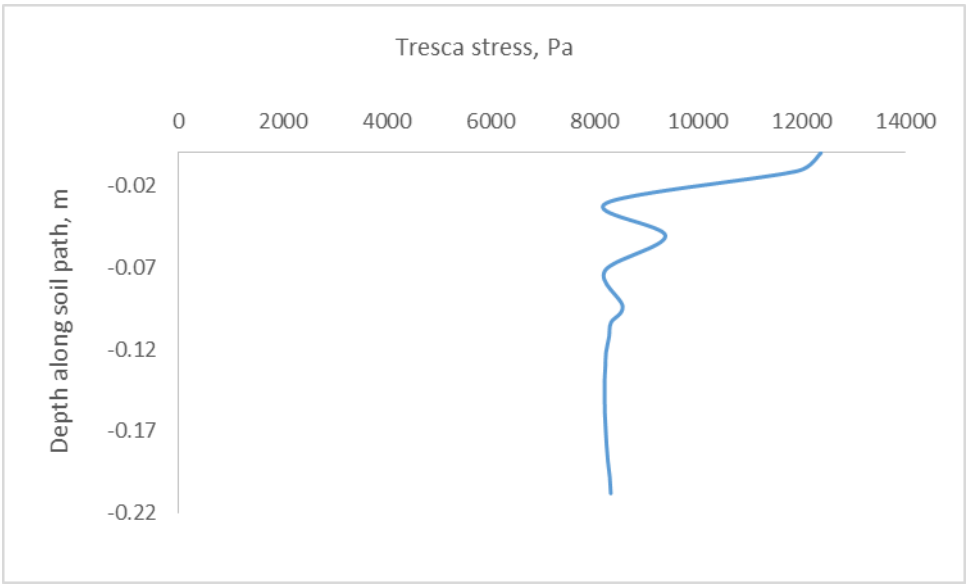

Figure D-4 Series-1a: Tresca stress distribution

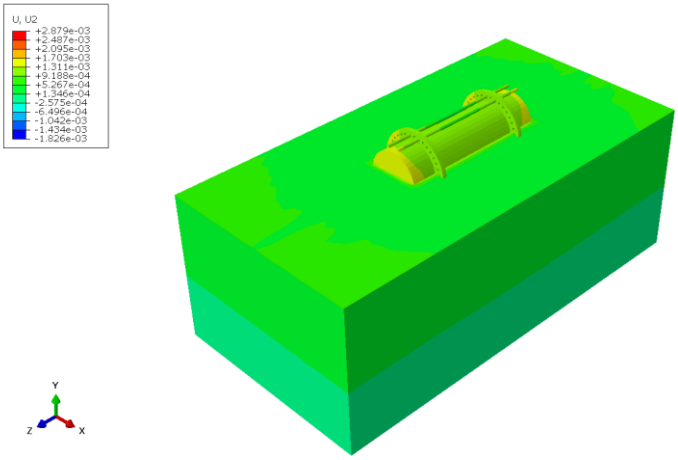

Figure D-5 Series-1a: vertical soil settlement after 6-hours of treatment

Appendix E **Phase-3: Series-2**

E.1 Flow behaviour

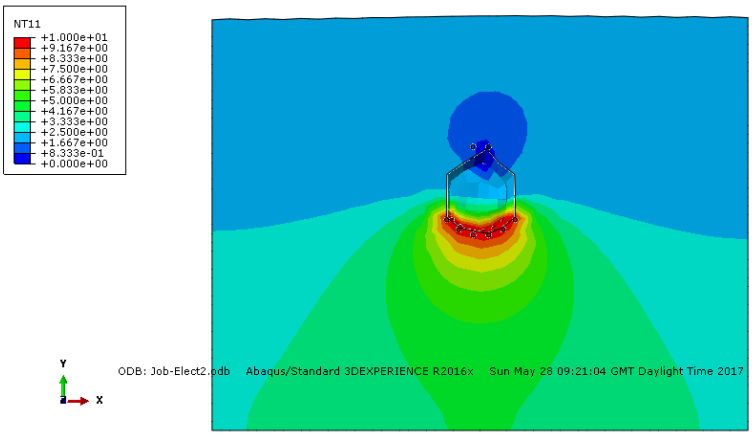

Figure E-1 Series-2a: section view of electrical field distribution with depth and along the horizontal soil surface

E.2 Soil Stress Distribution

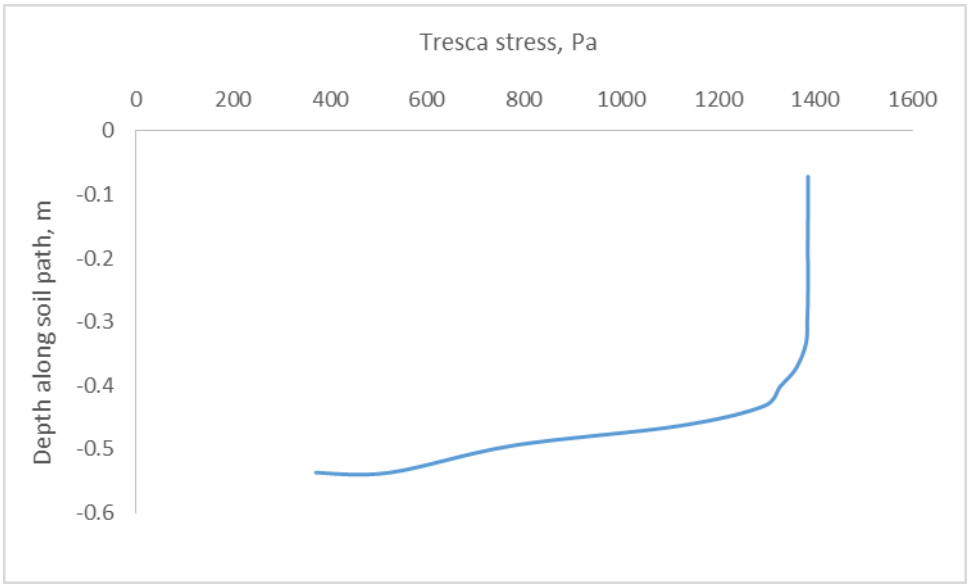

Figure E-2 Series-2a: soil Tresca stress distribution

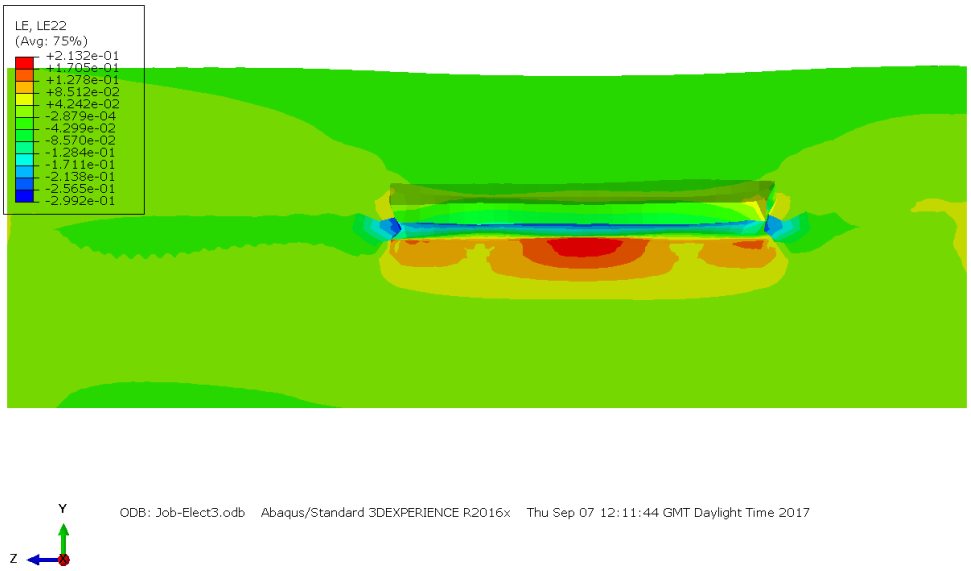

Figure E-3 Series-2a: contour plot of Soil Strain distribution

E.3 Soil Settlement Distribution

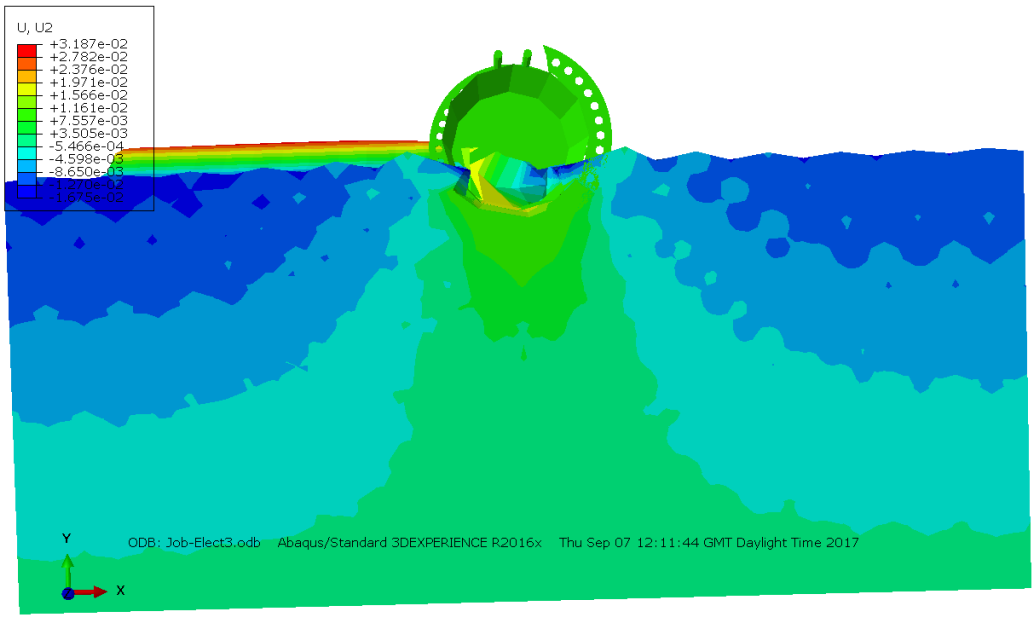

Figure E-4 Series-2a: section view of vertical soil settlement distribution within and along the soil surface

Appendix F **Phase-3: Series-3**

F.1 Flow Behaviour

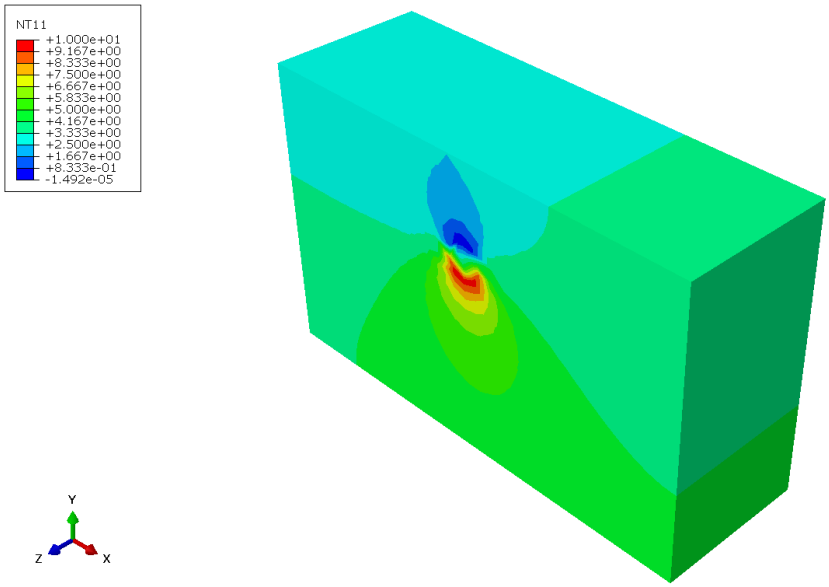

Figure F-1 Vertical penetration model Series-3a: electrical field distribution along the soil surface

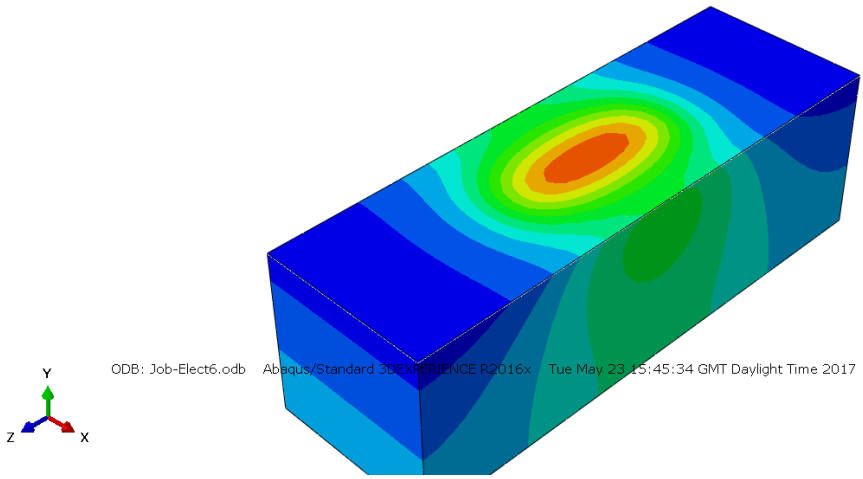

Figure F-2 axial model series-3a: electrical field distribution along the soil horizontal surface.

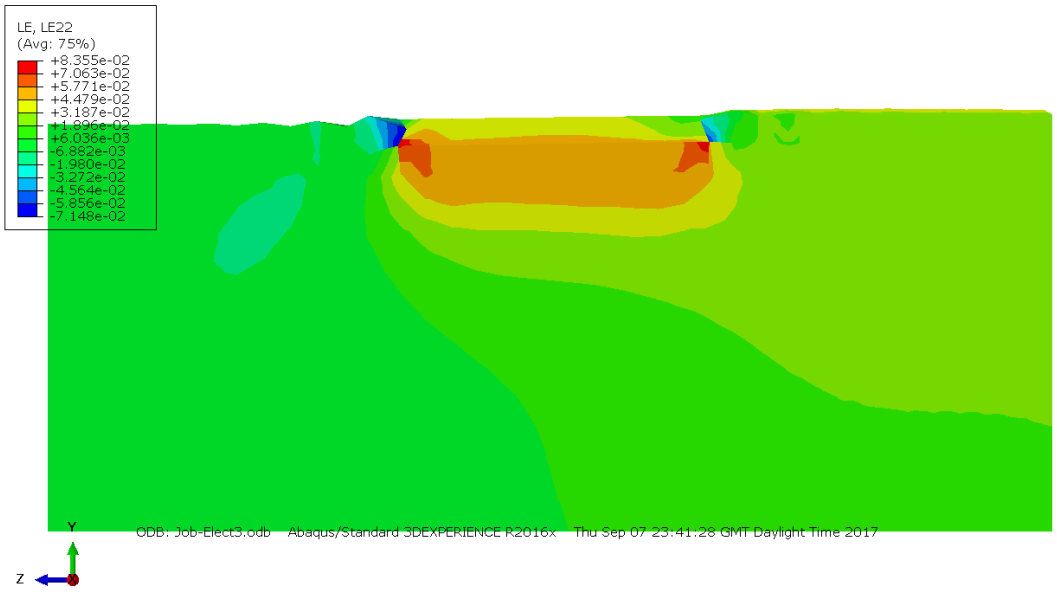

Figure F-3 axial model series-3a: contour plot of soil strain distribution